

Organic Photoconductive Materials: Recent Trends and Developments

Kock-Yee Law

Xerox Webster Research Center, 800 Phillips Road, 0114-39D, Webster, New York 14580

Received July 13, 1992 (Revised Manuscript Received October 19, 1992)

Contents

I. Introduction	449	B. Photogeneration Mechanisms in Organic Photoconductors	475
II. Background	450	1. Photogeneration in Phthalocyanines	475
A. History of Xerography	450	2. Photogeneration in Perylenes	476
B. The Xerographic Process	450	3. Photogeneration in Azo Pigments	477
C. Evolution of Xerographic Materials and Devices	450	C. Photogeneration Efficiency	477
D. General Requirements for Xerographic Photoreceptors	451	1. Effect of Molecular Structure	477
E. Xerographic Measurements	452	2. Effect of Molecular Architecture	478
III. Classes of Organic Photoconductive Materials	453	D. Photoinduced Electron-Transfer Reactions	480
A. Phthalocyanines	453	1. Effect of CGL/CTL Energetics on the Photosensitivity	480
1. Synthesis, Structural Variation, and Purification	453	2. Effect of CGL/CTL Energetics on the Residual Potential	481
2. Optical Absorption and Electronic Structure	453	V. Trends and Outlook	481
3. Polymorphism in Phthalocyanines	454	A. Trends in Materials Research	481
4. Photoconductivity	455	1. Basic Studies	481
5. Naphthalocyanines	457	2. Materials Design Concept	482
B. Squaraines	457	3. Visible versus IR	482
1. Synthesis and Structural Variation	458	4. Environmentally Safe Materials	482
2. Optical Absorption	459	B. Trends in Device Development	482
3. Solid-State Properties	459	C. Outlook and Other Opportunities	483
4. Photoconductivity	461		
5. Unsymmetrical Squaraines	462		
C. Azo Pigments	464		
1. Synthesis, Purification, and Structural Variation	464		
2. Electronic Structure of Photoconductive Azo Pigments	465		
3. Optical and Solid-State Properties	465		
4. Photoconductivity	466		
D. Perylene Pigments	467		
1. Synthesis, Purification, and Structural Variation	468		
2. Optical and Solid-State Properties	468		
3. Photoconductivity	470		
4. Perinones	471		
E. Miscellaneous Classes	471		
1. PVK-TNF Charge-Transfer Complex	471		
2. Thiapyrylium Salts	472		
3. 3,6-Diphenylpyrrolo[3,4-c]pyrrole-1,4-dithione	472		
4. Miscellaneous Photoconductors	473		
IV. Mechanistic Studies	474		
A. Definitions, Models, and Measurements of Photogeneration	474		
1. Definitions and Models	474		
2. Measurements of Photogeneration Efficiency	474		

I. Introduction

During and after the energy crisis in the 1970s, there was a projected severe shortage of fuel energy globally. A huge surge of research activities aimed at alternative clean energies, such as solar energy, took place. The conversion of sunlight to electricity and chemical fuel has been an attractive subject since. Early work on photovoltaic and photoelectrochemical devices has been focused on inorganic photoconductive (semiconductive) materials, such as silicon (crystalline and amorphous), CdS, Cu₂S, TiO₂, etc.¹⁻⁸ Much less attention was paid to organic materials, which had a stereotype of inefficient, impure, and unstable upon solar degradation, etc. Nonetheless, the advantages of using organic photoconductive materials in solar cells, such as low cost and ease of fabrication into large area, were recognized.⁹⁻²² In the 1980s, we came to realize that the global energy shortage is real but not as severe as it was forecasted. Moreover, we have also learned to use our fuels more efficiently and have been seeking alternative energy at every opportunity. The urgency of researching new photoconductors for solar energy conversion has lost its momentum. Meanwhile, an explosion of research activities, aimed at the development of cheaper and better organic photoconductors for xerographic photoreceptors in copiers and laser printers, has taken place in the copier industry. Today more than 90% of the xerographic photoreceptors are



Kock-Yee Law was born in Hong Kong. He received a B.S. with first class honors in chemistry from The Chinese University of Hong Kong in 1974 and a Ph.D. in organic photochemistry from The University of Western Ontario in 1978. He joined the Xerox Webster Research Center in 1981 and has been a Principal Scientist since 1989. Dr. Law is also a Principal Investigator of the NSF Photoinduced Charge-Transfer Center at the University of Rochester. He served as treasurer for the Inter-American Photochemical Society from 1984–1991. Dr. Law was given an "Excellence in Science and Technology" award by the Corporation Research Group at Xerox in 1987 and a Xerox Eagle Award for being one of the top patent winners within Xerox in 1992. Dr. Law was also a recipient of the Journal Award (Science) Honorable Mention by The Society of Imaging Science and Technology in 1991. His current research interests include molecular design, synthesis, and mechanistic studies of organic photoconductors and charge control additives.

made of organic photoconductors.^{23–26} The intention of this article is to provide an overview on the classes of organic photoconductive materials that have been studied and successfully developed in the photoreceptor industry. Critical scientific issues related to the mechanism of photogeneration and the subsequent electron-transfer processes are reviewed. Trends in the research of organic photoconductors and the future utilization of the materials and know-how developed in the photoreceptor industry for other electronic device applications are noted.

II. Background

A. History of Xerography

The term xerography originates from the Greek words *xeros* and *graphos*, which together mean "dry writing". In the early 1930s, out of the need of making carbon copies of legal documents in his own work, the inventor of xerography, Chester Carlson, envisioned the benefit of having a copying machine in the office. He studiously examined various light-related electrostatic phenomena. In 1938, he filed the first patent on what he called electrophotography.²⁷ The photosensitive devices Carlson examined were sublimed thin films of sulfur and anthracene on zinc plates. The photogenerated electrostatic images were developed by lycopodium powder. The road of commercialization of the electrophotographic process was quite dramatic.²⁸ Initially, Carlson failed to use his invention to impress the couple of dozen companies he contacted. It was not until 1944 that a group at Battelle Development Corporation, headed by Schaffert, took the responsibility to reduce the Carlson invention to practice. Subsequently, a small photographic film company in Rochester, the Haloid

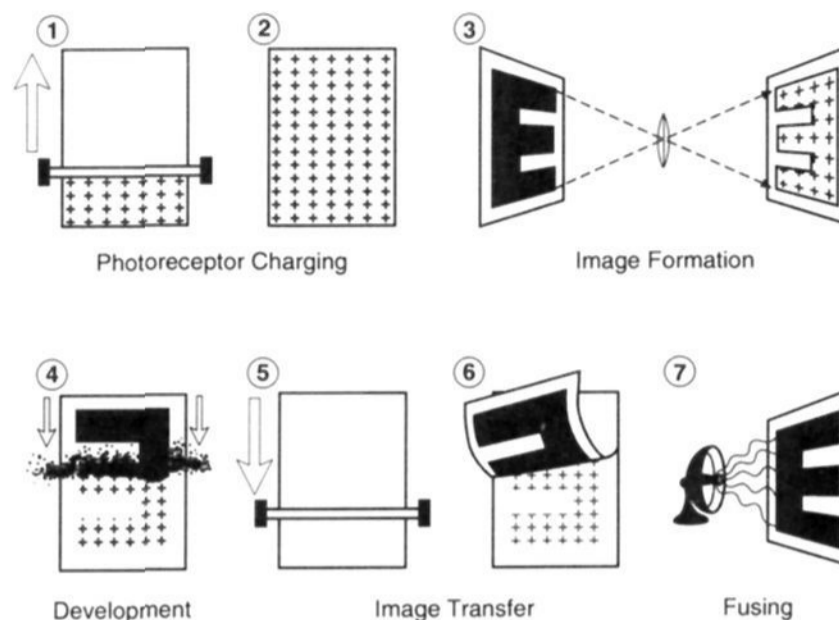


Figure 1. Basic steps in the xerographic process.

Company (the predecessor of Xerox Corporation), joined the effort in 1947. In 1949, the first copier machine, the Xerox Model A, was introduced. Model A basically consisted of three subunits, a charging and developing unit, a camera for exposure, and a radiant heat fusing unit. The copying process was totally manual, involving about a dozen steps before a photocopy could be produced. In addition, the copy quality was operator dependent and unpredictable. The need to automate the entire copying process to enable reliability and dependability was recognized. The work on automation took another 10 years. In 1959, the Xerox copier Model 914 was introduced. This was the world's first automated photocopy machine. It was one of the most successful single products in the history of business. It not only turned the small photographic company, Haloid, into a giant corporation, Xerox, but also revolutionized the way the modern office works, making the copier machine a nondisposable integral part of office appliances today. Now the xerographic process is used not only to duplicate the document, but also to create the document.

B. The Xerographic Process

The essence of the xerographic process is the generation of electrostatic images and the development of these images into hardcopy. The basic steps in the xerographic process are depicted in Figure 1. The process involves charging (steps 1 and 2) and imagewise photodischarge (step 3) of the photoreceptor device. The photogenerated electrostatic images are then developed by toner (or dry ink) electrostatically (step 4). After the transferral of the toned images to a piece of paper (steps 5 and 6), the toned images are then fused (step 7) to produce a photocopy. As seen in steps 1–4, one of the key elements in xerography is the photoreceptor device, which has to accept and retain charges in the dark and to undergo photodischarge upon light exposure. To achieve a high contrast potential between the imaged and nonimaged areas, a photoreceptor has to have a high level of charge acceptance and low conductivity in the dark and become conductive when it is illuminated.

C. Evolution of Xerographic Materials and Devices

In Carlson's early experiments, sublimed thin films of sulfur and anthracene were used as photoconductors.

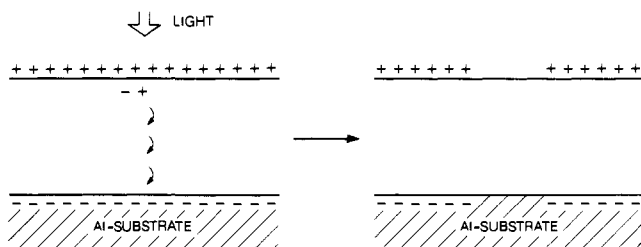


Figure 2. Schematics of the configuration and the photo-discharge process of a single-layer photoconductor.

By today's standard, these are very poor photoconductors because they do not absorb in the visible region and their efficiencies of photogeneration are low. For example, the quantum yield of photogeneration for anthracene was reported to be 10^{-4} .²⁹ Nevertheless, Carlson's concept of forming electrostatic images using a photoconductor was demonstrated. As soon as the Battelle group initiated their activity, alternative photoconductive materials were sought. The investigation eventually led to the development of the world's first visible-light sensitive photoconductor.³⁰⁻³² The photoconductive device consisted of a 10–50- μm -thick layer of selenium vacuum deposited onto an aluminum plate or drum. The configuration and the imaging mechanism of the device is given in Figure 2. Basically, the photoconductive device was charged positively in the dark and was then exposed imagewise. Electron-hole (e-h) pairs are generated at the front surface upon illumination. While the photogenerated electrons are neutralized at the front surface, the photogenerated holes migrate across the device and become neutralized also, forming electrostatic images of the original document. Selenium is an excellent photoconductor and its quantum efficiency of photogeneration is about unity. The photoresponse of selenium, however, decreases sharply at wavelengths $> 550 \text{ nm}$.³³ Subsequent activities on selenium devices have been focused on improving the spectral response in the visible region as well as extending it to the near-IR (750–850 nm), enabling selenium-based devices to be useful in diode laser printers.³⁴⁻³⁸

Organic photoconductive materials have always been associated with electrophotography, from the materials studied in Carlson's early invention to the organic photoconductors in the marketplace today. Even when the selenium photoconductor enjoyed its business success, research on organic photoconductors was active. The need of cheaper and better photoconductors, coupled with the environmental concerns of disposing selenium, has continuously motivated research on organic photoconductive materials. The first commercial organic photoconductor was based on a charge-transfer complex between poly(vinylcarbazole) and trinitrofluorenone.³⁹ Subsequent work at Eastman Kodak also led to the development of an aggregated photoconductor based on a thiapyrylium salt.⁴⁰ The configuration and the imaging process of these early organic photoconductors are similar to those shown in Figure 2.

In single-layer photoconductors, the photoconductor not only has to have a high quantum efficiency of photogeneration, but also a high charge mobility across the device, for both electrons and holes. Moreover, since the photoconductor is constantly in contact with other subsystems in the copier, it must also have a good

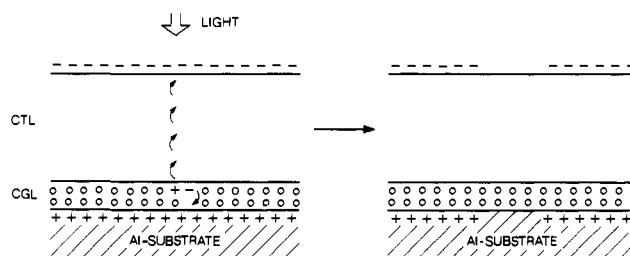


Figure 3. Schematics of the configuration and the photo-discharge process of a bilayer photoconductor: CGL, charge generation layer; CTL, charge transporting layer.

mechanical strength. This set of requirements is very stringent and sometimes the demands are opposing. Satisfying all these demanding requirements has become increasingly difficult. As a result, the concept of bilayer photoconductor device was developed. In the bilayer configuration, the charge generation and charge transport functions are separated into two discrete layers, the charge-generation layer (CGL) for generating the charges and the charge-transporting layer (CTL) for transporting the charges.⁴¹⁻⁴³ By design, the CGL absorbs most of the incoming light and its thickness varies from 0.2 to 2 μm , depending on the concentration of the photoconductor in the layer. The CTL not only has to transport the charges, it also serves as a protective layer for the CGL, enabling improvements in the mechanical properties of the entire photoconductor device. The thickness of the CTL can be anywhere from 15 to 30 μm . The configuration and the imaging mechanism of a bilayer photoconductor device are given in Figure 3. Since the technology of hole-transporting materials is more advanced than that of electron-transporting materials, most of the practical organic photoconductors to date are negatively charged at the surface as shown in Figure 3.⁴⁴

Illumination of the bilayer photoconductor device results in the formation of e-h pairs in the CGL. The photogenerated holes inject to the CTL wherein the injected holes migrate across the CTL and become neutralized. Electrostatic images are then formed. Organic photoconductive pigments of different chemical classes have been successfully used in bilayer photoconductor devices. The structures and the physical and the photoconductive properties of these materials are reviewed in section III. Fundamental issues related to the mechanism of photogeneration and the subsequent electron-transfer processes are the subjects of section IV. Although the electron- or hole-transport process in the CTL is photoinduced in the bilayer photoconductor device, the transport process, which involves hoppings of electrons between electroactive sites in the CTL, is a ground-state phenomenon.^{45,46} The subject itself is huge and is considered to be beyond the scope of this paper.

D. General Requirements for Xerographic Photoconductors

As noted earlier, the key steps in the xerographic process are the generation of electrostatic images and the development of these images into hardcopy. To achieve a high contrast potential for image development, the photoconductor must be an insulator or have low conductivity in the dark and become conductive upon

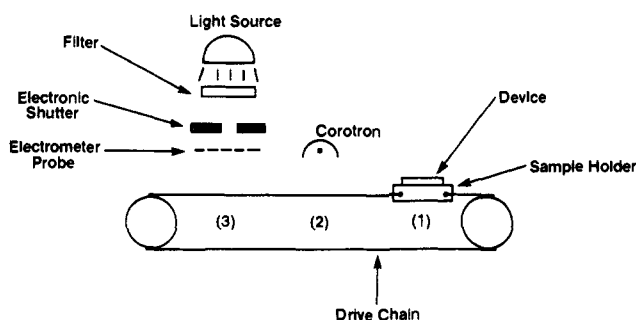


Figure 4. A schematic of a flat plate scanner apparatus.

exposure to light. Regardless of the device configuration, all photoinduced processes in the photoreceptor originate from the photoconductor. A highly sensitive photoconductor not only requires less energy to generate the electrostatic images, but also enables the photoreceptor to be operated at a higher speeds. Therefore, the photosensitivity and the dark conductivity (usually measured as the dark decay of the surface potential) of the photoreceptor are the first set of material parameters to be assessed. Furthermore, photoreceptors are used repetitively in a machine environment. As seen in section II.C, each charging/photodischarging process involves a sequence of photogeneration and electron-transfer processes. In practice, these processes should remain constant within the intended life of the device. Depending on the application, the intended life can be anywhere from a few thousand to a million cycles.

For copier applications, the only spectral requirement for the photoconductor is to be sensitive in the visible region, e.g., 400–650 nm. A tungsten lamp or a xenon lamp can be used as an illuminator. Due to the recent advances of laser and computer technologies, the digital age of xerography has already arrived. Xerography is no longer limited to making duplication, it is used to create the document as well. Recognized advantages of digital xerography include improvement of copy quality, editing, and coloring of the document. Among the lasers for xerographic printer applications, solid state (GaAs) diode lasers, which emit at 750–850 nm, are known to be low cost, compact, and highly efficient. They have been the preferred light source for various xerographic printers.⁴⁷ (The most common diode laser emits at 780 nm.) To capture these business opportunities, the photoconductor has to be sensitive at wavelengths where the lasers emit. Thus the search for IR-sensitive organic photoconductor for diode laser printers has been an active area of research for more than a decade.⁴⁸

In addition to the photoelectrical performance, the mechanical properties of the entire photoreceptor device, the cost of manufacturing, and the toxicity of the materials employed are issues one has to address prior to the commercialization of the device.

E. Xerographic Measurements

The photoelectrical properties of a xerographic device are usually studied on a flat plate scanner. A schematic of the apparatus is given in Figure 4. Typically, the photoreceptor device is mounted and grounded on the sample holder. The photoreceptor is then moved back and forth from its resting position (1) to the measuring

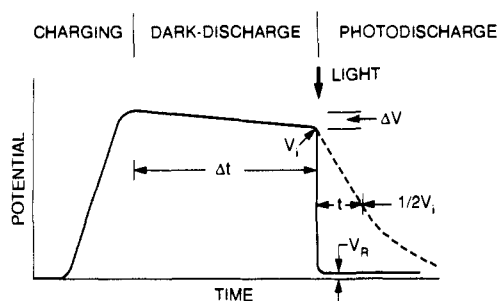


Figure 5. Schematics of photodischarge curves: —, photodischarge by an intense light; ---, photodischarge by a monochromatic light of intensity I .

station (3) by the drive chain. When the device is moving under the corotron device at position (2), it will be charged either positively or negatively. When the device is stopped at (3), its surface potential is measured by an electrometer. The output of the electrometer is displayed on either a strip-chart recorder or a personal computer. Schematics of the photodischarge curves are depicted in Figure 5. With the shutter closed, the dark conductivity (decay) of the device ($\Delta V/\Delta t$) is measured. With the shutter open, the device could be exposed to an intense erase light to determine the residual potential (V_R) or to a monochromatic light of known intensity (I in $\text{ergs cm}^{-2} \text{s}^{-1}$) to determine the photosensitivity of the device. The photosensitivity can be expressed as $E_{0.5}$, the energy required to photodischarge half of the initial potential (V_i). $E_{0.5}$ is the product of I and t , where t is the time for I to photodischarge the device from V_i to $0.5V_i$. This procedure is simple and all the first-order xerographic properties can be determined. It has been used extensively for materials evaluation and structure-property relationship study.

Another common variant for the xerographic experiment is a drum scanner.⁴⁹ In this case, the sample is mounted on a rotating conductive drum. Corotron charging devices, light sources, and surface potential probes are mounted around the circumference. Photodischarge curves analogous to those in Figure 5 can be generated by measurements from a series of potential probes. The advantage of the drum scanner is that one can vary the speed of the drum and examine the mobility of the charge during the photodischarge. Information on the kinetics of the photodischarge process can be obtained. Moreover, since each charging/photodischarge cycle can be completed in a short time, the drum scanner has frequently been used as a tool for stress tests, where the durability of the device for practical application is evaluated.

The xerographic gain (η) is defined as the quantum yield of e-h pairs formation after illumination of the xerographic device and can be expressed as⁵⁰

$$\eta = \frac{\epsilon}{4\pi deI} \left(\frac{dV}{dt} \right)_{V_i}$$

where ϵ is the dielectric constant, dV/dt is the rate of the photodischarge at V_i , d is the thickness of the device, e is the elementary charge, and I is the light intensity.

Since d , I , and dV/dt are measurable quantities, one can calculate η if one makes an assumption on ϵ . In a bilayer device such as that described in Figure 3, η is a complicated function of (1) the quantum efficiency

of photogeneration of the photoconductor (ϕ_{eh}) in the CGL, (2) the efficiency of hole injection from CGL to CTL, and (3) the hole mobility in CTL. Deconvolution of these extricate relationships is not simple. Hence information obtained for ϕ_{eh} is indirect. In practice, alternative procedures and device configurations are frequently used to determine ϕ_{eh} . The details of some of the measurements are given in section IV.A.2.

III. Classes of Organic Photoconductive Materials

In this section, organic materials that are known to be photoconductive are grouped into several categories on the basis of their chemical structures and their impacts in xerographic photoreceptors. For each class of compounds, the synthesis, optical absorption, and solid-state properties are first reviewed. Literature photoconductivity data are then compiled and discussed. Critical factors that influence the photoconductivity are highlighted.

A. Phthalocyanines

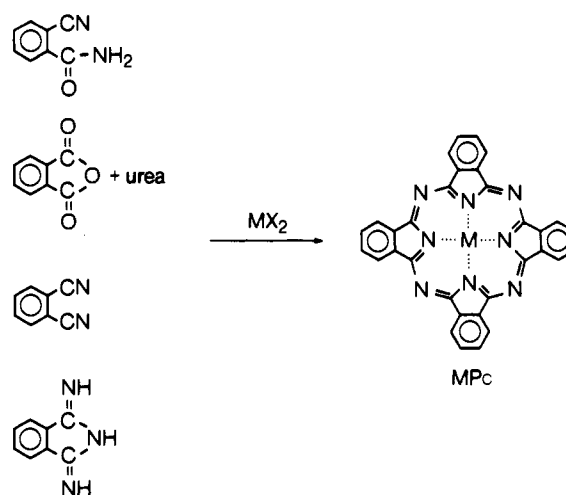
The synthesis of phthalocyanine was discovered by accident in 1907 when Braun and Tcherniac isolated a small amount of blue precipitate after heating *o*-cyanobenzamide in alcohol.⁵¹ In the early 1930s, Linstead and co-workers reported the synthesis of many phthalocyanines and suggested that a phthalocyanine ligand consists of four units of isoindole and has a highly conjugated system.⁵²⁻⁵⁵ The structure of phthalocyanine was established later by Robertson and co-workers who reported the X-ray single-crystal structures of nickel phthalocyanine, copper phthalocyanine, and platinum phthalocyanine.⁵⁶⁻⁵⁹ Phthalocyanines show intense absorption in the red and their appearances in the solid-state range from dark blue to metallic bronze to green, depending on the central metal, the crystalline form, and the particle size. They are widely used as colorants for plastics, inks, fabrics, and automobile paints. In addition, they have also been found to exhibit interesting optical, magnetic, catalytic, semiconductive, and photoconductive properties.^{60,61}

1. Synthesis, Structural Variation, and Purification

Since the early work by Linstead and co-workers, many procedures for phthalocyanines have been developed. These reactions are summarized in Scheme I. Depending on the metal salt and the valence of the metal, a variety of phthalocyanines can be synthesized. M can be two hydrogen atoms, such as in metal-free phthalocyanine, H₂Pc. It can be a monovalent or divalent metal such as Li₂Pc or MgPc. When M is trivalent, M can be a metal halide or a metal hydroxide, such as in AlClPc and AlOHPC. In the case of tetravalent metals, M can be a metal oxide, a metal dihalide or a metal dihydroxide, such as in TiOPc, SiCl₂Pc, and Si(OH)₂Pc. To date, nearly all metals and semimetals are known to form complexes with the phthalocyanine ligand.^{60,61}

In addition to the central metal ion, structural variation can be accomplished by substitutions on the phthalocyanine ring, such as sulfonic acid (or amide),^{62,63} carboxylic acid,⁶⁴ alkyl,⁶⁵ aryl,^{66,67} halide,^{68,69} nitro,⁷⁰ etc. Substituents usually enhance the solubility of phthalocyanines in solvents.

Scheme I



Due to the steric effect, they also induce morphological changes in the solid state. The change in morphology has frequently been found to affect the photoconductivity.

Phthalocyanines are usually purified by successive washings with organic solvents, alkali solution and boiling 5% hydrochloric acid solution after synthesis.⁷¹ Trace amounts of metal salt and organic impurities such as phthalonitrile, phthalimide, phthalic anhydride, and urea decomposition products, have been detected.^{72,73} These impurities are shown to adversely affect the xerographic properties of phthalocyanines in devices.⁷⁴⁻⁷⁶ To purify phthalocyanines to the "photoconductor" grade, the techniques of acid pasting (by reprecipitating the sulfuric acid solution of a phthalocyanine in ice-water)⁷⁷⁻⁷⁹ and sublimation^{74-76,80,81} are frequently used.

2. Optical Absorption and Electronic Structure

The absorption spectra of a number of phthalocyanines (H₂Pc, MgPc, TiOPc, VOPc, CrPc, FePc, CoPc, NiPc, CuPc, ZnPc, SnCl₂Pc, and PbPc) have been studied in solution by Edwards and Gouterman.⁸² VOPc, CoPc, NiPc, CuPc and ZnPc are stable in the vapor phase and their absorption spectra in the gaseous state were also recorded. These spectral data revealed that phthalocyanines have two absorption bands, one in the visible region at 600–700 nm (the Q-band) and the other in near-UV at ~300–400 nm (the Soret band). The vapor spectra are usually blue-shifted several hundred cm⁻¹ with respect to the solution spectra. While the spectrum of H₂Pc shows two clear vibronic bands at ~698.5 and 663 nm in 1-chloronaphthalene solution, most phthalocyanines exhibit only one absorption band and an absorption shoulder in the visible absorption. The visible absorption of phthalocyanine is not sensitive to the central metal ion. A summary of the absorption spectra data of phthalocyanines has been compiled in an earlier review by Lever.⁶⁰

Theoretical molecular orbital studies have been carried out for several phthalocyanines⁸³⁻⁸⁵ as well as H₂Pc.^{86,87} These calculations show that the visible absorption band (the Q band) primarily arises from the $\pi \rightarrow \pi^*$ transition within the delocalized phthalocyanine ring system. Specifically, the $\pi \rightarrow \pi^*$ transition involves a charge transfer from the outer benzene rings

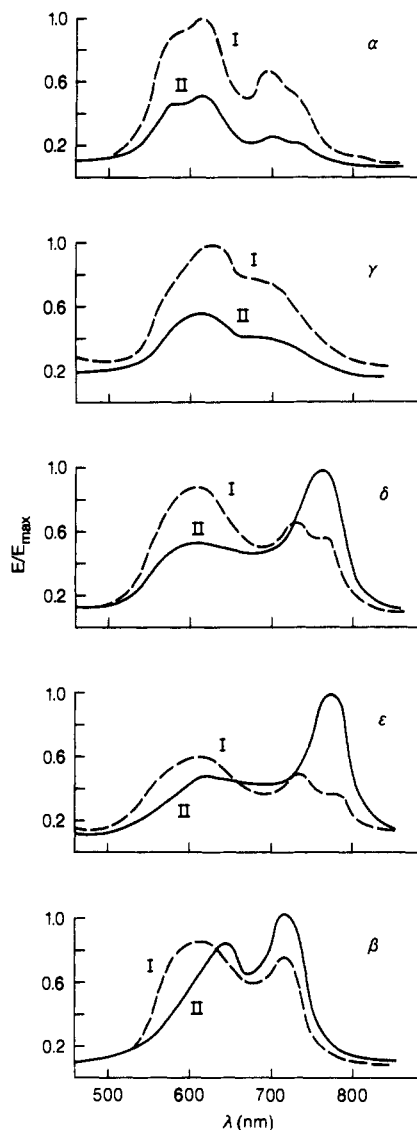


Figure 6. Dichroic spectra of pigment particles of the five polymorphs of CuPc. The direction of the light polarization is perpendicular (I, - - -) and parallel (II, —) to the longitudinal axis of the rodlike pigment aggregates. Reprinted from ref 88. Copyright 1978 Oil & Colour Chemists Association.

of phthalocyanine to the inner macrocyclic ring.⁸³ The calculation also predicts that the frequencies of the Q band are generally independent on the metal ion, which agrees well with experimental results. Finally, these MO calculations also consider interactions between the ligand MO's and the d orbitals of the metal ion. Qualitative predictions of the MO levels of several phthalocyanines have been reported.⁸³⁻⁸⁵

3. Polymorphism in Phthalocyanines

Polymorphism is a common phenomenon in phthalocyanines. This is because the intermolecular forces between phthalocyanine molecules are relatively weak and a variety of molecular stacking arrangements of similar interaction energies are possible. The color of each polymorph is different and dye chemists have been exploiting this property for some time. As it turns out, the variation of molecular stacking in the solid state has a profound influence on the photoconductivity too.

Among the phthalocyanines, CuPc has been the most studied compound because of its stability and its

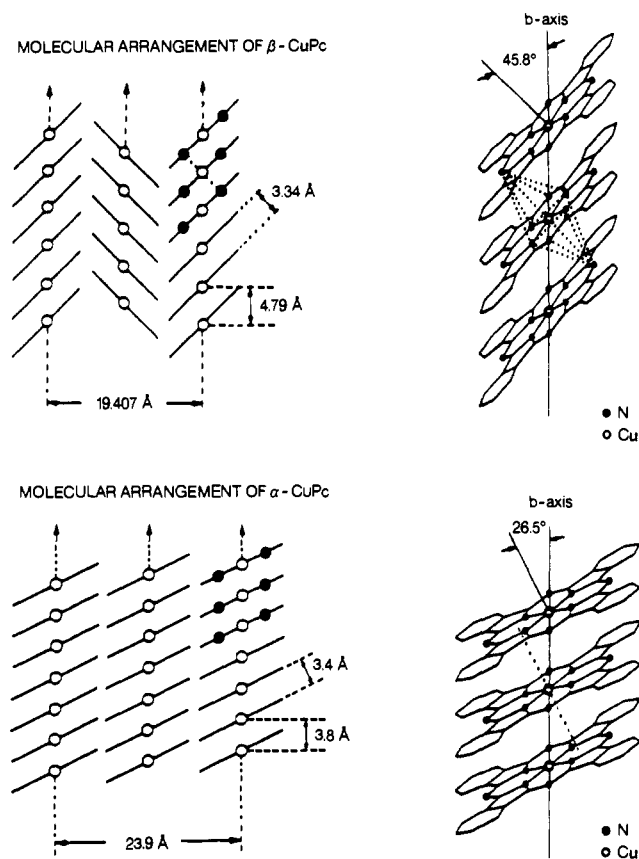


Figure 7. Molecular stacking arrangements of α -CuPc and β -CuPc. Reprinted from ref 88. Copyright 1978 Oil & Colour Chemists Association.

extensive use in the dye industry. Five polymorphs, namely the α -, β -, γ -, δ -, and ϵ -form of CuPc are known.⁸⁸ β -CuPc is the thermodynamically stable polymorph and is obtained directly from synthesis or recrystallization from other metastable polymorphs.⁸⁹ α -CuPc is obtained by acid-pasting β -CuPc.⁹⁰ The γ -, δ -, and ϵ -form of CuPc are obtained by precipitating a sulfuric acid solution of CuPc under different conditions.⁹¹⁻⁹⁴ α -, γ -, δ -, and ϵ -CuPc are metastable and can be converted to β -CuPc upon heating or solvent recrystallization. These five polymorphs of CuPc exhibit characteristic solid-state absorption spectra and X-ray powder diffraction patterns in the solid state. Neither the absorption spectra nor the X-ray diffraction patterns are available in a single publication for reproduction here, unfortunately. In Figure 6, the dichroic spectra of the five different polymorphs of CuPc, which give us the flavor of their solid-state absorption spectra, are shown. The data show that both δ - and ϵ -CuPc exhibit absorption bands with λ_{max} at ~ 770 nm that are significantly red-shifted from the solution absorption maximum (~ 678 nm). This red-shift indicates that there exists an intermolecular charge-transfer interaction between CuPc molecules in these two polymorphs. As shall be discussed in section IV, this intermolecular interaction is a prerequisite for the high photoconductivity. In fact, Yagishita et al.⁹⁵ and Enokida and Hirohashi⁹⁶ have reported that the xerographic performance of ϵ -CuPc is superior to other polymorphs of CuPc.

β -CuPc is thermodynamically stable and single crystals of β -CuPc have been grown for structural analysis.⁹⁷ In the case of α -CuPc, structural information

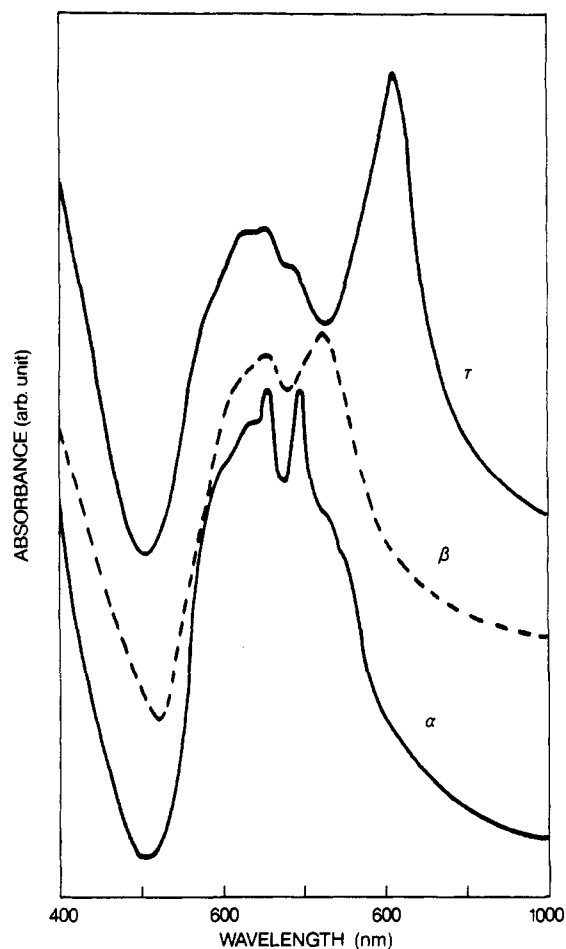


Figure 8. Absorption spectra of the α -, β -, and τ -forms of H_2Pc . Reprinted from ref 105. Copyright 1985 The Society for Imaging Science and Technology.

was obtained by comparing the X-ray powder pattern of α -CuPc with those of α -CuPcCl₄ and α -PtPc, and the single-crystal structure of α -PtPc.^{89,98} The stacking arrangements of CuPc molecules in the α - and β -polymorphs are depicted in Figure 7. Details of the stacking arrangements of δ -, γ -, and ϵ -CuPc are not available, probably due to experimental difficulties.

H_2Pc is known to exist in four different polymorphs in the solid state, namely α , β , X, and τ . Again β - H_2Pc is the thermodynamically stable polymorph and is obtained from either direct synthesis or recrystallization.⁹⁹ α - H_2Pc is obtained by acid pasting or sublimation in thin films.¹⁰⁰⁻¹⁰³ X- H_2Pc is prepared by neat milling α - H_2Pc for ~ 1 week,¹⁰⁴ and τ - H_2Pc can be obtained either by milling α - H_2Pc in a solvent^{105,106} or direct synthesis.¹⁰⁷ Figures 8 and 9 show the solid-state absorption spectra and the X-ray powder diffraction patterns of α -, β -, and τ - H_2Pc , respectively. The data of X- H_2Pc are known to be similar to those of τ - H_2Pc ,^{99,104} and cannot be incorporated in Figures 8 and 9 because they are from a different publication. The X-ray and absorption data, which are supported by recent solid-state ¹³C NMR spectral results,¹⁰⁸ indicate that each polymorph has a unique set of solid-state properties. Both X- and τ - H_2Pc are found to have photoconductivity of practical values.^{99,106,109} Incidentally, the longest wavelength absorption maxima of X- and τ - H_2Pc are also significantly red-shifted (by ~ 100 nm) relative to the solution absorption of H_2Pc .

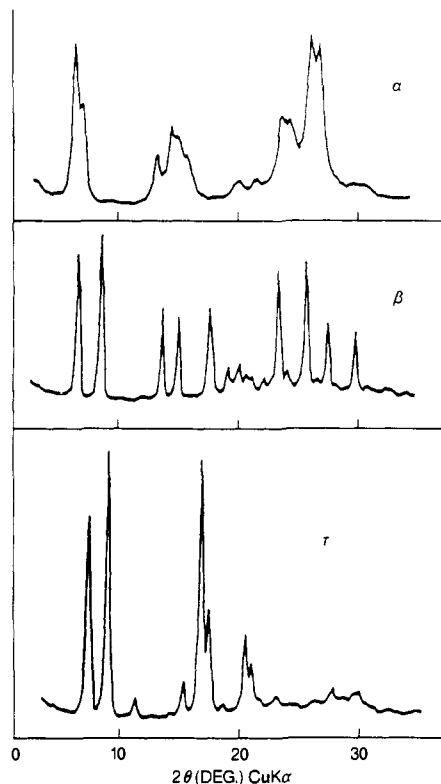


Figure 9. X-ray powder diffraction patterns of the α -, β -, and τ -forms of H_2Pc . Reprinted from ref 105. Copyright 1985 The Society for Imaging Science and Technology.

A tremendous amount of attention has been paid to TiOPc lately because of its interesting polymorphic behaviors and high photoconductivity. Besides the α - and β -polymorph, TiOPc is shown to form a variety of metastable polymorphs, some of which are found to be highly sensitive in xerographic devices. For example, Enokida et al.^{110,111} reported that, in addition to α - and β -TiOPc, which are obtained by acid pasting of TiOPc following by an acetone treatment, and by wet milling of crude TiOPc, respectively, they also synthesize an amorphous form, m - and γ -form of TiOPc by varying the processing conditions toward crude TiOPc. Fujimaki and co-workers^{112,113} reported the synthesis of TiOPc via the reaction of titanium tetra-*n*-butoxide and 1,3-diiminoisoindole. After acid pasting, three different polymorphs, Y, A, and B were isolated depending on the subsequent processing conditions. Tanako et al.¹¹⁴ reported a variant of solvent treatment at the same time, where the so-called phase 1, 2, and 3 of TiOPc were prepared. A glance at some of the absorption spectra and X-ray powder diffraction patterns indicates that some of the compositions reported between different laboratories are similar. The author has made no effort to sort them out here, but hopes that this review can stimulate a more thorough and careful characterization effort on these highly sensitive and interesting materials. A snapshot at the various polymorphs of photoconductive phthalocyanines is provided in Table I.

4. Photoconductivity

In the last decade, most of the photoconductivity studies of phthalocyanines have been with bilayer xerographic devices. Table II summarizes the xerographic data of several of the most mentioned phthalocyanines.

Table I. Polymorphic Forms and Structural Characterization of Some Phthalocyanines

MPc	polymorphs	method of preparation	characterization	ref(s)
CuPc	α	acid pasting	absorption, X-ray	89, 90
	β	as-synthesized, recrystallization	absorption, X-ray	89
	γ	acid pasting + solvent treatment	absorption, X-ray	93
	δ	acid pasting + solvent treatment	absorption, X-ray	94
H ₂ Pc	ϵ	acid pasting + solvent treatment	absorption, X-ray	91, 92
	α	acid pasting, sublimation	absorption, X-ray	100–103
	β	as-synthesized, recrystallization	absorption, X-ray	99
MgPc	X	neating milling	absorption, X-ray, IR	104
	τ	wet milling, as-synthesized	absorption, X-ray, CP MAS ¹³ C NMR	105–107
	α	sublimed film	absorption, IR, X-ray	115, 116
	β	as-synthesized	absorption, IR, X-ray	115, 116
ZnPc	aggregated ^a	CH ₂ Cl ₂ treatment of the α -form	absorption, IR, X-ray	115, 116
	α	acid pasting	X-ray, IR	117
CoPc	β	recrystallization	X-ray, IR	117
	α	as-synthesized	X-ray, absorption, IR	118
AlClPc	β	as-synthesized	X-ray, absorption, IR	118
	ϵ	as-synthesized	X-ray, absorption, IR	118
	β^b	sublimation	absorption, IR, X-ray	116
AlClPcCl	aggregated ^a	solvent recrystallization	absorption, IR, X-ray	116
	β^b	sublimation	absorption, IR	116, 119
AlOHPC	aggregated ^a	solvent recrystallization	absorption, IR	116, 119
	α^b	sublimed film	absorption, X-ray, IR	120
InClPc	aggregated ^a	solvent recrystallization	absorption, X-ray, IR	120
	β^b	sublimation, as-synthesized	absorption, X-ray	121, 122
VOPc	aggregated ^a	solvent recrystallization	absorption, X-ray	121, 122
	phase I	acid pasting	absorption, X-ray, IR	123
	phase II	heating, solvent recrystallization	absorption, X-ray, IR	123
TiOPc	phase III	heating	absorption, X-ray, IR	123
	α	sublimed film	absorption, X-ray, IR	110
	β	solvent recrystallization	absorption, X-ray, IR	110
	aggregated ^{a,c}	various acid pasting/solvent treatment combinations	absorption, X-ray, IR	110–114

^a The "aggregated" forms denote to polymorphs that exhibit near-IR absorption that are significantly red-shifted from their solution λ_{\max} . It is shown that the red-shift is the result of the intermolecular interaction between the phthalocyanine rings in the solid state.

^b This notation is assigned because this polymorph shows absorption similar to the corresponding polymorph of CuPc or H₂Pc. ^c At least nine different polymorphs of TiOPc that exhibit red-shifted absorption in the solid state have been reported.

Table II. Xerographic Data of Photoconductive Phthalocyanines

MPc	polymorph	CGL deposition technique	MPc conc in CGL	dark decay (V/s)	xerographic data ^a		spectral range ^e (nm)	ref
					visible ^b	near-IR		
H ₂ Pc	α	solution coating	50% ^d	-7.4	<i>e</i>		550–700	106
	β	solution coating	50% ^d	-2.5	<i>e</i>		550–700	106
	τ_1	solution coating	50% ^d	-5.1	<i>e</i>	4.5 at 780 nm	550 to >800	106
	τ_2	solution coating	50% ^d	-3.0	<i>e</i>	2.5 at 780 nm	550 to >800	106
	X	solution coating	30% ^f	-20		4.5 at 780 nm	550 to >800	124
CuPc	α	solution coating	50% ^d	<i>g</i>	<i>g</i>			96
	β	solution coating	50% ^d	-22	11		550–700	96
	ϵ	solution coating	50% ^d	-11	17	15 at 770 nm	550 to >800	96
MgPc	aggregated	solution coating	30% ^f	-80		30 at 810 nm	550 to >800	124
VOPc	phase II	solution coating	30% ^f	-30		4.1 at 810 nm	550 to >800	124
AlClPc	aggregated	solution coating	30% ^f	-55		10.0 at 810 nm	550 to >800	124
AlClPcCl	aggregated	evaporation	100%			~3 ^h at 800 nm	550 to >800	119
InClPc	aggregated	solution coating	30% ^f	-60	16	8.0 at 810 nm	550 to >800	125
TiOPc	aggregated	evaporation	100%	-45	4.5	2.6 at 810 nm	550 to >800	122
	α	solution coating	50% ^d	-65		2.6 at 790 nm	550 to >800	110
	β	solution coating	50% ^d	-45		3.6 at 790 nm	550 to >800	110
	γ	solution coating	50% ^d	-54		1.8 at 790 nm	550 to >800	110
	m	solution coating	50% ^d	-60		2.4 at 790 nm	550 to >800	110
	amorphous	solution coating	50% ^d	-58		1.9 at 790 nm	550 to >800	110
	Y	solution coating	50% ^d	-13		0.75 at 800 nm	550 to >800	112
	A	solution coating	50% ^d	-32		2.5 at 800 nm	550 to >800	112
	B	solution coating	50% ^d	-85		1.6 at 800 nm	550 to >800	112

^a All data were obtained from bilayer devices of very similar device geometry. ^b These are white light exposure (400–700 nm). ^c Estimated from the absorption spectra. ^d CGL binder: poly(vinyl butyral). ^e The $E_{0.5}$ values for the α , β , τ_1 , and τ_2 forms were determined to be 5.99, 9.13, 0.90, and 0.77 lux s under white light exposure. ^f CGL binder: PE200, a commercial polyester from Goodyear Chemicals. ^g The charge acceptance of the device was too low for any meaningful measurements. ^h Estimated from ref 119.

cyanines in the literature. In addition, a number of phthalocyanines, such as Ge(OH)₂Pc,¹²⁶ Si(OH)₂Pc,¹²⁶ InBrPc,¹²⁷ etc., have also been disclosed in the patent literature to have a similar sensitivity range. It is

obvious that, because of the polymorphic behavior, comparison of the photoconductivity between different phthalocyanines is difficult. This is especially so because some of the data are generated in different

laboratories where the fabrication conditions, device geometry, and evaluation procedures are often different.

The data in Table II indicate that both dark decay and photosensitivity vary over a wide range. Since there is evidence that impurities primarily increase the dark decay of phthalocyanines in devices,^{74,75} we can focus the discussion here on factors that influence the photosensitivity. Probable factors that affect the sensitivity are fabrication effect, photogeneration efficiency, injection efficiency of the photogenerated holes to the CTL, and the mobility of the holes in the CTL. Since most of the data given in Table II have been optimized with respect to the latter two parameters, they should not contribute significantly to the sensitivity variation. On the other hand, even though phthalocyanine is pigmentary, device fabrication and photogeneration efficiency are closely tied together because fabrication can induce polymorphic changes. The molecular stacking arrangement of phthalocyanine molecules in the microcrystals, which influences the photosensitivity, varies as a result (section IV). In any event, the data in Table II suggests that the different polymorphs of TiOPc are more sensitive than H₂Pc and many other phthalocyanines. On the basis of the red-shift in the solid-state absorption spectra of these polymorphs relative to the solution absorption spectrum of TiOPc,¹¹⁰⁻¹¹⁴ one can safely conclude that TiOPc molecules are adapting into an arrangement in the solid state such that extensive intermolecular charge-transfer interactions occur. What is uncertain is the overall contribution of this stacking arrangement to the high sensitivity. Theoretical calculations and molecular simulations of the effect of the stacking arrangement on the electronic properties of TiOPc are warranted. With the recent advent in scanning tunneling microscopy and atomic force microscopy, the structures of some of these interesting TiOPc polymorphs may soon be accessible. The origin for the high sensitivity of Y-TiOPc will then be comprehensible.

Fujimaki and co-workers^{112,113} reported that the xerographic gain of a device incorporating Y-TiOPc is 90% under a xerographic field of ~ 30 V/ μ m. This implies that the quantum yield of photogeneration for Y-TiOPc must be $\geq 90\%$. From the $E_{0.5}$ values in Table II, one can estimate that the xerographic gains for most phthalocyanines are 10–90%. This is significantly higher than the values reported for similar phthalocyanines in photoelectrochemical devices, from which power energy conversion efficiencies of less than a couple of percent are obtained.^{14,22,129-133} The higher gains obtained in xerographic devices are ascribable to the design of the xerographic device, which minimizes e-h pair recombination by the uses of high electric field across the device and hole-transporting molecules in the CTL. The function of the latter is to remove the photogenerated holes out of the recombination range.

A typical spectral response curve for a xerographic device incorporating a photoconductive phthalocyanine is given in Figure 10. The data show that the phthalocyanine device exhibits flat and high photoresponses from 600 to 850 nm. The sensitivity between 450–550 nm is rather poor due to the lack of optical absorption, indicating that phthalocyanines are not suitable for copier applications. On the other hand, the spectral range matches well to the diode laser wavelengths (750–

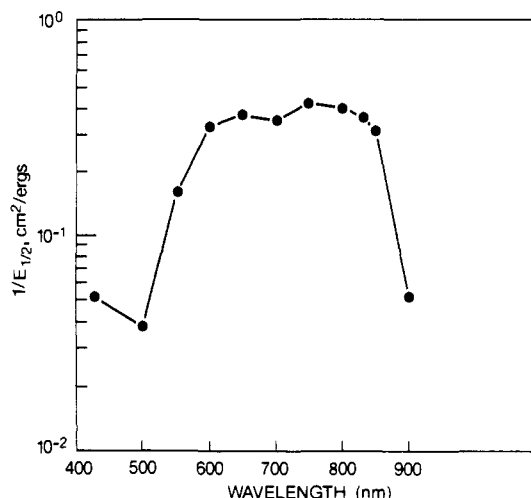
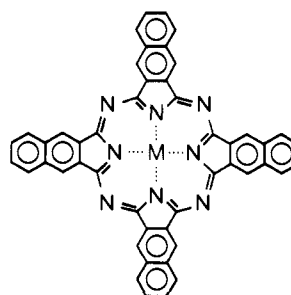


Figure 10. Spectral response curve of an InClPc bilayer photoreceptor device. Reprinted from ref 122. Copyright 1987 The Society for Imaging Science and Technology.

850 nm). Thus phthalocyanines are primarily developed as IR photoconductors for diode laser printers.

5. Naphthalocyanines

Probably out of scientific curiosity, naphthalocyanines were synthesized by reacting either 1,2-dicyanonaphthalene or 2,3-dicyanonaphthalene with a metal salt.¹³⁴ The synthesis is very similar to that of phthalocyanine. While the naphthalocyanine isolated from 1,2-dicyanonaphthalene may consist of a mixture of geometrical isomers, a pure naphthalocyanine compound can be isolated from the 2,3-dicyanonaphthalene synthesis (structure I).



Naphthalocyanines are metallic green powders in the solid state. Due to the extended conjugation, the solution λ_{\max} of naphthalocyanines are at 750–850 nm, red-shifted by ~ 100 nm relative to those of phthalocyanines.¹³⁵ The optical absorption is compatible with the diode laser wavelengths and has prompted the investigation of these materials for diode laser printer applications.¹³⁶⁻¹³⁸ However, the low yield of the naphthalocyanine synthesis, coupled with the success of phthalocyanines as IR photoconductors, make naphthalocyanines unlikely candidates for further development.

B. Squaraines

Condensation of squaric acid with a *N,N*-dimethylaniline derivative in an azeotropic solvent at reflux results in a 1,3-disubstituted product, an intensely absorbing colorant.¹³⁹ Because of the unique electronic

Table III. Synthesis and Absorption Spectral Data of Squaraines

D — A — D

squaraine	substituents	% yield (procedure)	λ_{\max}^a (log ϵ) ^b	ref (synthesis, absorption)
Sq-1	R ₁ = R ₂ = CH ₃ , X = H	40–60 (acid route) 45 ± 3 (ester route)	627.0 (5.49)	154, 156
Sq-2	R ₁ = R ₂ = C ₂ H ₅ , X = H	6 (acid route) 6.7 (ester route)	634.1 (5.51)	154, 156
Sq-3	R ₁ = R ₂ = C ₃ H ₇ , X = H	9 (acid route)	638.8 (5.53)	146, 156
Sq-4	R ₁ = R ₂ = C ₄ H ₉ , X = H	7.4 (acid route)	640.0 (5.53)	146, 156
Sq-5	R ₁ = R ₂ = CH ₃ , X = OH	~95 (acid route) 85 (ester route)	635.9 (5.52)	146, 156
Sq-6	R ₁ = R ₂ = C ₂ H ₅ , X = OH	~95 (acid route) 90 (ester route)	641.1 (5.57)	146, 156
Sq-7	R ₁ = R ₂ = C ₄ H ₉ , X = OH	~90 (acid route)	648.2 (5.56)	156
Sq-8	R ₁ = R ₂ = CH ₃ , X = F	23 (acid route) 19 (ester route)	630.0 (5.09)	154, 156
Sq-9	R ₁ = R ₂ = CH ₃ , X = CH ₃	30 (acid route) 56 ± 2 (ester route)	643.5 (5.42)	154, 156
Sq-10	R ₁ = R ₂ = CH ₃ , X = C ₂ H ₅	24 (acid route) 8.3 (ester route)	643.0 (5.40)	154, 156
Sq-11	R ₁ = R ₂ = CH ₃ , X = OCH ₃	9.5 (acid route) 8.1 (ester route)	631.8 (5.40)	154, 156
Sq-12	R ₁ = CH ₃ , R ₂ = CH ₂ C ₆ H ₅ , X = H	63 (acid route) ^c	628.2 (5.56)	147
Sq-13	R ₁ = CH ₃ , R ₂ = CH ₂ C ₆ H ₄ Cl, X = H	63 (acid route) ^c	626.4 (5.55)	147
Sq-14	R ₁ = CH ₃ , R ₂ = CH ₂ C ₆ H ₅ , X = F	29 (acid route) ^c	632.6 (5.50)	147
Sq-15	R ₁ = CH ₃ , R ₂ = CH ₂ C ₆ H ₄ F, X = F	28 (acid route) ^c	630.9 (5.49)	147
Sq-16	R ₁ = CH ₃ , R ₂ = CH ₂ C ₆ H ₄ Cl, X = F	29 (acid route) ^c	630.6 (5.30)	147
Sq-17	D =	77–85 (acid route)	660 ^d	157
Sq-18	D =	17 (acid route)		158
Sq-19	D =	81 (acid route)		159
Sq-20	D =	34 (acid route)	638.4 ^d (5.46)	160
Sq-21	D =	~60 (acid route)	661.0 (5.53)	156
Sq-22	D =	95 (acid route)	668 ^d (5.48)	161

^a Unless specified, absorption spectra were recorded in methylene chloride, λ_{\max} in nm. ^b Molar extinction coefficient, in cm⁻¹ M⁻¹. ^c The azeotropic solvent used in these syntheses was 1-heptanol under reduced pressure. ^d In chloroform.

structure, the nomenclature of this class of compounds had not been systematic; they have been named as cyclotrimethine dyes,¹⁴⁰ substituted 3-oxo-1-cyclobutenolates,¹³⁹ cyclobutenediylum dyes,¹⁴¹ cyclobutenediyl dyes,¹⁴² squarylium dyes,¹⁴³ etc. In 1981, Schmidt proposed the name squaraine for them.¹⁴⁴ We find the Schmidt nomenclature system very systematic and compounds of a variety of substitution, either at the nitrogen or in the phenyl ring can be named unambiguously. (See Table III for structures.)

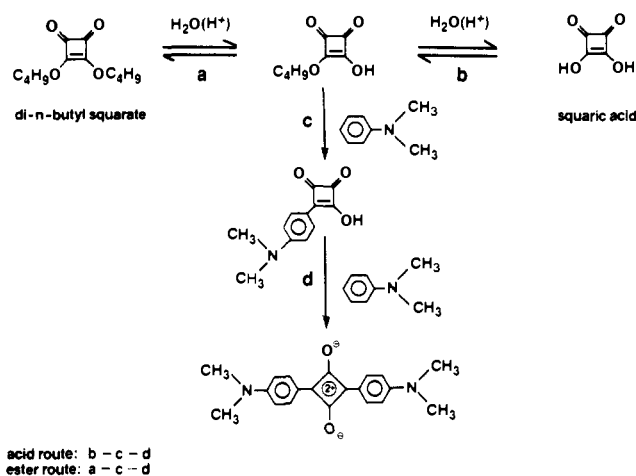
Squaraines were initially used as sensitizers for ZnO photoconductors.¹⁴⁵ The photoconductivity of squaraines was first recognized in 1974, when Champ and Shattuck demonstrated that squaraines could photogenerate e-h pairs in bilayer xerographic devices.¹⁴³ Early work on squaraines has been focused on

solar energy conversion.^{15–21} As it turns out, squaraines exhibit intense absorption in the near-IR (700–850 nm) in the solid state. The absorption matches well to the diode lasers and stimulated a rapid development of squaraines in the 1980s.⁴⁸

1. Synthesis and Structural Variation

Traditionally, squaraines are synthesized by condensing 1 equiv of squaric acid and 2 equiv of *N,N*-dialkylaniline in an azeotropic solvent.¹⁴¹ Water is the byproduct of the synthesis and is removed azeotropically. Since the synthesis starts with squaric acid, we shall refer to it as an acid route (Scheme II). The acid route synthesis is simple and versatile. Structural variation can simply be achieved by using different aniline precursors.^{139–141,146–151} Squaraines synthesized

Scheme II



by this procedure are, however, often found to exhibit high dark decay and low charge accepting properties in xerographic devices.^{152,153} An additional purification procedure to improve the xerographic properties is needed and has yet to be developed. Structural modification of squaraines improves their solubility in organic solvents, enabling them to be purified by conventional techniques; substitution, however, perturbs the solid-state properties of squaraine and results in a decrease in photoconductivity.¹⁴⁷ Law and Bailey reported that squaraines could also be synthesized from dialkyl squarate and *N,N*-dimethylaniline derivatives (ester route, Scheme II).¹⁵⁴ Although the synthetic efficiency and scope of this new route are similar to the acid route, xerographic measurements showed that squaraines synthesized by this procedure consistently exhibit better xerographic properties, namely lower dark decay and higher charge acceptances.¹⁵⁵ It was concluded from a mechanistic study that, due to the change in reaction condition, the microcrystalline squaraine products from the ester route are smaller in particle size and have a different crystallographic orientation. This morphological change results in "purer" squaraine samples and improvements in xerographic properties. The synthetic data of the squaraines synthesized from these two routes are summarized in Table III.

2. Optical Absorption

In solution, squaraines exhibit sharp and intense visible absorption at 620–670 nm, depending on the substituent in the phenyl ring or at the nitrogen.¹⁵⁶ Their extinction coefficients are very high, $\geq 10^5 \text{ cm}^{-1} \text{ M}^{-1}$. The solution absorption data are also given in Table III. The electronic structures of both the S_0 and S_1 states of **Sq-1** have been studied theoretically by Bigelow and Freund.¹⁶² These authors showed that both S_0 and S_1 states are intramolecular donor-acceptor-donor charge-transfer (D-A-D CT) states. The anilino moieties and the oxygen atoms are electron donors and the central four-membered ring is an electron acceptor. They further showed that there is a charge-transfer during the $S_0 \rightarrow S_1$ electronic excitation, but the CT is primarily confined in the central C_4O_2 unit ($\sim 80\%$). It is believed that this localization of electronic transition has resulted in the narrow absorption band (half bandwidth $\sim 750 \text{ cm}^{-1}$) observed in these compounds.

In agreement with the CT character, electron-releasing groups, either at the nitrogen or in the phenyl ring, induce bathochromic shifts on the λ_{max} . It is, however, important to point out that the bathochromic effect is relatively small as compared to other polar molecules having intramolecular CT states. The small substituent effect is consistent with the electronic structure calculated by Bigelow and Freund, merely confirming that the structural variation in the anilino moiety has only a minor influence on the central C_4O_2 unit of squaraine.

3. Solid-State Properties

Squaraines exist as microcrystalline powders in the solid state. Highly photoconductive squaraines, such as **Sq-1**, -5, and -8-11 are pigmentary. Their solid-state properties can be characterized by solid-state absorption spectroscopy and X-ray powder diffraction technique.¹⁶³ The solid-state absorption spectrum of **Sq-1** is broad and panchromatic, consisting of two bands, one at longer wavelengths and the other at shorter wavelengths relative to the monomeric absorption (Figure 11a). In the X-ray powder pattern, three diffraction lines at $2\theta \sim 11.5^\circ$, 14.5° , and 26° are observed (Figure 11a). The solid-state absorption spectra and X-ray powder diffraction patterns of **Sq-5** and -8-11, which are also given in Figure 11b-f, are found to be similar to those exhibited by **Sq-1**. The similarity not only suggests that the solid-state properties of these squaraines are similar, but also that the C-2 substituent in the phenyl ring has very little effect on the intermolecular CT interaction.¹⁵⁵

In 1982, Wingard¹⁶⁴ reported a crystal structure of **Sq-9**. He showed that there exist extensive intermolecular interactions between the anilino moiety and the central C_4O_2 unit of squaraine and that the interplanar distance is $\sim 3.5 \text{ \AA}$. He also proposed that the broad absorption observed in the solid state is a direct consequence of the intermolecular charge-transfer interaction. A similar conclusion was also reached by Tristani-Kendra and Eckhardt in their study of the structure and the solid-state absorption of **Sq-6**.¹⁶⁵ Because of the similarity of solid-state properties among **Sq-1**, -5, and -8-11, we believe that these squaraines form similar aggregates in the solid state. A schematic of the intermolecular D-A interaction is given in Figure 12a.

N-Alkyl and *N*-benzyl substituents disturb the intermolecular CT interaction between the squaraine chromophores due to the steric effect. The splittings between the two absorption bands in the solid state become smaller and sometimes the absorption appears just as a broad band centered around the monomeric solution absorption. The conclusion from absorption spectral data are supported by the X-ray powder diffraction patterns of *N*-alkyl- and *N*-benzylsquaraines, which are found to be different from those of **Sq-1**.¹⁶³

Recently, squaraines bearing *N*-pyrrolidino rings (**Sq-19** and -20) have been synthesized.^{159,160} Unlike *N*-alkyl- or *N*-benzylsquaraines, these squaraines are photoconductive and exhibit solid-state properties resembling that of **Sq-1**.¹⁶⁰ This observation suggests that *N*-pyrrolidino substitution is unique. The attainment of minimal perturbation to the solid-state properties is probably due to the small size and the rigidized *N*-pyrrolidino ring structure.

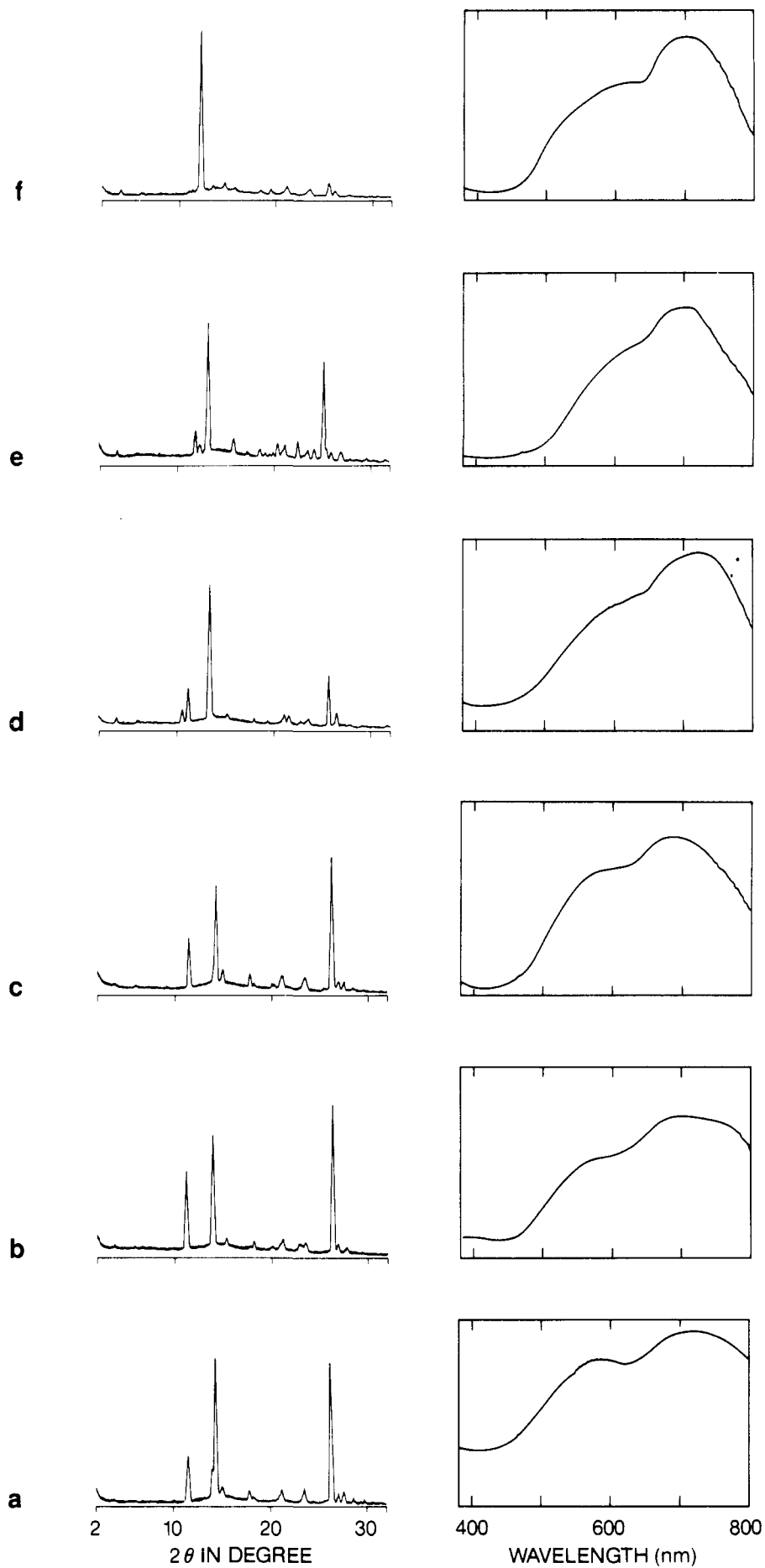


Figure 11. Solid-state absorption spectra and X-ray powder diffraction patterns of (a) Sq-1, (b) Sq-5, (c) Sq-8, (d) Sq-9, (e) Sq-10, and (f) Sq-11.

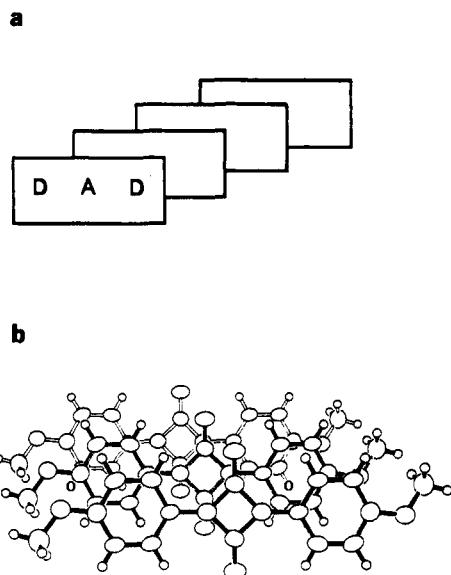


Figure 12. (a) A schematic of the intermolecular interaction of **Sq-1** in the solid state; (b) the stacking arrangement of **Sq-23** in the solid state.

In addition to the D–A interaction between the anilino moiety and the central C_2O_4 unit of squaraine, a different kind of intermolecular interaction has also been observed in a special case, the solid state of bis-(4-methoxyphenyl)squaraine (**Sq-23**, D = $p\text{-CH}_3\text{O-C}_6\text{H}_4\text{-}$). Single-crystal structural analysis of **Sq-23** revealed that the interplanar distance is ~ 3.5 Å, however, the major intermolecular interaction is from the polarized C–O dipoles, through a staircase arrangement (Figure 12b).¹⁶⁶ The change in molecular stacking (from **Sq-1**) is presumably due to the decrease in polarization of the π -electron in **Sq-23**. While intermolecular D–A interactions are expected to dominate in the solid state of most squaraines, dipolar C–O interactions do exist and have been observed in Langmuir–Blodgett films fabricated from surfactant squaraines.¹⁶⁷

4. Photoconductivity

The photoconductivities of most squaraines have been examined in bilayer xerographic devices. The data are summarized in Table IV. Although these data were obtained from devices of similar configuration, quantitative comparisons are difficult, especially between results obtained in different laboratories. The data show that the dark decay values vary from -10 to -115 V/s. Since impurities in squaraines are primarily responsible for the high dark decay,¹⁴⁷ the variation seen in Table IV indicates that there is a variation of “purity” among the squaraine samples even though they are supposed to be chemically “pure”.

Structural variation of squaraines has a large effect on the photosensitivity. $E_{0.5}$ values ranging from 2.9 to >1000 ergs/cm² are reported. Known factors that may contribute to this sensitivity variation are impurities, particle size, morphology (crystallinity and aggregated form), and fabrication effect. Since the photosensitivity was obtained from bilayer devices, the efficiency of hole injection from CGL to CTL could be critically important also. Impurities are known to affect the dark decay primarily,¹⁴⁷ and the variation of particle size is expected to be small, at least between the Xerox laboratories.

Table IV. Xerographic Data of Squaraines

squaraine	xerographic data		ref
	dark decay (V/s)	$E_{0.5}$ at 600, 800 nm (ergs/cm ²)	
Sq-1	-95	3.7, 4.5	155
Sq-2	-10	insensitive ^a	163
Sq-4	-10	insensitive ^a	163
Sq-5	-100	5.6, 6.3	155
Sq-6	-35	314, 350	163
Sq-7		insensitive ^a	163
Sq-8	-60	3.8, 2.9	155
Sq-9	-30	11.7, 13.6	155
Sq-10	-10	insensitive ^a	163
Sq-11	-80	insensitive ^a	163
Sq-12	-35	38.2, 44	147
Sq-13	-95	10.9, 8.1	147
Sq-14	-105	16.8, 13.6	147
Sq-15	-75	10.2, 8.2	147
Sq-16	-115	5.9, 5.9	147
Sq-17	-15	(10.0 at 830 nm)	124
Sq-18	-35	(5.5 at 830 nm)	124
Sq-19	-26	(4.2 at 820 nm)	159
Sq-20	-70	3.9, 4.6	160
Sq-21		insensitive ^a	163
Sq-22	-15	(50 at 830 nm)	124

^a Insensitive defined as $E_{0.5} > 1000$ ergs/cm².

Thus major contributors to the observed sensitivity variation are (1) the morphology of the squaraine particles in the CGL, (2) fabrication effects, and (3) hole injection from CGL to CTL. A negative effect generated by any of them is expected to lower the photosensitivity of the device.

Data for the xerographic sensitivities of **Sq-1**, **-5**, and **-8–11** are available from one laboratory.¹⁶³ These squaraines are pigmentary and have shown to have similar solid-state properties (Figure 11a–f). Thus, any negative effects resulting from device fabrication and morphology should be minimal. The most likely candidate for the sensitivity variation is the difference in hole-injection efficiency. This is indeed the case. Law et al.¹⁶³ reported the redox potentials of a series of squaraines and the use of the oxidation potentials to estimate the energy levels of the HOMOs of squaraines in devices. In the case of **Sq-1**, **-5**, and **-8–11**, the photosensitivity was found to decrease as the energy level of the HOMO increases. The data indicate that the sensitivity loss is the result of the decrease in hole-injection efficiency, which becomes increasingly inefficient as the injection process becomes less favorable thermodynamically. Additional credence to the importance of hole-injection efficiency on the photosensitivity comes from the xerographic data of **Sq-17** and **-18**. Since the substituent effect on the oxidation potential is additive,¹⁶³ it is then predicted, on the basis of the electrochemical data, that **Sq-17** and **-18** should be less sensitive than **Sq-5** and **-8**, respectively, but that they should be more sensitive than **Sq-9**. The data in Table IV agree with this prediction, reassuring the crucial role of hole injection on the photosensitivity. Further discussion on the effect of the energetics of the CGL and CTL on the sensitivity is given in section IV.D.1.

Due to the *N*-alkyl groups, *N*-alkylsquaraines **Sq-2–4**, **-6**, **-7**, **-21**, and **-22** show enhanced solubility in organic solvents and their aggregations in the solid state are perturbed from the photoconductive aggregated form. The photosensitivities of these compounds are

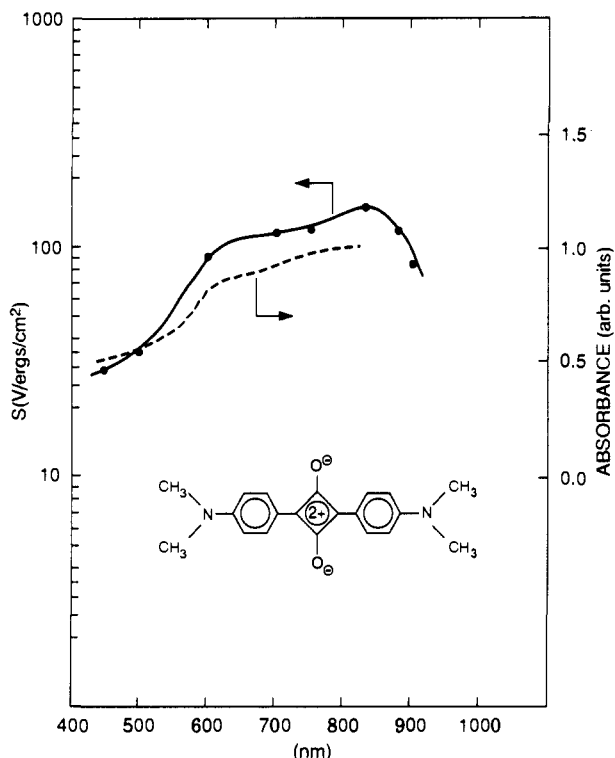


Figure 13. Spectral response curve and absorption spectrum of **Sq-1** in a bilayer photoreceptor device. Reprinted from ref 175. Copyright 1992 The American Chemical Society.

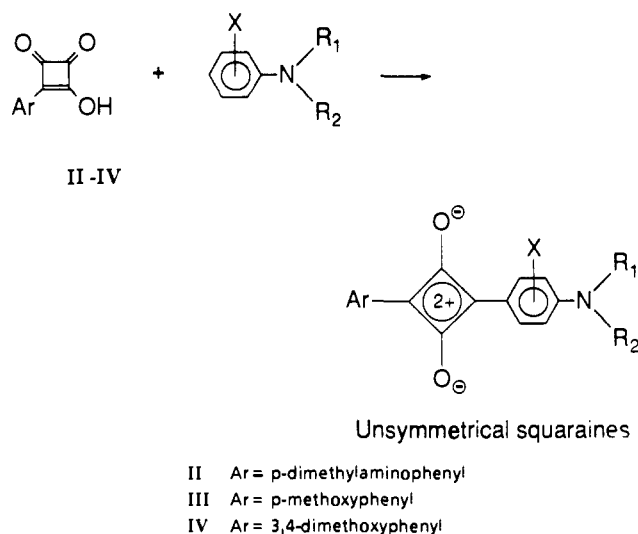
low ($E_{0.5} > 50$ ergs/cm²) and are attributable to the combination of fabrication and morphological effects. In contrast, *N*-benzyl substitution exerts only a relatively minor effect on the solubility of squaraine. Their oxidation potentials are high relative to **Sq-1** due to the electron-withdrawing *N*-benzyl group. Despite these positive attributes, the photosensitivities of *N*-benzylsquaraines vary from comparable to **Sq-1** to low sensitivity. The observation is attributable to be an aggregational effect, because it was shown, by solid-state absorption spectra and X-ray powder diffraction patterns, that the aggregations in these compounds are different from that of **Sq-1**.¹⁶³ The difference is presumably induced by the *N*-benzyl substitution.

N-Pyrrolidino-substituted squaraines are exceptions. The *N*-pyrrolidino group seems to have very little effect on either the solubility or the aggregation. As a result, **Sq-19**¹⁵⁹ and **20**¹⁶⁰ are highly sensitive. The attainment of minimal perturbation on the solution and solid-state properties of these materials is, again, attributable to the small size and the rigidized *N*-pyrrolidino ring structure.

The spectral responses of squaraines parallel their solid-state absorption spectra. A typical spectral response curve of **Sq-1**, along with its absorption in the CGL, is given in Figure 13. The photosensitivity is flat from 600 to 850 nm, making it an ideal candidate for diode laser printer applications. The photosensitivity, however, decreases at wavelengths < 600 nm, suggesting that squaraines are not suitable for use in copiers, where a flat response from 450 to 650 nm is essential.

As in the case of phthalocyanines, one can crudely estimate the xerographic gains from the $E_{0.5}$ values of the squaraine devices in Table IV. The gains are ranging from 5–50% for **Sq-1**, -5, and -8–11 and are significantly higher than the power conversion efficiencies of similar

Scheme III



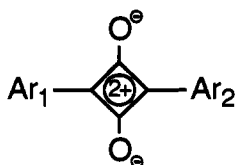
materials in photovoltaic devices, which are < 1%.¹⁵ Again, the uses of high electric field and hole-transporting molecules to inhibit the e–h recombination in xerographic devices are contributing to the high gains.

5. Unsymmetrical Squaraines

Early work by Chang and co-workers^{162,163} revealed that squaraines exhibit high dark decay and low charge acceptance in photoreceptor devices. This observation was confirmed by Law and Bailey.¹⁶⁵ In addition, the synthetic yields for highly sensitive squaraines, such as **Sq-1** and -8 are low. In an attempt to circumvent the yield–performance dilemma, Yanus,¹⁶⁸ Kazmaier et al.,¹⁶⁹ and Law et al.¹⁷⁰ reported the syntheses and the use of mixed squaraine compositions in xerographic devices. These mixtures were synthesized by reacting either squaric acid or dibutyl squarate with a mixture of *N,N*-dimethylaniline derivatives. The mixtures are found to exhibit very similar solution and solid-state properties when compared to **Sq-1**. Structural analyses indicated that each mixture consists of two symmetrical squaraines and one unsymmetrical squaraine. The observation of favorable photoconductive properties from these compositions was an initial surprise because it is generally believed that high chemical purity is a prerequisite for the high sensitivity. The observation not only suggests that mixture of squaraines can cocrystallize to form photoconductive aggregates, it also expands the design space for new squaraines, since it suggests that the asymmetry in the squaraine structure has no adverse effect on the photoconductivity.

In 1988, Kazmaier et al.¹⁷¹ disclosed the synthesis of a number of unsymmetrical squaraines by condensing 1-[*p*-(dimethylamino)phenyl]-2-hydroxycyclobutene-3,4-dione (II) with *N,N*-dimethylaniline derivatives (Scheme III). The precursor for the synthesis was synthesized either via the acid dichloride of squaric acid or diethyl squarate. Several unsymmetrical squaraines were prepared, but no detailed structural characterization data were provided.

A more ambitious synthetic scheme for unsymmetrical squaraines was pursued by Law and Bailey.¹⁷² In this case, the precursor (II) was synthesized by a [2 + 2] cycloaddition reaction between *p*-nitrophenyl ketene and tetraethoxyethylene, followed by a hydrolysis

Table V. Synthesis and Optical Properties of Unsymmetrical Squaraines

squaraine	Ar ₁	Ar ₂	% yield	λ_{\max}^a (log ϵ) ^b	ref
USq-1			52	621.6 (5.30)	172
USq-2			22	632.5 (5.30)	172
USq-3			33	627.3 (5.07)	172
USq-4			3.8	625.0 (5.03)	172
USq-5			67	578.8 (5.37)	173
USq-6			86	563.6 (5.20)	173
USq-7			73	583.5 (5.32)	173
USq-8			32	581.1 (5.40)	173
USq-9			43	583.6 (5.23)	173
USq-10			77	587.0 (5.34)	173
USq-11			87	572.1 (5.20)	173
USq-12			83	592.4 (5.35)	173
USq-13			59	590.4 (5.32)	173

^a Absorption maximum, in nm, in chloroform. ^b Molar extinction coefficient, in $\text{cm}^{-1} \text{M}^{-1}$.

reaction and a reductive-alkylation reaction. The entire squaraine synthesis was accomplished without using squaric acid, an expensive reactant. The yields and the optical properties of several unsymmetrical squaraines, USq-1-4, are tabulated in Table V. These unsymmetrical squaraines not only exhibit similar solution and solid-state properties as compared to their symmetrical photoconductive analogs, their photoconductivities are very similar as well. The benefit of having an unsymmetrical squaraine with better photoconductivity has not materialized, so far.

In an attempt to overcome all the technology shortfalls of squaraines, specifically low synthetic yield, high dark decay, and poor photoresponse at wavelengths < 600 nm, etc., Law and Bailey reported the synthesis of a new class of unsymmetrical squaraines, by substituting one of the aniline rings in squaraine with an anisole ring.¹⁷³ The precursors for the synthesis, III and IV (structures in Scheme III), were synthesized by a [2 + 2] cycloaddition reaction between *p*-methoxyphenyl ketene, or 3,4-dimethoxyphenyl ketene with tetraethoxyethylene, followed by a hydrolysis reaction. Unsymmetrical squaraines can then be prepared by condensing III or IV with an aniline derivative. The goal of synthesizing squaraines without using squaric acid is accomplished. The synthetic and absorption spectral data of these unsymmetrical squaraines (USq-5-13) are given in Table V as well. The solid state properties of USq-5-13 have been studied by solid-state absorption spectroscopy and X-ray powder diffraction.¹⁷⁴ The data indicate that these unsymmetrical squaraines form photoconductive aggregates similar to that of Sq-1. Law concluded that the unsymmetrical structure has very little effect on the solid-state properties, and he attributed the observation to the similarity in molecular size and electronic properties between the aniline ring and the anisole ring. It is important to point out that, due to the substitution of the aniline ring by a weaker electron donor, the solution λ_{\max} of USq-5-13 are blue-shifted relative to squaraines having two aniline rings. The solid-state absorption spectral data show that there is an increase in absorption at 450 to 600 nm as the result of the solution blue-shifts.¹⁷⁴ This change in optical absorption has led to a panchromatic visible photoresponse for xerographic devices incorporating USq-5-13.¹⁷⁵

The photoconductivity of USq-5-13 have been studied in bilayer xerographic devices.¹⁷⁴ Although fabrication effect, purity, and hole-injection efficiency have been shown to be important factors that influence the photoconductivity of USq-5-13. USq-13 was identified as the most outstanding squaraine so far. Specifically, USq-13 is shown to have a low dark-decay value (-15 V/s) and high sensitivity in xerographic devices, where $E_{0.5}$ values of 3.1 and 1.9 ergs/cm² at 600 and 790 nm, respectively, are reported.¹⁷⁵ The sensitivity appears to surpass all squaraines reported in the literature (Table IV). In fact, the sensitivity performance of USq-13 compares favorably to one of the best IR photoconductors, namely the Y-TiOPc recently reported by Fujimaki and co-workers.¹¹²

The spectral response curve of USq-13 is depicted in Figure 14, along with its absorption in the CGL. The data indicate that the spectral response of USq-13 parallels its absorption. The response is flat from 450-650 nm in the visible region and has a peak sensitivity at 790 nm. By comparison with the spectral response of Sq-1 (Figure 13), an improvement in spectral response in the visible region, at 450-600 nm, is evident. Law¹⁷⁵ concluded from the sensitivity data and the spectral response curve that USq-13 would be useful not only in copiers, but also in diode laser printers and multifunctional printer-copiers. This makes USq-13 one of the most versatile photoconductors reported to date.

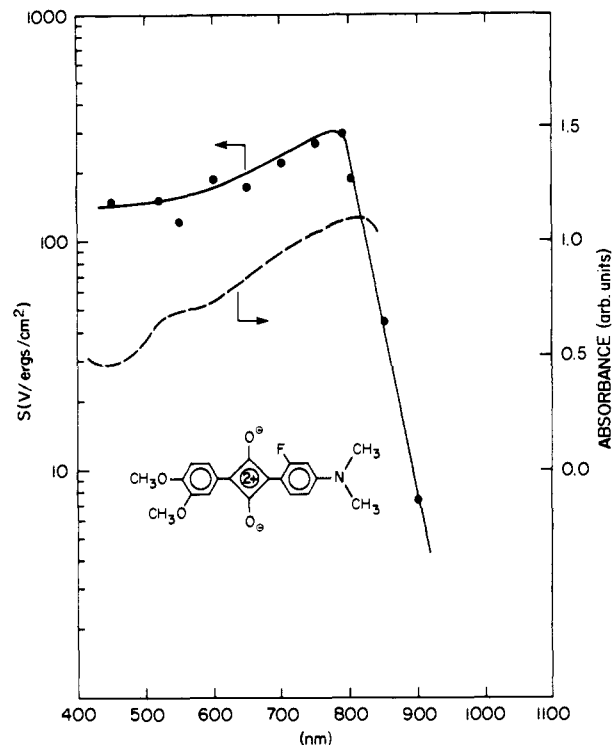
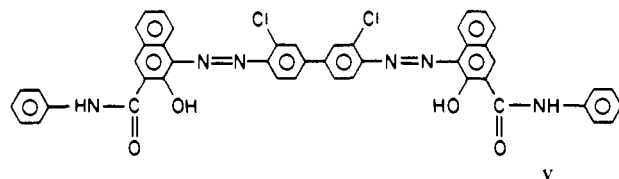


Figure 14. Spectral response curve and absorption spectrum of USq-13 in a bilayer photoreceptor device. Reprinted from ref 175. Copyright 1992 The American Chemical Society.

C. Azo Pigments

Azo dyes and pigments belong to a class of colorants which consist of azo chromophore ($-\text{N}=\text{N}-$) linking aromatic groups. The preparative procedures for azo compounds, by the classic azotization and coupling reaction, are relatively simple. This simplicity has enabled azo compounds to become the largest group of synthetic colorants to date. The photoconductive properties of azo compounds were reported as early as 1969 by Rau who observed photocurrents from thin layers of 1-(phenylazo)naphthol.¹⁷⁶ Several years later, Champ and Shattuck reported the use of bisazo pigment Chlorodiane Blue (V), 4,4'-[(3,3'-dichloro[1,1'-biphenyl]-4,4'-diyl)bis(azo)]bis[3-hydroxy-*N*-phenyl-2-naphthalenecarboxamide] as a photogenerating pigment in xerographic devices.¹⁷⁷ This earlier work coupled with the ease of the synthesis has led to a fierce research

effort in the photoreceptor industry, where uncounted thousands of azo pigments of a variety of structures have been synthesized and screened for xerographic photoreceptor applications.



1. Synthesis, Purification, and Structural Variation

A typical reaction scheme using the synthesis of bisazo pigments from 2,7-diaminofluorenone and substituted 2-hydroxy-3-naphthanilides (general structure VI) as an example is illustrated in Scheme IV.

The azotization and coupling reaction are normally carried out in an ice bath (0–5 °C). The coupling reaction is base catalyzed, and a variety of bases, e.g., NaOAc, NaOH, triethylamine, etc., can be used. The synthesis is very efficient (~90%). Most of the synthesized pigments, however, have to be purified prior to use as photoconductors. In general, purification is achieved by repetitive washings with water, DMF, and/or DMSO.^{178–181} The washing sequence, the number of washings, and the time and temperature of each washing are known to be critical to the photoelectrical properties. What is not clear at present is the role of these washings on the photoconductivity. Nonetheless, it has been reported that photoconductive azo pigments can undergo morphological changes in ketonic solvents at elevated temperatures.¹⁸²

As shown in Scheme IV, the design of new azo structures, by varying the structures of the aromatic amine and/or the coupler, is almost unlimited. A literature survey indicates that azo pigments from 2-naphthol couplers are consistently found to exhibit moderate to high photoconductivity. Examples of notable aromatic amines and major classes of couplers (VII–X) that have been studied are tabulated in Table VI. The pace of further innovation on new structures of aromatic amine and coupler continues. More recently, the synthesis of unsymmetrical azo pigments has been reported. The synthesis can be accomplished either by using an unsymmetrical amine precursor²⁰⁰

Scheme IV

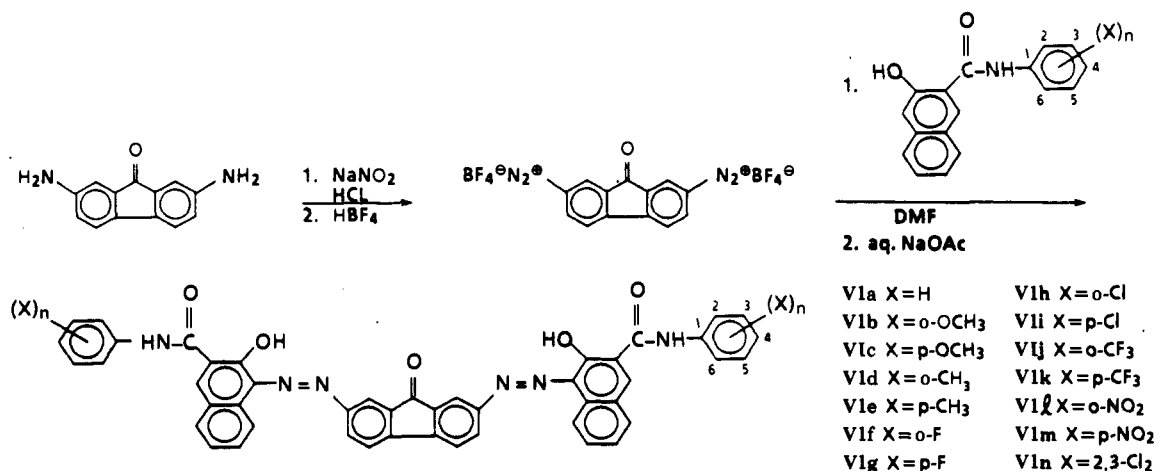
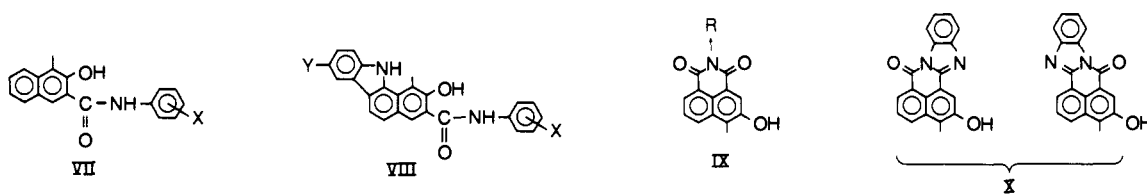


Table VI. Examples and Structures of Photoconductive Azo Pigments

no.	aromatic amine	type of couplers ^a	ref(s)
1	3,3'-dichlorobenzidine	VII	177
2	2,7-diaminofluorenone	VII, VIII	183, 184
3	2,6-diaminoanthraquinone	VII, VIII	185, 186
4	2,7-diaminoanthraquinone	VII, VIII	185, 186
5	3,6-diaminocarbazole	VII, VIII	184, 187
6	<i>N</i> -ethyl-3,6-diaminocarbazole	VII, VIII	187
7	2,7-diamino-9-xanthone	VII-IX	188
8	bis(<i>p</i> -aminophenyl)phenylamine	VII-IX	189
9	tris(<i>p</i> -aminophenyl)amine	VII, VIII	184, 190, 191
10	2,7-diaminodibenzothiophene sulfone	VII, VIII	183, 192
11	2,7-diaminodibenzothiophene	VII, VIII	192
12	2-(<i>p</i> -aminophenyl)-6-aminobenzoxazole	VII-IX	193, 194
13	bis(<i>p</i> -aminophenyl)amine	VII-X	195
14	<i>N</i> -methylbis(<i>p</i> -aminophenyl)amine	VIII	196
18	2,5-bis(<i>p</i> -aminophenyl)-1,3,4-oxadiazole	VII, IX, and X	180, 197
19	1,6-diaminopyrene	VII-IX	198
20	1,5-diaminonaphthalene	VII-IX	199

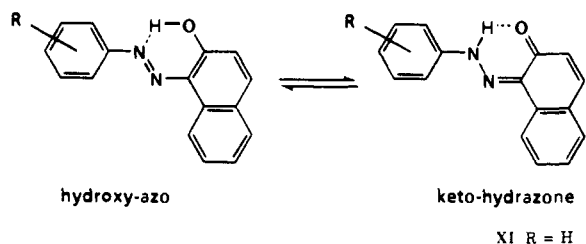
^a Couplers are as follows:



or a symmetrical amine precursor but coupling it sequentially with different couplers.^{201,202} There is evidence that the unsymmetrical structure may improve the photosensitivity of the pigment.²⁰²

2. Electronic Structure of Photoconductive Azo Pigments

The hydroxy-azo/keto-hydrazone tautomerism of 1-(phenylazo)-2-naphthol (XI) and its derivatives is well documented, both in solution and in the solid state.²⁰³⁻²⁰⁶



It has been calculated theoretically that the keto-hydrazone form is thermodynamically favored,²⁰⁷ and that electron-withdrawing functionality^{204,205} and H-bonding (both inter and intra)^{207,208} are key driving forces that shift the equilibrium in favor of the keto-hydrazone form. This conclusion is supported by X-ray analyses of several 1-(phenylazo)-2-naphthols bearing electron-withdrawing groups.^{209,210}

X-ray structural analysis was also reported for 1-(2',5'-dichlorophenylazo)-2-hydroxy-3-naphtho-2'',5''-dimethoxyanilide, and the data indicate that it has a keto-hydrazone structure in the solid state.²¹¹ Owing to the large molecular sizes and the pigmentary nature of most photoconductive azo pigments, single crystals of these compounds could not be grown for X-ray structural determination. Their electronic structures and their stacking arrangements in the solid state are not well-known.

Law et al.²¹² have recently studied the electronic structure of a number of photoconductive bisazo pigments by cross-polarization magic-angle spinning ¹³C NMR spectroscopy. The data, which are complemented by IR spectra data, indicate that photoconductive bisazo pigments from 2-hydroxy-3-naphthalenide derivatives (coupler type VII in Table VI) have a keto-hydrazone structure exclusively in the solid state. Both intra- and intermolecular H-bonding are cited to be contributors to the observation. Work has also been extended to trisazo and polyazo pigments that contain couplers of types VIII-X. Without exception, all photoconductive azo pigments have been found to exist as keto-hydrazones in solids.²¹³

3. Optical and Solid-State Properties

Photoconductive azo pigments are practically insoluble in common organic solvents. Their optical absorption can only be examined in the solid state (in KBr pellet or in a polymeric binder). The absorption spectrum of a bisazo pigment, 2,7-[(9-oxofluorene-2,7-diyl)bis(azo)]bis[2-hydroxy-3-naphthalenecarboxamide] (VIa), is given in Figure 15a. Further spectral data that probe the substituent effect on the absorption of bisazo pigments are depicted in Figure 15b-e. The data clearly show that substituent in the anilide ring of the coupler moiety has very little effect on the pigment absorption. Since the absorbing chromophore is the keto-hydrazone unit and it is known that substituent in the anilide ring has no effect on the hydroxy-azo/keto-hydrazone tautomerism,²¹² the lack of any substituent-induced spectral changes is reasonable. By the same token, the absorption wavelength is not expected to be sensitive to the structure of the aromatic amine or the number of azo linkages. This has indeed been observed.²¹⁴ Thus most of the photoconductive azo pigments are sensitive in the visible region (450-650 nm) primarily.

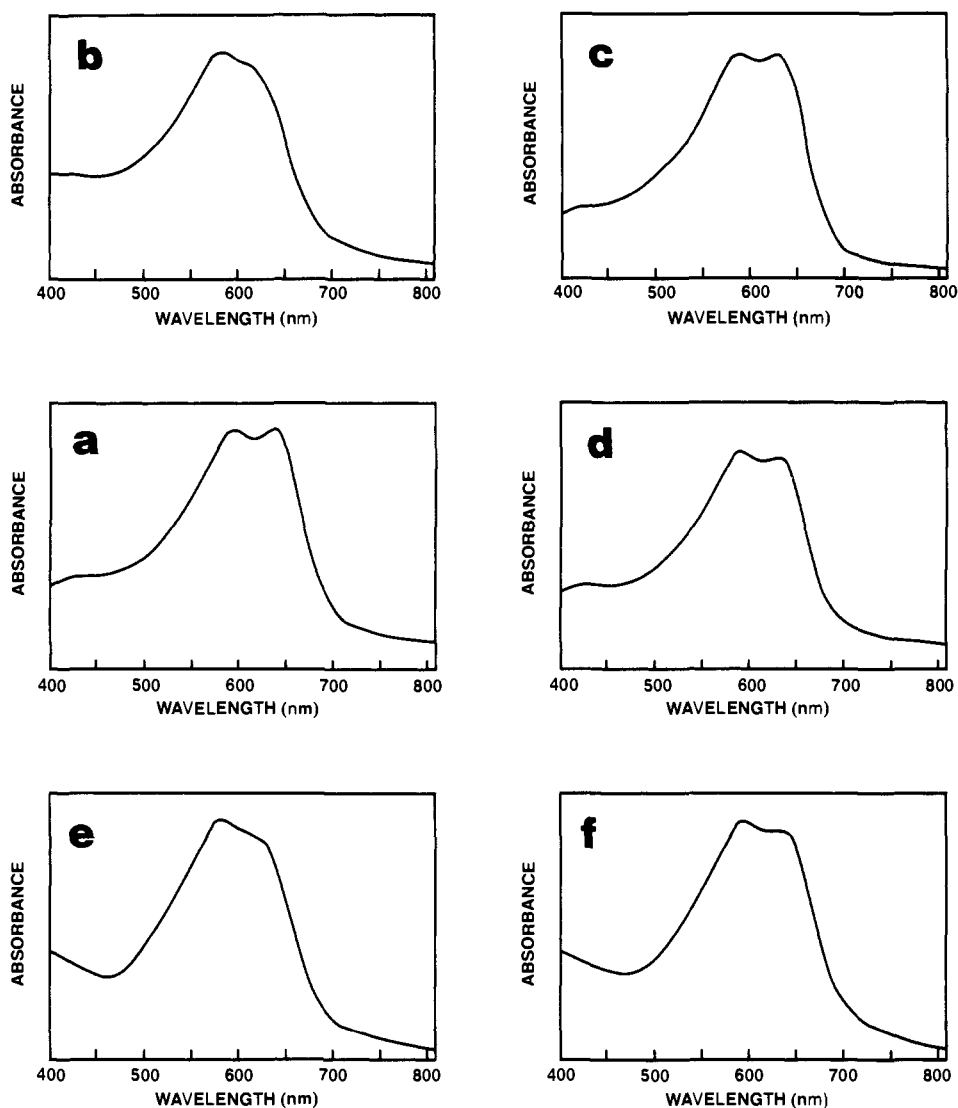


Figure 15. Solid-state absorption spectra of bisazo pigments (a) VIa, (b) VIb, (c) VIc, (d) VIj, (e) VII, and (f) VI m.

Extension of the conjugation of the keto-hydrazone unit through the use of coupler type VIII leads to a red-shift of the visible absorption. In fact, bisazo pigments from *N*-methylbis(*p*-aminophenyl)amine²¹⁵ and trisazo pigments from tris(*p*-aminophenyl)amine^{184,216,217} are known to absorb beyond 700 nm, and they have been shown to be sensitive at the diode laser wavelengths (780 nm).

Finally, azo pigments are generally found to be less crystalline than those of phthalocyanines and squaraines according to X-ray powder diffraction patterns.²¹⁸ One, however, cannot conclude that azo pigments are "amorphous" because broad and featureless patterns can also be obtained from materials that have very small crystallite sizes. The observation of high photoconductivity from azo pigments, which requires efficient exciton and carrier diffusions, implies that a certain degree of ordering must exist microscopically in these materials.

4. Photoconductivity

The number of azo pigments that have been disclosed in the patent literature are just too numerous to be tabulated here. Instead, a handful of known high performers and their xerographic data are given (Table VII). Both visible and visible-IR sensitive azo pigments

are known. The spectral response curves of representing pigments are given in Figures 16 and 17.

The data in Table VII show that the dark decay values of azo pigments are relatively low as compared to those of phthalocyanines and squaraines (Tables II and IV). The low dark decay is likely due to the lack of free carriers in bilayer devices incorporating azo pigments because charge carriers are only generated at the CGL/CTL interface and are neutralized in the photodischarge process (see Section IV.B.3). The high purity of these materials may also contribute to the low dark decay.

By comparing analogous sensitivity data in Tables II and IV, one can conclude that the photosensitivities of high-performance azo pigments are as high as the best in the phthalocyanine and squaraine series. Very little is known about the origin of the high sensitivity. Recent work by Hashimoto indicated that the photosensitivity may follow a Hammett relationship.¹⁸¹ Despite the insufficient understandings on the electronic structure, the photogeneration mechanism and the structure-photoconductivity relationship, the pace of developing new azo pigments is incredibly rapid. The technological advantages of azo pigments are (1) they are adaptable to low-cost solution-coating manufacturing technology, (2) they are highly sensitive, and (3) they have a wide spectral range, 450 to ≥ 800 nm. Additionally, the

Table VII. Structures and Xerographic Data of Photoconductive Azo Pigments

	structure	dark decay (V/s)	$E_{0.5}$ (ergs/cm ²)	spectral range, (nm)	ref
Visible Pigments					
V		-21	15.7 at 570 nm	450-650	214
VIh		~-1	~3 ^a at 600 nm	450-650	219
VIIn		-12	3.3 at 590 nm	450-650	214
		-13	2.4 at 600 nm		
XII		-11	6.0 at 560 nm	450-650	214
		-11	4.5 at 600 nm		
XIII				450-650	180
			~5 at 600 nm		
XIV			~2 ^b at 600 nm	450-650	202
Visible-IR Pigments					
XV		-25	3.6 at 790 nm	450 to ≥800	217
XVI		-2	10.2 at 780 nm	450 to ≥800	215

^a Estimated from the photodischarge curve in Figure 5 of ref 219. ^b Estimated from the spectral sensitivity curve in ref 202.

photoelectrical stability of azo pigments have been shown to be excellent.^{180,202,216}

D. Perylene Pigments

Perylene pigments are diimides and bis imidazoles of perylene-3,4,9,10-tetracarboxylic acid. Perylenes

have good light and water fastnesses and are best known for their use as colorants for automobile paints and plastics. The photoconductivity of perylenes was recognized as early as 1972 when Regensburger and Jakubowski studied the xerographic properties of a number of perylenes in bilayer devices.²²⁰ The motivation for the investigation was simply because

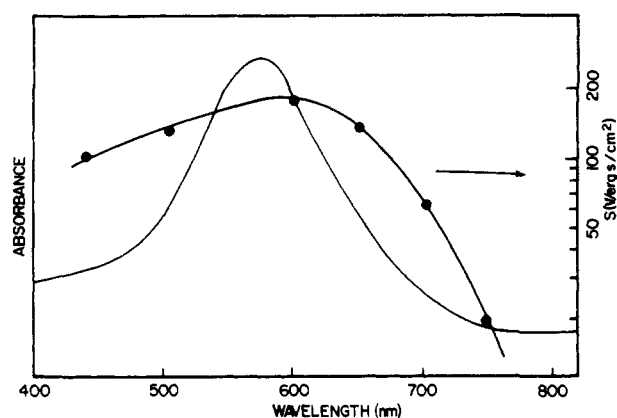


Figure 16. Spectral response curve and absorption spectrum of bisazo pigment VI in a bilayer photoreceptor device.

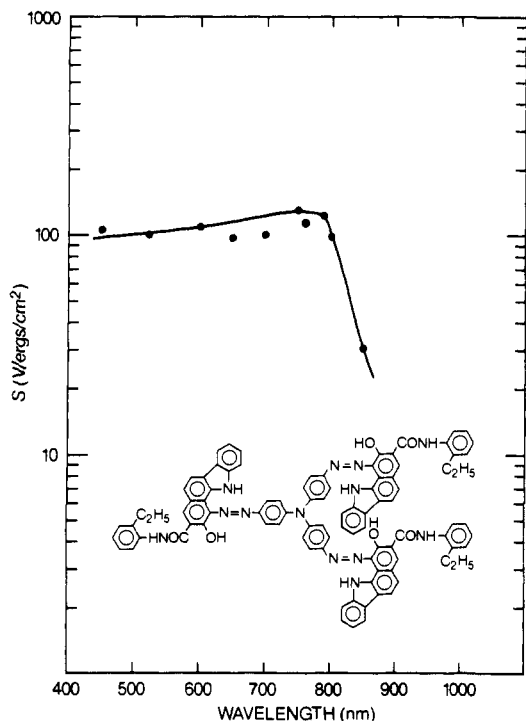


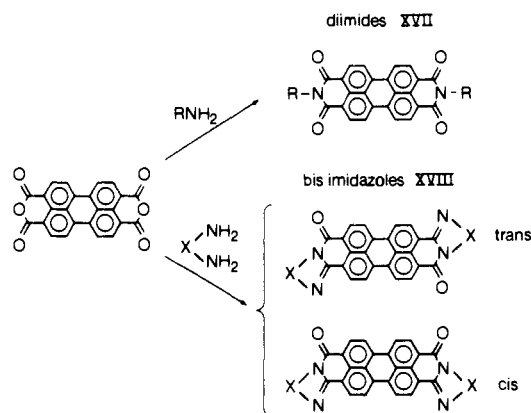
Figure 17. Spectral response curve of trisazo pigment XV in a bilayer photoreceptor device.

perylene are visibly absorbing and available. At that time, perylenes offered no cutting-edge advantages, in terms of sensitivity, diode laser compatibility, and ease of manufacturing, over other photoconductors. More recently, Popovic et al. showed that the photogeneration of e-h pairs for the perylene photoconductor is primarily at the CGL/CTL interface of the bilayer xerographic device.²²¹ The exciton of perylene undergoes either an electron-transfer reaction with the hole-transporting molecule or decay nonradiatively to the ground state. This unique interfacial photogeneration process has received considerable amount of attention lately²²²⁻²²⁴ and has shown promises in alleviating problems of charge transport and interfacial trapping commonly observed in organic photoreceptors.²²²

1. Synthesis, Purification, and Structural Variation

Perylenes are synthesized by condensation of perylene-3,4,9,10-tetracarboxylic dianhydride with amines in a solvent.²²⁵ The synthesis is extremely efficient and

Scheme V



isolated yields are normally $\geq 90\%$. A general reaction scheme is given in Scheme V.

The condensation reaction is stepwise.²²⁶ Since the starting dianhydride, the reaction intermediate and the perylene product are not soluble in the reaction solvent, the synthesis typically involves the transformation of one red solid to another. Contamination of the perylene product by the starting dianhydride and/or the intermediate is unavoidable. While the concentration of impurities in perylenes usually does not affect their performance as colorants, impurities are certainly undesirable for photoconductive devices. Techniques to purify perylenes, by washing perylenes with alkaline solutions, in which the starting dianhydride and the intermediate become hydrolyzed and soluble, by acid pasting, and by vacuum sublimation are known in the dye industry.²²⁵⁻²²⁷ For materials evaluation, the photoconductivity of many perylenes have been examined using vacuum-deposited CGLs, so that the purification and the CGL fabrication can be achieved in one step.

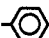
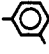
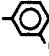
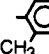

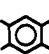
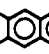
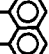
Structural variation of perylenes can simply be accomplished by using different amine precursors. The chemical structures of various photoconductive perylenes (general structures XVII and XVIII) are shown in Table VIII. An additional dimension for modifying the perylene structure was reported by Duff et al.²²⁸ These authors show that sulfonation of perylene-3,4,9,10-tetracarboxylic dianhydride with chlorosulfonic acid leads to the formation of 1,12-sulfonylperylene-3,4,9,10-tetracarboxylic acid (XIX), which upon deoxygenation and dehydration yields perylo(6,6a,6b,7-bcd)-thiophene-3,4,9,10-tetracarboxylic dianhydride (XX) (Scheme VI). Compound XX can then be used as a starting material to generate a new set of perylene diimides and bisimidazoles.

Unsymmetrical perylene pigments have also been reported.^{229,230} For example, reaction of perylene-3,4,9,10-tetracarboxylic dianhydride with 1 equiv of an amine results in a monoanhydride monoimide. This monoanhydride monoimide can then be reacted with a secondary primary amine to produce a variety of unsymmetrical perylene pigments.

2. Optical and Solid-State Properties

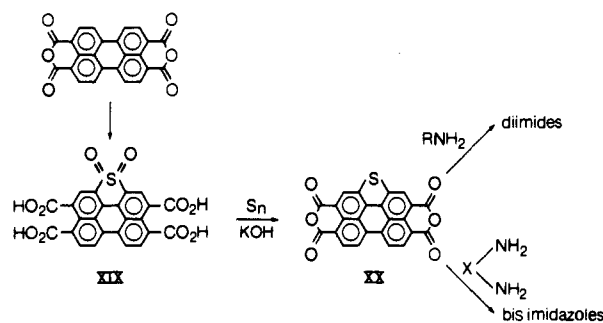
Perylene pigments have a red (or orange-red), red-brown, or purple blue appearance depending on the structure of the N-substituents. Their solubility in common solvents is very low. In organic solvents, *N,N'*-dialkyl or *N,N'*-diaryl diimide perylenes exhibit ab-

Table VIII. Structures and Xerographic Data of Perylene Pigments

perylene	CGL appearance	xerographic data ^a				ref(s)	
		dark decay (V/s)	$E_{0.5}^b$ (ergs/cm ²)	sensitivity ^c (V/ergs/cm ²)	spectral range ^d (nm)		
Diimides							
XVIIa	R=H	red	-10	60		450-600	222
XVIIb	-CH ₃	red	-15	24		450-600	222
XVIIc	- <i>n</i> -C ₃ H ₇	black			~100	450-650	223
XVIId	- <i>n</i> -C ₅ H ₁₁	red brown			~120	450-600	223
XVIIe	-CH ₂ CHCH ₃ C ₂ H ₅	red			~170	450-600	223
XVIIf	-CHCH ₃ C ₃ H ₇	red			~50	450-600	223
XVIIg	-CHC ₂ H ₅ C ₂ H ₅	red			~10	450-600	223
XVIIh	-CHCH ₃ - <i>i</i> -C ₃ H ₇	red			~120	450-600	223
XVIIi	- <i>neo</i> -C ₆ H ₁₁	red			~160	450-600	223
XVIIj	- <i>n</i> -C ₁₀ H ₂₁	red brown			~30 ^e	450-600	223
XVIIk	- <i>n</i> -C ₁₅ H ₃₁	red brown			~75	450-600	223
XVIIl	- <i>n</i> -C ₂₀ H ₄₁	red brown			~75	450-600	223
XVIIm	-CH ₂ CH ₂ C ₆ H ₅	black		3 ^f	180	450-680	223, 224
XVII n		red	-36	13		450-550	222
XVII o		red	-30	13		450-550	222
XVII p		red	-76	12		450-550	222
XVII q		red	-12	>100		450-550	222
Bis-imidazoles							
XVIII a		purple blue	-10	3.5		450-700	222
XVIII b			-10	6.7		450-700	222
XVIII c			-36	6.7		450-700	222
XVIII d			-60	>50		450-700	222

^a Data obtained from bilayer xerographic devices, the CGLs are fabricated by a vacuum-deposition technique, 0.1-0.3 μm . ^b White light exposure, 400-700 nm. ^c Estimated from the maximum of the photoresponse curves from ref 223. ^d Estimated from the absorption spectra. ^e The OD of the sample at the maximum is 0.4. ^f Estimated from the photodischarge curve in ref 224.

Scheme VI



sorption at λ_{max} 510-530 nm with an extinction coefficient of $(5-10) \times 10^4 \text{ cm}^{-1} \text{ M}^{-1}$.²³¹ The λ_{max} is not sensitive to the structure of the N-substituent. On the other hand, substituent in the perylene ring can induce either a bathochromic or a hypsochromic shift on the λ_{max} , depending on the nature and the position of the substituent. The magnitude of the ring-substituent-induced shift is in the order of 50 nm. The generally small spectral shift suggests that the π, π^* transition of perylene is localized in the perylene ring.²³¹

Bisimidazole perylenes absorb at longer wavelengths relative to those of diimide perylenes. For example,

the λ_{max} of XVIIIa is at 636 and 586 nm in concentrated sulfuric acid, whereas the λ_{max} of VIIa is at 595 and 552 nm in the same solvent.²²² The observed bathochromic shift is attributable to the extended π -conjugation in the perylene structure of XVIIIa.

While the solution absorption wavelengths of *N,N'*-dialkyl diimide perylenes are independent of the *N*-alkyl group, the shapes of their solid-state absorption bands are very sensitive to the structure of the *N*-alkyl group.^{223,224} The appearances of thin films of *N,N'*-dialkyl diimide perylenes vary from red to red-brown to black. The effect of the *N*-alkyl group on the crystallographic properties and the solid-state absorption of *N,N'*-dialkyl diimide perylenes have been studied by Graser and Hadicke,²³² and more recently by Duff et al.^{223,224} These authors have systematically shown that the solid-state absorption of *N,N'*-dialkyl diimide perylenes are dependent on the extent of the intermolecular interactions in the solid state. When the intermolecular interaction is strong, such as in the case of *N,N'*-di-*n*-propyl diimide perylene, the absorption is panchromatic and the appearance is black (Figure 18a). As the intermolecular interactions decrease, the absorbance of the long wavelength component decreases.

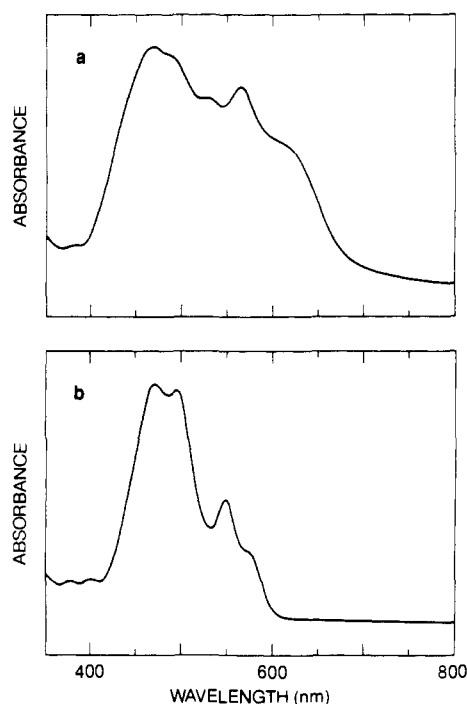


Figure 18. Absorption spectra of evaporated thin films of perylene pigments (a) XVIIc and (b) XVIII. Reprinted from ref 223. Copyright 1991 The Society for Imaging Science and Technology.

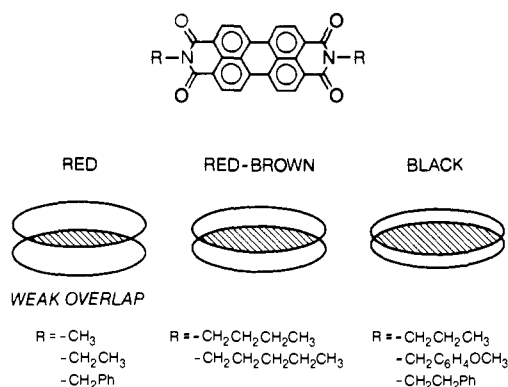


Figure 19. Molecular and idealized crystal structures for N,N' -dialkyl diimide perylene pigments. Reprinted from ref 223. Copyright 1991 The Society for Imaging Science and Technology.

es. As a result, the appearance of the pigment changes from black to red-brown to red. An example of a red-appearing perylene (N,N' -dineopentyl diimide perylene) is given in Figure 18b. Schematics of the three possibilities of intermolecular interactions are given in Figure 19.

The absorption spectra of several thin films of N,N' -diaryl diimide perylenes (XVIIIn-q) have also been reported. No substituent effect on the absorption is found. Since the N -phenyl ring in XVIIIn has already been twisted from planarity due to steric repulsion, the lack of an effect is ascribable to the small conformational differences among these materials.²²²

The solid-state absorption of bis-benzimidazole perylene XVIIIa is very broad and consists of two bands, one at longer wavelengths and the other at shorter wavelengths relative to the solution absorption. The broad absorption and the red-shift in the absorption edge are attributable to the strong intermolecular

interaction of XVIIIa in the solid state, which is enabled by the planar molecular structure. Structural modification of XVIIIa, such as in XVIIIb-d, results only in small spectral shifts. The small shifts reconfirm that the electronic transition of perylene pigments is primarily localized in the perylene ring.

Polymorphism has been reported for perylene pigments. For instance, depending on the sample history, XVIIIa was shown to form four different polymorphs as powders.²²² Perylene XVIIIm forms an amorphous thin film when prepared by vacuum deposition technique. Upon exposure of the amorphous thin film to solvent vapor, a crystalline thin film is obtained.²³³ Detailed structural characterization of these polymorphs and the connectivity of the structural changes to the photoconductivity have not been reported.

3. Photoconductivity

The photoconductivities of perylene pigments have primarily been studied in bilayer xerographic devices and the data are summarized in Table VIII. Generally speaking, the dark decay values are lower than those in Tables II and IV. The low dark decay is at least in part attributable to the high purity of these materials in devices where the perylene CGLs are prepared by a vacuum evaporation technique.

A glance at the sensitivity data indicates that the sensitivity variation is quite small despite the structural changes. N,N' -Dialkyl diimide perylenes XVIIIf-l are slightly soluble in methylene chloride, the coating solvent for the CTL. The low sensitivity obtained from these materials may be resulted from device fabrication. For example, the lowerings of the sensitivity in devices of XVIIIf-l are found to parallel to the solution absorption of the perylene spectrally.²²⁴ The mirror-image relation between the sensitivity loss and the solution absorption indicates that some of the perylene molecules have been converted to the "dissolved" state during the device fabrication, and these molecules compete for the light absorption with the perylene aggregates in the xerographic device. In the case of XVIIIf, the low absorbance of the device is also contributing to the low sensitivity. After consideration of the fabrication effect, one can preliminarily conclude that the structural effect on the sensitivity of N,N' -dialkyl diimide perylenes is small. In section IV, we will show that the photogeneration mechanism of perylene XVIIIa involves exciton diffusion after optical excitation and e-h pairs formation at the CGL/CTL interface (or at the contact point between the microcrystalline perylene and the CTL). If the same photogeneration mechanism is operating for XVIIIf-l, the photosensitivity of these perylenes should be a dependence of the exciton diffusion length, since recombination of the e-h pairs at the CGL/CTL interface is unlikely under the electric field. The lack of sensitivity variation among perylenes XVIIIf-l implies that their exciton diffusion lengths are very similar. In the case of perylene XVIIIa, Popovic et al. estimated that the exciton diffusion length is $\sim 2700 \text{ \AA}$.²²¹ This is in the same order of magnitude as compared to the thicknesses of the CGLs of XVIIIf-l.²²³ The lack of any structural dependence on the photoconductivity is then, not unreasonable.

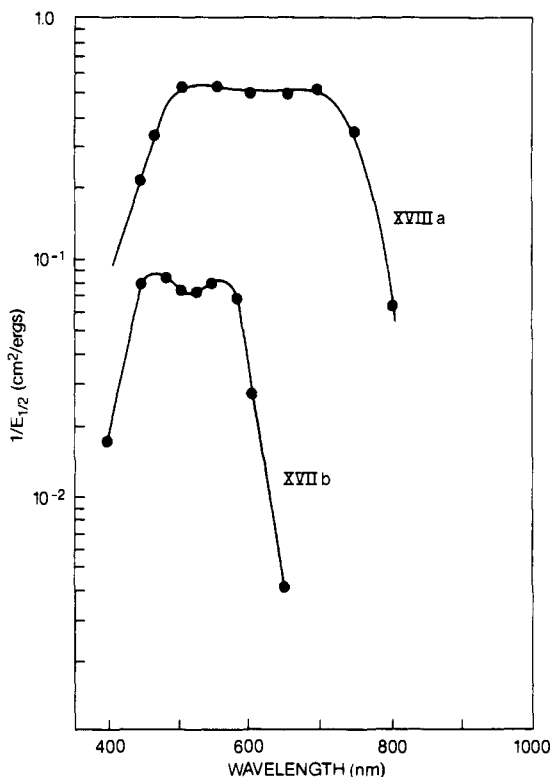


Figure 20. Spectral response curves of perylene pigments XVIIb and XVIIIa in bilayer xerographic devices. Reprinted from ref 222. Copyright 1989 The Society for Imaging Science and Technology.

N,N'-Diaryl diimide perylenes (XVIIIn–q) are generally less sensitive than their *N,N'*-dialkyl analogs. The relatively low sensitivity is probably due to the weak intermolecular interactions in these materials. For example, the *N*-phenyl ring in XVIIIn has been shown to be twisted from the molecular plane of the perylene ring due to steric repulsion.²²² Thus the intermolecular distance in the microcrystals of these materials will be longer, which leads to low sensitivity. The fact that XVIIq is the least-sensitive compound in the series is consistent with this argument because the twisting angle in XVIIq is expected to be the largest due to the *o*-methyl group.

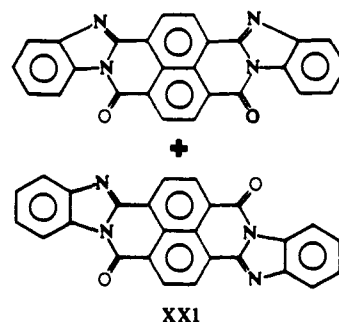
Among the bis-imidazole perylenes studied, XVIIIa is the most sensitive compound. Molecular modeling studies indicate that XVIIIa is the most planar molecule among XVIIIa–d. Again, a closer intermolecular interaction is attained, which results in a higher photosensitivity.²²²

The quantum efficiencies of photogeneration for XVIIIm and XVIIIa in xerographic devices are reported to be ~43%²³³ and 36%²²¹ at an electric field of ~30 V/μm. These quantum yields are significantly higher than the power conversion efficiencies of similar materials in photoelectrochemical devices, which are in the range of 1–2%.^{10,234} The high yields obtained in xerographic devices again are the result of the lack of charge recombination due to the high electric field and the use of a CTL.

Typical spectral responses of diimide and bis-imidazole perylenes are given in Figure 20. The data show that perylene pigments are sensitive in the visible region only. They are not candidates for photoreceptors in diode laser printers.

4. Perinones

In 1975, Regensburger and Jakubowski²³⁵ reported their study on the photodischarge of a commercial perinone pigment (XXI, bis-benzimidazole, perinone) in xerographic devices. Compound XXI is synthesized by condensing 1,4,5,8-naphthalenetetracarboxylic dianhydride with *o*-phenylenediamine. The product is a mixture of the *trans* and *cis* isomer.



The photoconductivity of XXI was studied in some detail by Loutfy et al.²³⁶ They reported that the photosensitivity of XXI is comparable to those of perylenes ($E_{0.5} \sim 10$ ergs/cm², white light exposure). The spectral response of XXI is quite narrow (450–520 nm) which obviously limits the practical value of XXI in device applications. An effort was made to broaden the spectral response and bis-naphthimidazole perinone was synthesized. While the spectral response is improved, covering from 450 to 650 nm, a decrease in photosensitivity is observed.²³⁶

E. Miscellaneous Classes

1. PVK–TNF Charge-Transfer Complex

Poly(vinyl carbazole) (PVK) is a commercial polymer obtained by free-radical polymerization. PVK itself is photoconductive, but only in the UV region.²³⁷ Numerous efforts were made in the early development of organic photoconductors to render PVK photoconductive in the visible region. Hoegl²³⁸ and Lardon et al.²³⁹ investigated the use of dopants in PVK to enhance the photosensitivity, and electron acceptor molecules were found to be particularly beneficial. Regensburger⁴¹ reported the use of a thin film of selenium as a spectral sensitizer for PVK. Dye sensitization of PVK has also been reported.^{240–242} Along with these activities, the first commercial organic photoconductor, based on the charge-transfer complex of PVK:TNF (trinitrofluorenone) was introduced.³⁹ The photoconductive composition is a 1:1 charge-transfer complex between the carbazole moiety and TNF. The photoconductor is a 13-μm single-layer device and is prepared by casting a THF solution containing PVK and TNF onto an aluminum substrate.²⁴³ The chemical structures and the spectral response curve of the photoconductor are given in Figure 21. Although the PVK:TNF photoconductor had been phased out of the marketplace due to the low photosensitivity, the toxicity of TNF, and the poor mechanical strength, studies on the photoconductivity of CT complexes of PVK and similar materials, and the dye sensitization of PVK remain a fascinating research topic.^{244–248}

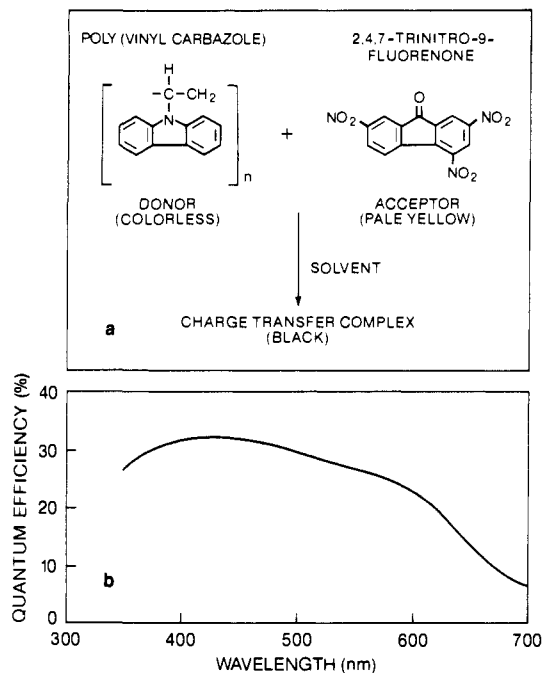
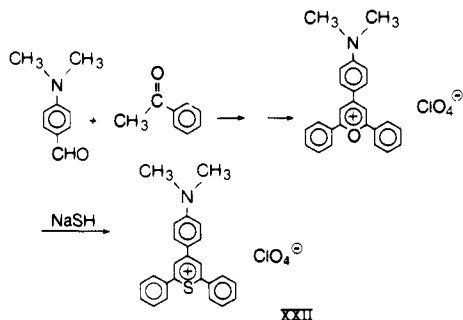


Figure 21. (a) Chemical structures and (b) spectral response curve of a PVK:TNF charge transfer complex device. Reprinted from ref 243. Copyright 1971 IBM Corporation.

Scheme VII



2. Thiapyrylium Salts

The most mentioned thiapyrylium salt is XXII, 4-[4'-(dimethylamino)phenyl]-2,6-diphenylthiapyrylium perchlorate). It was synthesized by first condensing *p*-(dimethylamino)benzaldehyde with 2 equiv of acetophenone in perchloric acid to form a pyrylium perchlorate,^{249,250} followed by sulfurization of the pyrylium perchlorate with sodium hydrosulfide to yield XXII (Scheme VII).²⁵¹

The photoconductivity of XXII was discovered by Light,⁴⁰ who observed a color change and an increase in photoresponse speed when polymer films incorporating XXII were exposed to solvent vapor. The composition of the actual photoconductor was reported by Dulmage et al.^{252,253} These authors showed that photoconducting thin (5–10- μm) films of XXII are prepared by casting a methylene chloride solution containing XXII, bis[2-methyl-4-(diethylamino)phenyl]phenylmethane (a hole transporting molecule) and a polycarbonate polymer onto a substrate. The as-formed film is homogeneous according to X-ray powder diffraction analysis. It exhibits an absorption band analogous to the monomeric absorption of XXII, at λ_{max} 580 nm (Figure 22). Upon exposure of the homogeneous film to methylene chloride vapor, a dye

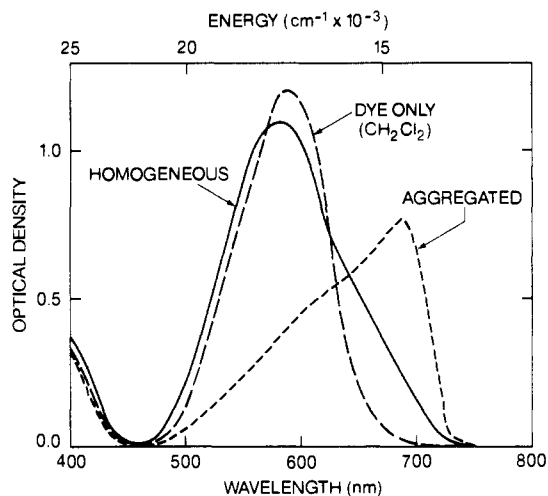


Figure 22. Absorption spectra of thiapyrylium salt XXII. Reprinted from ref 252. Copyright 1978 The American Institute of Physics.

aggregate, which is essentially a "complex" between XXII and the diphenol-A polycarbonate polymer, is formed. The formation of the dye aggregate results in a bathochromic shift on the λ_{max} , from 580 to 690 nm (Figure 22). Subsequent spectroscopic, electrochemical, and structural studies (on both the photoconducting film and a model aggregate) suggest that the electronic states of XXII are intramolecular charge-transfer states and that there exists extensive intermolecular charge-transfer interactions in the aggregate. The interplanar distance of XXII in the aggregate is $\sim 3.4 \text{ \AA}$.²⁵⁴ A schematic of the structure of the aggregate is given in Figure 23. The photoconductivity of XXII was studied by the xerographic discharge technique. The data show that the film that contains aggregate of XXII is ~ 150 times more sensitive than its precursor film (Figure 24). The quantum yield of photogeneration for the aggregate of XXII was determined to be $\sim 20\%$ at 30 $\text{V}/\mu\text{m}$. Mechanistic investigations suggest that the photogenerated e-h pairs are formed at the surface of the aggregates between the diffused exciton and, presumably, the hole-transporting molecule.²⁵⁵

As seen in Scheme VII, there is a lot of room in designing new thiapyrylium salt photoconductors. Many synthetic routes are known.²⁵⁶ Thus far only the photoconductivity of XXII has been detailed. The difficulty of uncovering more photoconductive thiapyrylium salts may be a molecular architecture issue rather than a synthetic issue because of the stringent stacking requirement in the photoconductive aggregate of XXII.

Finally, XXII is sensitive from 450 to 700 nm and is not suitable for diode laser printer applications. Several approaches have been reported in the literature to extend the photoresponse to 780 nm. These include the synthesis of thiapyrylium salts with more double bonds, selenopyrylium salts, and telluropirylium salts.^{257–259}

3. 3,6-Diphenylpyrrolo[3,4-c]pyrrole-1,4-dithione

The photoconductivity of 3,6-diphenylpyrrolo[3,4-c]pyrrole-1,4-dithione (XXIII) was first reported by Mizuguchi and Rochat in 1988.²⁶⁰ Compound XXIII was reported to be synthesized from the corresponding

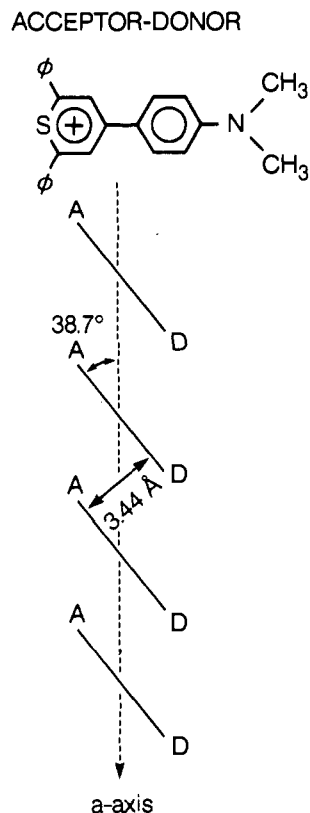


Figure 23. A schematic of the quasi-one-dimensional thiopyrylium salt assembly projected along the *a* axis. Reprinted from ref 254. Copyright 1982 Academic Press.

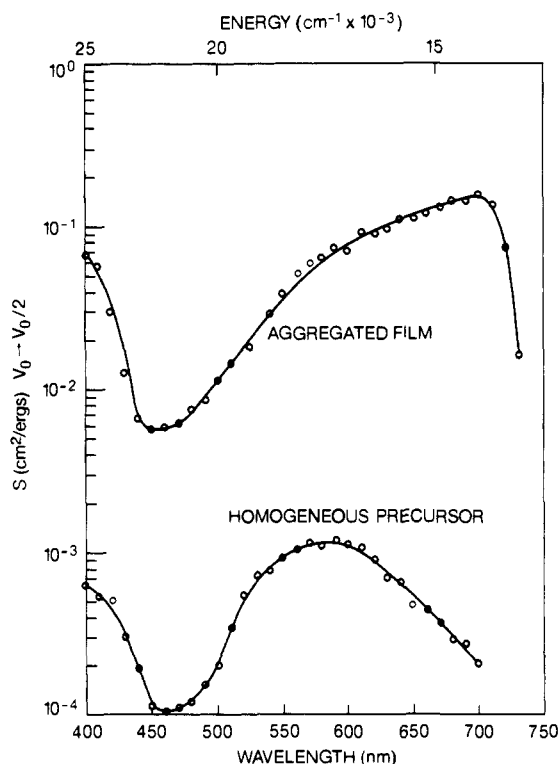


Figure 24. Spectral response curve of a single-layer photoceptor incorporating XXII: untreated device (lower curve) and solvent vapor treated device (upper curve). Reprinted from ref 252. Copyright 1978 The American Institute of Physics.

diketo precursor and Lawesson's reagent. Apparently, the crude product from the synthesis is very impure and has to be washed 3–4 times with solvents and then

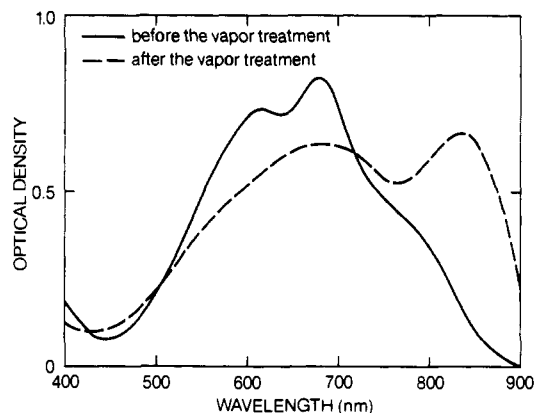
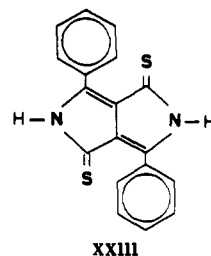


Figure 25. Absorption spectra of an evaporated thin film of XXIII (~ 1200 -Å thick). Reprinted from ref 260. Copyright 1988 The Society for Imaging Science and Technology.

sublimed 4 times under an argon atmosphere prior to device fabrication.



Both the solution and solid-state absorption, as well as the polymorphism of XXIII have been briefly investigated.^{260–262} The photoconductivity was examined in a bilayer configuration using a vacuum vapor-deposited CGL as well as a solution-coated CGL. It was shown that a disordered thin film (1200 Å) of XXIII was obtained by vacuum deposition. Upon exposure of the film to solvent vapors, the crystallinity of the film increases, along with an increase in absorptivity in the near-IR at λ_{\max} 860 nm (Figure 25). Mizuguchi et al. proposed that there is an increase in intermolecular CT interactions in the thin film of XXIII after solvent vapor treatment. Concurrently, a 100-fold increase in photoconductivity was noted in the vapor treated film.

In principle, many derivatives of XXIII can be synthesized.²⁶³ So far only the properties of XXIII have been reported.

4. Miscellaneous Photoconductors

By definition, organic colorants are aromatic compounds that absorb visible light. There are two usual "organic means" to reduce the excitation energy of aromatic molecules and make them visibly absorbing. While the photographic industry has been successful in using π -double bond conjugation,²⁶⁴ the dye industry has been relying on the introduction of intramolecular CT states. As a result of the CT character and their commercial availability, the photoconductivities of many colorants have been examined. Notable examples are dihaloanthranthone,^{265,266} epindolidione,²⁶⁷ trihalopyranthredione,²⁶⁸ quinacridone,²⁶⁹ tetrachloroindigo,²⁷⁰ azulonium dyes,²⁷¹ etc. Even though some of these compounds are highly sensitive, they have not been studied at any great length. The practical successes of phthalocyanines, squaraines, azo pigments,

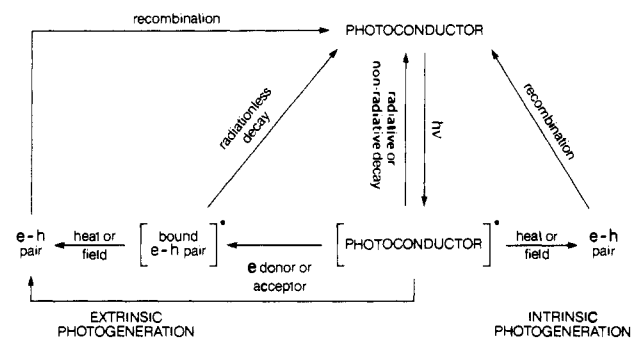


Figure 26. Definitions of the intrinsic and extrinsic photogeneration processes.

and perylenes are probably contributing to the lack of attention to these materials.

IV. Mechanistic Studies

In a bilayer photoreceptor device such as that shown in Figure 3, excitation of the photoconductor results in the generation of e-h pairs in the CGL. The photogenerated holes then inject to the CTL and migrate across the CTL to discharge the device. In this section, scientific studies on factors that influence the photogeneration and the subsequent interfacial electron-transfer processes are reviewed.

A. Definitions, Models, and Measurements of Photogeneration

1. Definitions and Models

By definition, the mechanism of photogeneration for a photoconductor can either be intrinsic or extrinsic. The conceptual scheme is given in Figure 26. Essentially, after excitation of a photoconductor, the excited photoconductor, in most cases the exciton, can either fluoresce or decay nonradiatively to the ground state. If this excited state ionizes and forms an e-h pair, regardless of the mode of activation (thermal or electric field assisted), the photogeneration process is defined as intrinsic. On the other hand, if the excited state needs to react with an electron donor/or acceptor prior to the formation of the e-h pair, the photogeneration process is defined as extrinsic. In extrinsic photogeneration, an intermediate bound e-h pair, such as an exciplex or an excited charge-transfer complex, may be

involved. Radiative decay processes, such as fluorescence from the exciplex,²⁷² or delayed luminescence resulted from recombination of the e-h pair,²⁷³ are known to occur. These radiative decay processes have been omitted in Figure 26 for simplicity. Finally, Figure 26 is intended only for definition purposes and does not imply that a photoconductor can only have one photogeneration mechanism.

Amorphous selenium is an intrinsic photogenerator. The quantum yield of photogeneration was shown to be a strong dependence on the excitation wavelength, temperature, and electric field.²⁷⁴ A diffusion model based on the Onsager theory^{275,276} has been successfully applied to analyze the diffusive motion of opposite charges in the presence of an applied field (Figure 27a). The model assumes that there is an activation barrier for the ionization process. If the excitation does not result in ionization, the probability of recombination increases. The barrier for the ionization process can be overcome by exciting the photoconductor to a "hot" state, or it can be activated by thermal energy or an applied electric field. Similar to the photogeneration of selenium, the photogeneration of anthracene^{277,278} and poly(vinyl carbazole)²⁷⁹ are also dependent upon the excitation wavelength, temperature, and applied electric field. These are intrinsic organic photoconductors and the Onsager model has been found to be applicable in analyzing the results.

In the case of most organic photoconductors, due to the rapid rate of internal conversion, the quantum yield of photogeneration is wavelength independent. To account for this diversion, the Onsager model has been modified by Noolandi and Hong (Figure 27b).²⁸⁰ The theoretical analyses have been shown to fit well with experimental data on the fluorescence quenching and quantum yield data for X-H₂Pc. More recently, the model has been extended to analyze results obtained from β -H₂Pc,²⁸¹ InClPc,²⁸² and perylene pigments.²²¹

2. Measurements of Photogeneration Efficiency

As pointed out in section II, the xerographic photodischarge method offers the simplest way to determine the xerographic gain (η), the quantum yield for e-h pairs formation in the entire device. In a single-layer photoreceptor, one can determine η as a function of the applied electric field (E) or temperature. The data can then be analyzed by the Onsager model or the Noolandi Hong model (Figure 27) from which the quantum yield of photogeneration (ϕ_{eh}), the thermal-

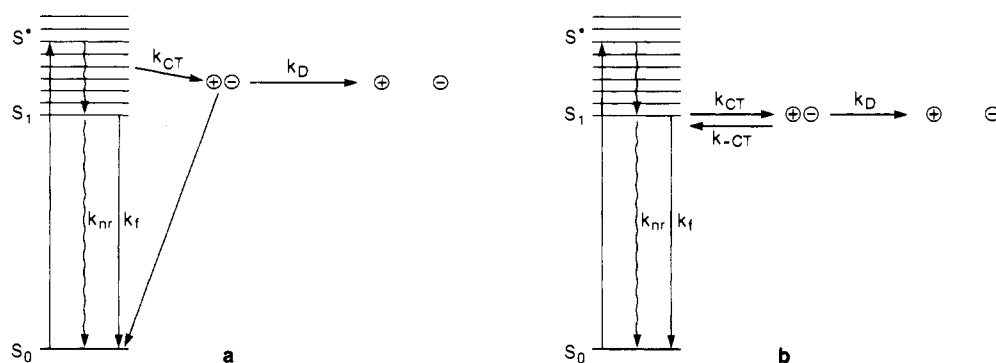


Figure 27. (a) A schematic representation of photogeneration as described by the usual Onsager Model; (b) a schematic representation of photogeneration as described by the Noolandi and Hong model. Reprinted from ref 280. Copyright 1979 The American Institute of Physics.

ization distance and the activation energy are calculated. This methodology has been applied to the analyses of organic photoconductors.

In the bilayer configuration, η is a function of ϕ_{eh} , the hole-injection efficiency from CGL to CTL and the hole mobility in the CTL. To determine the photogeneration efficiency (ϕ_{eh}) of the photoconductor in the CGL, one can study the CGL in a sandwich photoelectrical cell alone and measure the photocurrent of the layer.²⁸³ Alternatively, Popovic^{284,285} has shown that the quantum yield can be determined from the potential drop of a capacitance photoelectric cell after excitation by a laser pulse (pulsed photoconductivity).

In addition to photoelectrical measurements, two fundamentally sound, nonelectrical approaches based on the photophysics of the excited state have been reported. According to Figure 27b, if the photoconductor is fluorescing, one can use the technique of electric field induced fluorescence quenching to probe the photogeneration process. The quantum yield of e-h pair formation (ϕ_{eh}) is given by

$$\phi_{\text{eh}} = \left[\frac{k_{\text{CT}}}{k_{\text{CT}} + k_{\text{f}} + k_{\text{nr}}} \right] \phi_{\text{D}}$$

where ϕ_{D} is the probability of the bound e-h pair to dissociate to form a free e-h pair. At high field, $\phi_{\text{D}} \approx 1.0$, and ϕ_{eh} can be written as

$$\phi_{\text{eh}}^{\text{E}} = \frac{k_{\text{CT}}^{\text{E}}}{k_{\text{CT}}^{\text{E}} + k_{\text{f}} + k_{\text{nr}}} \quad (1)$$

The fluorescence quenching efficiency can be experimentally defined as

$$\phi_{\text{q}} = \frac{F^0 - F^{\text{E}}}{F^0} \quad (2)$$

where F^0 is the fluorescence intensity of the CGL and F^{E} is the intensity of the CGL under an electric field E .

From the photophysical processes of the excited state, ϕ_{q} can also be expressed as

$$\phi_{\text{q}} = \frac{k_{\text{CT}}^{\text{E}} - k_{\text{CT}}}{k_{\text{CT}}^{\text{E}} + k_{\text{f}} + k_{\text{nr}}} \quad (3)$$

By combining eqs 1 and 3, the relation between $\phi_{\text{eh}}^{\text{E}}$ and ϕ_{q} is given by

$$\phi_{\text{q}} = \frac{\phi_{\text{eh}}^{\text{E}} - \phi_{\text{eh}}}{1 - \phi_{\text{eh}}} \quad (4)$$

Since ϕ_{q} is an experimentally accessible quantity, one can then study ϕ_{eh} from the relationship between eqs 2 and 4. Details of the experimental procedure and the mathematical derivation have been provided in Popovic's publications.^{286,287}

Another nonelectrical measurement for ϕ_{eh} was reported by Tam using photoacoustic spectroscopy.²⁸⁸ He assumes that, if the major photophysical processes of the photoconductor are photogeneration of e-h pairs and charge recombination to generate heat, one can study the photogeneration process by monitoring the acoustic signal (S) of the photoconductive device as a function of E after optical excitation. The assumption is quite reasonable because the fluorescence quantum

yield and the yield of photochemical reaction of the photoconductor are usually very small. Thus

$$S = KI \quad (5)$$

$$S^{\text{E}} = K[1 - \phi_{\text{eh}}^{\text{E}}]I \quad (6)$$

where K is a machine constant and I is the light intensity.

By rearranging (5) and (6), we have

$$\phi_{\text{eh}}^{\text{E}} = \frac{S - S^{\text{E}}}{S} \quad (7)$$

Essentially, $\phi_{\text{eh}}^{\text{E}}$ is determined by measuring the acoustic signal S as a function of E . The Tam's model, however, fails to take into account the nonradiative decay process of the excited photoconductor (k_{nr}). The $\phi_{\text{eh}}^{\text{E}}$ obtained by this procedure is only relative.

B. Photogeneration Mechanisms in Organic Photoconductors

In this section, literature studies on the photogeneration mechanism (intrinsic vs extrinsic) of organic photoconductors are reviewed. Of the four main photoconductor classes, studies on the photogeneration mechanisms of phthalocyanines, perylenes, and azo pigments have been reported. The mechanism for squaraines remains to be investigated. Evidence so far suggests that most organic photoconductors are extrinsic photogenerators.

1. Photogeneration in Phthalocyanines

Although phthalocyanine is by far the most studied class of organic photoconductors and studies of the photogeneration mechanism have been reported, details of the photogeneration processes have yet to be unraveled totally. This is partly due to experimental difficulties because phthalocyanines are usually in the form of microcrystalline powders or thin films, and partly due to the rapid pace of technology development in the industry. In 1978, Menzel and Jordan²⁸⁹ reported the fluorescence emission of microcrystalline X-H₂Pc powder by laser-induced fluorescence technique. Subsequent experiments showed that the fluorescence is quenched by an applied electric field. The existence of a good correlation between the fluorescence quenching and photogeneration data suggests that the first excited singlet state (S_1) is the precursor state for the photogeneration.²⁹⁰ Loutfy and Menzel²⁸³ later reported an elegant investigation on the photogeneration mechanism of X-H₂Pc, in the presence of an electron acceptor/donor, using a combination of fluorescence quenching data and photogeneration efficiency data obtained from sandwich photoelectrical cells. These authors first studied the fluorescence quenching of X-H₂Pc microcrystalline powder by various electron acceptors and donors, which were surface coated onto the particle of X-H₂Pc at a monolayer coverage. Quenching efficiency as high as 92% was recorded for *o*-chloranil. Since controlled experiments demonstrated that H₂Pc molecules do not form any ground-state complexes with various electron acceptors or donors, Loutfy and Menzel proposed that an exciplex is formed at the surface of X-H₂Pc particles between H₂Pc and the electron ac-

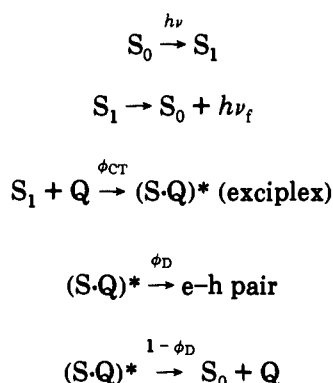
Table IX. Dependence of X-H₂Pc Photogeneration Efficiency (ϕ_{eh}) Fluorescence Intensity (F), Exciplex Formation Probability (ϕ_{CT}), and Exciplex Dissociation Efficiency to Free Carriers (ϕ_D), on TNF Concentration

TNF (mg/g)	ϕ_{eh} (%) ^a	F	ϕ_{CT}	ϕ_D
0	27	3.90	0.00	0.00
33	54	0.70	0.82	0.33
67	66	0.86	0.86	0.45
133	75	0.47	0.88	0.55
267	82	0.40	0.90	0.72

^a Reproducibility was better than $\pm 5\%$. (Data taken from ref 283.)

ceptor/donor. The formation of the exciplex leads to fluorescence quenching. The high quenching efficiency of these surface dopants indicates that the exciton migration range of X-H₂Pc must be very large. Indeed, exciton migration ranging between 200–400 Å, which is comparable to the dimension of the particles of X-H₂Pc (1000 × 300 × 300 Å), has been reported.^{291–293} The overall quenching data can be rationalized in terms of exciton migration, followed by fluorescence quenching due to the formation of the exciplex at the particle surface.

Using trinitrofluorenone (TNF) as an electron acceptor, particles of X-H₂Pc were surface coated at varying surface coverage, up to a monolayer coverage. The fluorescence quenching data and the photogeneration efficiency data from these samples are tabulated in Table IX. As the surface coverage of TNF increases, the photogeneration efficiency (ϕ_{eh}) increases and the fluorescence intensity F decreases. The photophysics of X-H₂Pc can be rationalized according to the following model:



where ϕ_{CT} is the probability of exciplex formation after optical excitation and ϕ_D is the probability of the exciplex to dissociate to an e–h pair.

In the absence of quenchers, the fluorescence intensity is F^0 and the photogeneration efficiency is ϕ_{eh}^0 . Addition of quencher to the system leads to a fluorescence F

$$F = F^0(1 - \phi_{CT})$$

and the photogeneration efficiency ϕ_{eh} becomes

$$\phi_{eh} = \phi_{eh}^0 + \phi_{CT}\phi_D$$

The calculated ϕ_{CT} and ϕ_D values are given in Table IX also. The increase of ϕ_D with increasing TNF coverage indicates the TNF aids not only the exciplex formation, but also the e–h pair formation. The mechanism of photogeneration for X-H₂Pc in the

presence of an electron donor or acceptor is therefore extrinsic, namely excitation of X-H₂Pc results in an exciton, which diffuses to the surface and forms an exciplex with an electron acceptor/or donor, before dissociation to form an e–h pair.

The question that remains is the photogeneration mechanism in the absence of an electron acceptor/or donor. Loutfy and Menzel indicated that the exciplexes of X-H₂Pc decay to regenerate the S₁ state, which can generate an e–h pair in the presence of an electric field. They postulated that O₂ may play a role in the photogeneration process, forming an exciplex and then dissociating to an e–h pair.²⁸³ The critical role of O₂ in the photogeneration of X-H₂Pc was also reported by Ahuja and Hauffe,²⁹⁴ who showed that O₂ is responsible for the photogeneration of X-H₂Pc in alkane solvents.

Complementary results on the need of O₂ in the photogeneration of phthalocyanine were reported in some detail by Mizuguchi. He showed by X-ray photoelectron spectroscopy that O₂ is desorbed from a thin film of β -CuPc at temperatures ≥ 90 °C under a vacuum of 6×10^{-8} Torr.²⁹⁵ Concurrent photocurrent measurements of the thin film showed that photocurrent increases as temperature increases from room temperature to ~ 90 °C. The rate of the increase in photocurrent slows down from ~ 90 to ~ 140 °C. At temperatures > 140 °C, the photocurrent decreases as the temperature increases.²⁹⁶ The decrease in photogeneration at temperatures > 90 °C, along with the O₂ desorption experiments indicate the O₂ is involved in the photogeneration process of β -CuPc. The increase in photogeneration between room temperature to 90 °C is attributable to thermal-assisted photogeneration.

In Loutfy and Menzel's mechanistic study of X-H₂Pc, an exciplex intermediate was proposed as a precursor CT state for photogeneration, but it was never observed experimentally. On the other hand, an exciplex intermediate was detected in the case of β -H₂Pc when Popovic studied the photogeneration mechanism of β -H₂Pc by delayed-collection-field and delayed fluorescence techniques.²⁸¹ Even though these literature data do not imply that all phthalocyanines are extrinsic photogenerators, most reported results on phthalocyanines, so far, can be rationalized within the exciton diffusion/surface ionization framework. In addition to O₂, Fujimaki²⁹⁷ recently showed that adsorbed water molecules on the surface of Y-TiOPc particles are also playing a role on the photoconductivity of TiOPc.

2. Photogeneration in Perylenes

The photogeneration mechanism of perylene XVIIIa was studied by Popovic, Loutfy, and Hor, using xerographic, pulsed photoconductivity and fluorescence measurements.²²¹ The device investigated is bilayer in configuration (Figure 3) and consists of a thin evaporated film of XVIIIa (2200 Å) and a CTL, which contains 35% of a hole-transporting molecule and 65% of a polycarbonate polymer, successively deposited on a semitransparent aluminized substrate. The fluorescence intensity of the thin film of XVIIIa is quenched (by 90%) after it is overcoated by the CTL. Controlled experiments by replacing the CTL with a polycarbonate coating or by coating the CGL film of XVIIIa with the hole transporting molecule indicate that the hole transporting molecule is responsible for the fluorescence

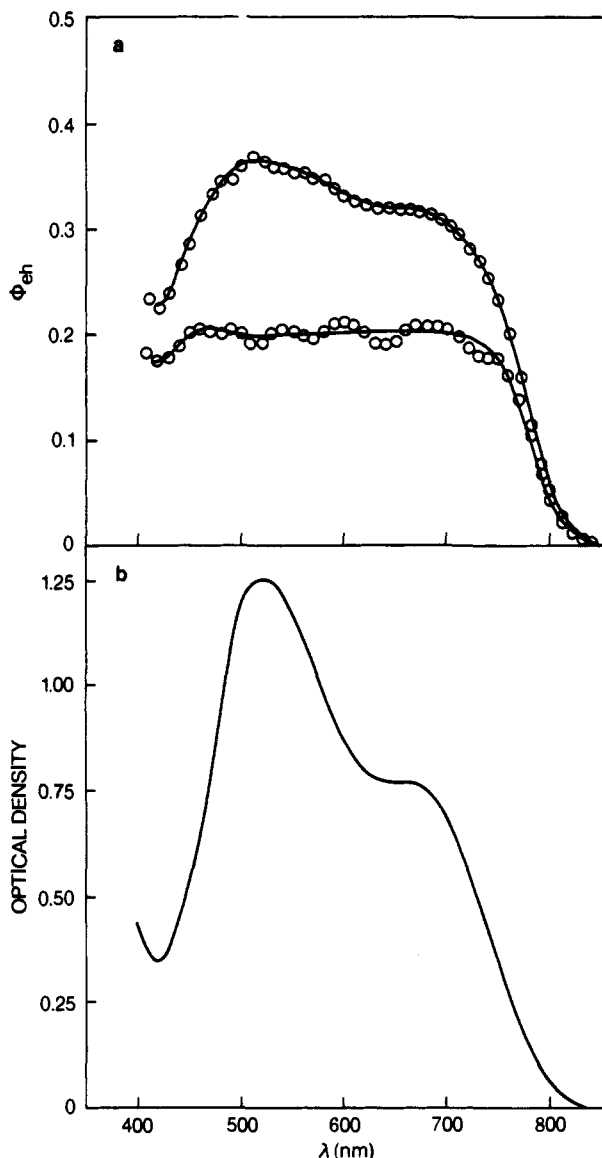


Figure 28. (a) Action spectra of perylene XVIIIa in a bilayer photoreceptor device: upper curve, illumination through the CTL; lower curve, illumination through the semitransparent aluminum substrate; (b) absorption spectrum of an evaporated film of XVIIIa ($\sim 1700 \text{ \AA}$). Reprinted from ref 221. Copyright 1988 North-Holland.

quenching alone. Since the fluorescence quenching data correlate well with the xerographic photodischarge and photogeneration data, the involvement of the S_1 of XVIIIa in the photogeneration process is indicated. The specificity of the fluorescence quenching suggests that the photogeneration of XVIIIa is extrinsic, namely exciton diffusion after excitation and e-h pair formation at the CGL/CTL interface between the exciton and the hole transporting molecule. Additional evidence to substantiate this model comes from photogeneration data obtained by illuminating the device (1) through the CTL and (2) through the semitransparent aluminum substrate. When the data is taken by illumination through the CTL, the action spectrum matches to the absorption spectrum (Figure 28a,b). On the other hand, when the photogeneration data is obtained by illumination through the semitransparent aluminum substrate, the photogeneration efficiency is relatively low and is independent of the excitation wavelength (Figure 28a). The wavelength independence provides evidence

for the exciton diffusion mechanism. For instance, at wavelengths where XVIIIa absorb strongly, the excited photogenerator is closer to the aluminum and the exciton diffusion length is long, whereas at wavelengths where XVIIIa is weakly absorbing, the excitation penetrates the entire CGL. The inefficient light absorption is compensated by the shorter distance for exciton diffusion. From the shape of the action spectra and the absorption of the CGL, Popovic et al. estimated that the exciton diffusion length for the evaporated thin film of XVIIIa is $\sim 2700 \text{ \AA}$.²²¹

The photogeneration efficiency of XVIIIa was shown to be less field dependent than that predicted by the Onsager model. It is uncertain whether this is a result of the direct formation of e-h pair without going through an exciplex or not. The theoretical framework for the low electric field dependence has not been developed.

3. Photogeneration in Azo Pigments

A study on the photogeneration mechanism of azo pigment VIh was reported by Umeda, Nimi, and Hashimoto in 1990.²⁹⁸ The CGL in the study is 1700 \AA in thickness and consists of 70% by weight of the bisazo pigment dispersed in a poly(vinyl butyral) binder. These authors showed by the xerographic photodischarge method that the quantum efficiency of photogeneration of the bilayer layer device is significantly higher than that of the single-layer device (same CGL without CTL). Since absorbance measurement indicates that the CGL is illuminated throughout, these authors propose that the photogeneration mechanism of bisazo pigment VIh involves exciton diffusion after excitation and e-h pairs formation at the CGL/CTL interface. The proposed mechanism is similar to that of perylene XVIIIa.

Law and Popovic²⁹⁹ studied the photogeneration mechanism of several bisazo pigments of the general structure of VI by fluorescence quenching technique. The correlation between xerographic and fluorescence quenching (by the CTL) data indicates that the S_1 state is the precursor state for the photogeneration process. Since controlled experiments suggest that the hole-transporting molecule is the only active species involved, the data indicate that the e-h pair formation involves an electron transfer between the exciton and the hole-transporting molecule. The need of a hole-transporting molecule is also suggested by Murakami et al.²⁰² in their study of the photogeneration of an unsymmetrical azo pigment XIV. Very recently, Umeda and Hashimoto³⁰⁰ reported a study of the photogeneration mechanism of triazo pigment XVI. Again, these authors showed that the photogeneration of XVI involves exciton diffusion after exciton and e-h pairs formation at the CGL/CTL interface of the bilayer device. Thus, there is compelling evidence to suggest that azo pigments are extrinsic photogenerators also.

C. Photogeneration Efficiency

1. Effect of Molecular Structure

In section III, the photoconductivity data of a large number of organic photoconductors are summarized. Because of the variation in device fabrication conditions and hole-transporting molecules, comparisons of the performance of different photoconductors are only

Table X. Quantum Yields of Photogeneration (ϕ_{eh}) of Various Photoconductors

photoconductor	ϕ_{eh} (%)	field strength (V/ μm)	method	ref
χ -H ₂ Pc	18	50	sandwich photoelectrical cell	287
VOPc (phase II)	~20	45	xerographic photodischarge	301
Y-TiOPc	~90	~30	xerographic photodischarge	112
Sq-5	22	50	sandwich photoelectrical cell	15
azo XIII	40	30	xerographic photodischarge	202
azo XIV	50	30	xerographic photodischarge	202
perylene XVIIIm	43	30	xerographic photodischarge	233
perylene XVIIIa	36	30	xerographic photodischarge	221
thiapyrylium salt XXII	~20	30	xerographic photodischarge	255

qualitative, especially between different laboratories. The xerographic photodischarge technique is simple and has served its purpose as a reliable tool for materials evaluation. For an accurate comparison of the photoconductivity of different photoconductors, quantum yield data are needed. Although the quantum yields of photogeneration (ϕ_{eh}) are not routinely measured, enough attention has been paid to photogenerators that are highly efficient. The ϕ_{eh} values of several organic photoconductors are tabulated in Table X. Undoubtedly, Y-TiOPc is the most efficient photoconductor in the group. The origin of its superiority as compared to other polymorphs of TiOPc and other phthalocyanines is still under active scrutiny. Comparison of the ϕ_{eh} values of all other photoconductors indicates that their photogeneration efficiencies are amazingly similar, ranging from ~20% to 50%. This is despite the wide structural variation among the chemical classes. Moreover, when compared to the effect of the molecular stacking arrangement in the microcrystalline state on the photogeneration efficiency (next section), the impact of the molecular structure is actually very small.

Although photoconductors from different chemical classes are structurally different, most of their electronic states are intramolecular CT states. For instance, theoretical calculations by Schaffer, Gouterman, and Davidson showed that the π, π^* transition of phthalocyanine involves a transfer of charge from the outer benzene ring to the inner macrocyclic ring.⁸³ This CT was confirmed spectroscopically in the case of VOPc dyes.³⁰² The electronic states of both squaraines^{156,163} and thiapyrylium salt²⁵⁴ are shown to be CT states also, by electrochemical and spectroscopic techniques. Although the electronic structure of perylene is not well understood, there is an indication from the aggregational behavior of these materials that its electronic state should have some CT character.³⁰³ As pointed out earlier, azo pigments are keto hydrazones. Both MO calculations³⁰⁴ as well as electrochemical results³⁰⁵ indicate that the electronic states of keto hydrazones are intramolecular CT states as well. The interesting outcome here is that, the key molecular requirement for an organic photoconductor is to have an intramolecular CT state that absorbs in the visible region.

2. Effect of Molecular Architecture

Polymorphism is a very common phenomenon in organic photoconductors. Usually, as the morphology of the microcrystal changes, the photoconductivity varies. Although the molecular stacking arrangement of the photoconductive molecules varies along with the

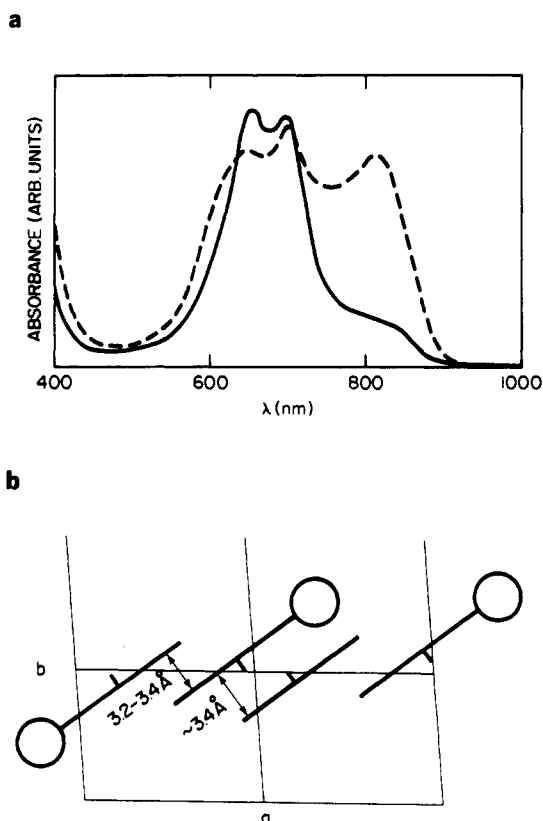


Figure 29. (a) Absorption spectra of *t*-Bu_{1,4}VOPc in polystyrene [before (—) and after (---) ethyl acetate vapor treatment]; (b) a schematic illustration of the intermolecular interaction of *t*-Bu_{1,4}VOPc molecules in the solid state. Reprinted from ref 309. Copyright 1988 The American Chemical Society.

morphological changes, the connectivity between photoconductivity and stacking arrangement is weak and indirect. The connectivity is usually masked by factors, such as impurity, particle size, crystallite size, or crystallographic preference, that are associated with the different preparations of each polymorph. In this section, several examples that clearly show the effect of stacking arrangement on the photogeneration efficiency are summarized. The importance of the precise stacking arrangement on the photogeneration efficiency is illustrated. The common molecular architecture among several highly efficient photogenerators is noted.

***t*-Bu_{1,4}VOPc Single-Layer Photoreceptors.** *t*-Bu_{1,4}VOPc is a composite VOPc dye that was synthesized by co-reacting 4-*tert*-butylphthalonitrile and phthalonitrile at a ratio of 1:11 with vanadium trichloride.³⁰² It exhibits good solubility in organic solvents due to the solubilizing *tert*-butyl groups. The number of *tert*-butyl groups on the VOPc ring is specifically designed in such a fashion that *t*-Bu_{1,4}VOPc molecules can self-assemble to the photoconductive aggregated form of VOPc (phase II) in the microcrystalline state. Figure 29a (solid curve) shows the absorption spectrum of a thin film of *t*-Bu_{1,4}VOPc in polystyrene (PS) on a transparent Mylar substrate. By comparison with its absorption in chloroform solution,³⁰² the absorption spectra of the metastable glassy phase (I) and the crystalline phase (II) of *t*-Bu_{1,4}VOPc and VOPc,^{123,302} Law³⁰⁶ concluded that *t*-Bu_{1,4}VOPc precipitates primarily as the phase I in PS during the film formation. Ethyl acetate vapor treatment (24 h) of the film causes

Table XI. Xerographic Data of *t*-Bu_{1,4}VOPc Single-Layer Photoreceptor Devices^a

	untreated	treated ^a
corotron (kV)	+5.5	+5.6
V _i (V)	+900	+920
ΔV/Δt (V/s)	+10	+35
V _R (V)	+250	+10
E _{0.5} at 600 nm (ergs/cm ²)	>10 ⁴	33

^a 10% by weight of *t*-Bu_{1,4}VOPc in polystyrene, 10-μm thick.

^b Ethyl acetate vapor treated for 8 h. (Data taken from ref 309.)

a change in color, from blue-green to blue-blue. In the absorption spectrum (Figure 29a dashed curve), a decrease in absorption in the visible region and an increase in absorption in the near-IR region ($\lambda_{\text{max}} \sim 810$ nm) are observed. Since the near-IR absorption is the unique characteristic of the crystalline phase II of VOPc and *t*-Bu_{1,4}VOPc, the absorption spectral data in Figure 29a suggest that the phase I of *t*-Bu_{1,4}VOPc is crystallized to the phase II upon exposure to ethyl acetate vapor.³⁰⁶ This conclusion is supported by X-ray powder diffraction data. A schematic of the stacking arrangement of *t*-Bu_{1,4}VOPc molecules in the phase II form is depicted in Figure 29b, in accord with the crystal structure of the phase II of VOPc.³⁰⁷

Table XI summarizes the xerographic photodischarge data of a 10-μm-thick, single-layer photoreceptor device of *t*-Bu_{1,4}VOPc in PS before and after the ethyl acetate vapor treatment. Results show that there is a slight increase in dark decay ($\Delta V/\Delta t$), a significant decrease in residual potential (V_R) and a dramatic increase in photosensitivity (lower $E_{0.5}$ value) after the ethyl acetate vapor treatment. Transmission electron microscopy results reveal that *t*-Bu_{1,4}VOPc particles (~ 0.1 – 0.15 μm) distribute uniformly within the layer and that there is neither a change in particle distribution nor in particle size after the vapor treatment. Since absorption spectral data and X-ray results show that *t*-Bu_{1,4}VOPc crystallizes from the glassy phase I to the crystalline phase II upon the vapor treatment, the change in xerographic properties is thus attributable to this phase change. The increase in dark conductivity (decay) and reduction in V_R are consistent with the increased crystallinity because crystalline materials are known to have higher conductivity than glassy materials.³⁰⁸ The most striking result in Table XI is the >300 times improvement in photosensitivity after the ethyl acetate vapor treatment. The result suggests that the quantum efficiency of photogeneration of *t*-Bu_{1,4}VOPc increases drastically as the intermolecular CT interaction between the VOPc rings is enhanced due to the crystallization.³⁰⁹

Squaraine Bilayer Photoreceptors. Sq-1 and Sq-23 form different aggregates in their microcrystalline state (Figure 12a,b). Their photoconductivities have been studied in parallel by xerographic photodischarge technique using bilayer photoreceptor devices.³⁰⁹ Results (Table XII) show that device of Sq-1 exhibits higher dark decay and higher V_R values as compared to that of Sq-23. These differences can be caused by intrinsic or extrinsic factors (e.g., impurities). More detailed experimentation is needed to elucidate all the possibilities. While the dark decay and V_R values differ only by a factor of 2, the difference in photosensitivity between them is over a factor of 100. The low sensitivity of Sq-23 is not due to an impurity effect because

Table XII. Xerographic Data of Sq-1 and Sq-23 in Bilayer Photoreceptor Devices^a

	Sq-1	Sq-23
corotron (kV)	-6.1	-4.8
V _i (V)	-970	-920
ΔV/Δt (V/s)	-90	-45
V _R (V)	-50	-20
E _{0.5} at 600 nm (ergs/cm ²)	3.3	390

^a CGL: ~ 0.5 -μm thick, consists of 30% by weight of a squaraine in a polycarbonate binder. CTL: ~ 30 -μm thick, consists of 40% by weight of a triarylamine hole-transporting molecule in a polycarbonate binder. (Data taken from ref 309.)

impurities primarily affect the dark decay of the device.¹⁴⁷ The low photosensitivity should not be due to any energy mis-match between CGL and CTL because the oxidation potential of Sq-23 is expected to be higher than that of Sq-1.¹⁶³ It is also not due to any fabrication effect because similar differences in photosensitivity are observed when Sq-1 and Sq-23 are tested in different device configurations. Law attributed the low photosensitivity of Sq-23 to an aggregational effect on the photogeneration efficiency.³⁰⁹ The result illustrates that while crystallinity may be required, high photogeneration efficiency can only be obtained when the aggregate fulfills its architectural requirements as an efficient photoconductor.

The xerographic results on *t*-Bu_{1,4}VOPc/PS single-layer photoreceptor devices show that there is a drastic increase in photogeneration efficiency when the glassy phase I is crystallized to phase II. A similar improvement in photosensitivity was observed by Dulmage and co-workers in an analogous single-layer photoreceptor based on thiapyrylium salt (XXII).²⁵² These authors showed that there is a 150 times increase in photogeneration efficiency when the as-coated, glassy, and homogeneous device is treated with methylene chloride vapor, which induces XXII to co-crystallize with the polycarbonate polymer as an aggregate. A perylene thin film of XVIIIm was shown to transform from amorphous to crystalline upon solvent vapor treatment and the transformation is accompanied by an increase in photogeneration efficiency.²³³ Mizuguchi and Rochat reported that solvent vapor increases the crystallinity of thin films of 3,6-diphenylpyrrolo[3,4-*c*]pyrrole-1,4-dithione (XXIII) and the increase in crystallinity also leads to a 100 times increase in photogeneration efficiency.²⁶⁰ All four photoconductors bear remarkable similarity, namely an increase in photoconductivity after solvent vapor treatment. The significance here is that, despite the wide structural variation among them, the molecular architecture of these molecules in their microcrystalline states, in terms of the intermolecular CT interactions, are similar (see Figures 23 and 29).

In the squaraine systems, Sq-1 and Sq-23 form different aggregates in solid and different photosensitivities are observed. The difference is attributable to an aggregational effect on the photogeneration efficiency. The most fascinating observation here is the high photosensitivity of Sq-1 because Sq-1 is shown to form aggregates having extensive intermolecular charge-transfer interactions (Figure 12a) similar to those of *t*-Bu_{1,4}VOPc, XXII and XXIII. These findings thus illustrate that, although crystallinity is a prerequisite for the high photogeneration efficiency, the precise

stacking arrangement in the aggregate is ultimately important.

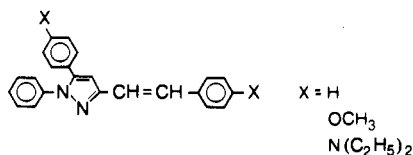
There are plenty of examples that support this view indirectly. The data in Table II show that the X- and the τ -form of H₂Pc are more sensitive than the α - and β -form. ϵ -CuPc is more photoconductive than α -CuPc and β -CuPc. The aggregated forms of MgPc, VOPc, AlClPc, AlClPcCl, and InClPc are superior to the respective α - or β -forms. The common feature of these sensitive polymorphs is their strong absorption in the near-IR region (~ 750 – 850 nm), which is red-shifted from their solution absorption maxima by 100–150 nm. The spectral changes are identical to that of *t*-Bu_{1,4}-VOPc, indicating that the intermolecular CT interactions in these materials are very similar. *It thus becomes clear that the architectural requirement of the photoconductive molecules in the solid state dominates the photoconductivity.* An efficient photoconductor should have (1) large charge mobility upon optical excitation (charge transfer states), (2) short interplanar distances (~ 3.5 Å), and (3) strong intermolecular CT interactions in solid.

D. Photoinduced Electron-Transfer Reactions

Regardless of the photogeneration mechanism, excitation of the photoconductor in a bilayer device, formally results in the formation of e–h pairs in the CGL. The photogenerated holes inject into the CTL and migrate across the device to neutralize the surface charges. The photogenerated electrons travel through the CGL to the ground of the conductive substrate. Fundamental understanding of these photoinduced interfacial electron-transfer processes is obviously of great practical values. Of the two processes, the electron-transfer between CGL and the grounded substrate has seldom been examined. Some efforts have been made to understand the energetic requirements between CGL and CTL on the xerographic performance.

1. Effect of CGL/CTL Energetics on the Photosensitivity

The injection efficiency of the photogenerated holes from CGL to CTL plays a crucial role in the xerographic gain of bilayer photoreceptor devices. The importance of the energetics between CGL and CTL was recognized as early as 1979. Melz and co-workers⁴² reported an investigation on the effect of hole transporting molecules on the photosensitivity of different bilayer devices. Three pyrazoline molecules were employed.



Although the oxidation potentials of these three molecules were not reported, one intuitively expects that it decreases as X changes from H \rightarrow OCH₃ \rightarrow N(C₂H₅)₂. Three different CGLs, namely a SeTeAs layer, a Chlorodiane Blue layer, and a Sq-9 layer, were examined in coupled with these CTLs. Without

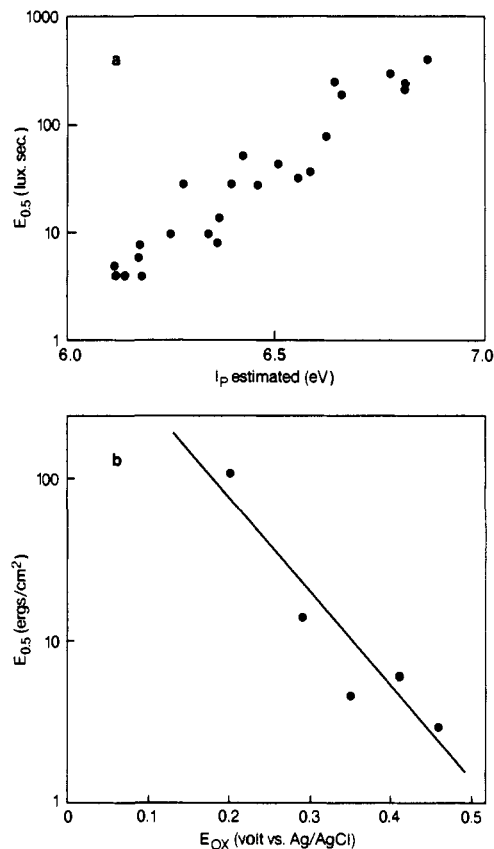


Figure 30. (a) A plot of $\log E_{0.5}$ vs I_p (CGL, Chlorodiane Blue/binder; CTL, hole-transporting molecules of varying ionization potential (I_p)); (b) a plot of $\log E_{0.5}$ vs E_{OX} (CGL, squaraines of varying oxidation potential; CTL, a triarylamine in a polycarbonate polymer). Part a reprinted from ref 310. Copyright 1981 IEEE Industry Applications Association.

exception, photosensitivity increases as X changes from H \rightarrow OCH₃ \rightarrow N(C₂H₅)₂. Since the fabrication and geometry of all devices are identical within a series of experiments, the results indicate that the efficiency of hole injection from CGL to CTL increases as the exothermicity of the injection process increases.

Kakuta, Mori, and Morishita³¹⁰ proposed the use of the " ω " technique, along with polarographic oxidation potential measurements to estimate the HOMOs of different CTLs. Using bisazo pigment Chlorodiane Blue as a photogenerator in the CGL, the xerographic sensitivities ($E_{0.5}$ values) of 25 bilayer devices containing hole-transporting molecules of varying oxidation potentials were determined. A plot of $\log E_{0.5}$ vs I_p (ionization potential) is given in Figure 30a. The data can be rationalized in terms of a hole-injection efficiency model, namely hole-injection efficiency and photosensitivity increase as the exothermicity of the injection process increases. The correlation between $\log E_{0.5}$ and I_p seems genuine since a similar plot was also obtained by Shi in his study of bilayer devices of ϵ -CuPc and different pyrazoline hole-transporting molecules.³¹¹

A similar description of the energetic requirement between CGL and CTL was provided by Law et al.¹⁶³ These authors reported the oxidation potential of a hole-transporting molecule (TPD) along with the oxidation potentials of 26 photogenerating squaraines in methylene chloride solution. By making the assumption that the oxidation potential of a squaraine in the CGL is similar to that in solution, the relative energy

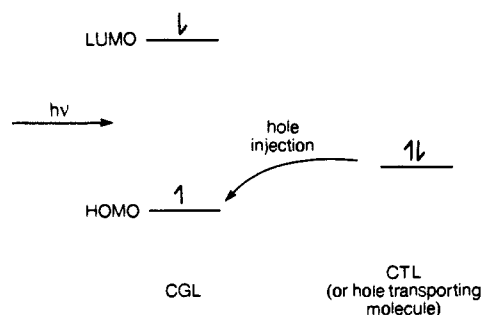


Figure 31. A schematic of an energetically favorable hole-injection process between CGL and CTL.

level of the HOMOs of various squaraines in CGLs can be assessed. Similarly, the energy level of the CTL is estimated. For a series of squaraines (Sq-1, Sq-5, and Sq-8-11) in which the fabrication, morphological, and particle size effects are minimal, the variation of xerographic sensitivity is shown to parallel the oxidation potential (E_{OX}). It is interesting to note that when one plots the $\log E_{0.5}$ versus E_{OX} , a similar linear correlation is obtained (Figure 30b). The mathematical analysis of the energetic requirement on photosensitivity has not been worked out.

Finally, from the oxidation potential of TPD and those of squaraines, one can conclude that highly sensitive devices ($E_{0.5} < 10$ ergs/cm²) can only be obtained when the hole-injection process is isoenergetic or better. The energetic requirement for having a favorable hole injection from CGL to CTL is depicted schematically in Figure 31. The finding of Law et al. agrees well with the report of Kitamura and Yokoyama, who concluded from DC transient measurements that the hole injection between CGL and CTL should be very efficient when the ionization potential of the CGL is the same as, or more positive than, the CTL.³¹²

2. Effect of CGL/CTL Energetics on the Residual Potential

One of the key parameters in the photodischarge of a xerographic device is the residual potential (V_R). A high V_R value lowers the contrast potential of the photodischarge process, which leads to low image-development latitude and poor copy quality. More significantly, electrons or "space charges" that remain in the device are known to be a source of electrical instability and device fatigue.³¹³⁻³¹⁵ Using DC transient measurements, Kitamura and Yokoyama³¹² showed that V_R increases when the HOMO of the hole-transporting molecule is isoenergetic or lower than that of the CGL. It is understandable that when the hole-injection process becomes isoenergetic or even unfavorable thermodynamically, the injection process becomes inefficient. This inefficiency results in the formation of "space charges" in the CGL. A similar energetic conclusion on V_R was also reached by Scott and co-workers,³¹⁶ in their study of bilayer devices containing bisazo and squaraine pigments.

In conclusion, evidence is provided that an exothermic photoinduced electron-transfer process between CGL and CTL is essential for maximizing the photosensitivity and minimizing the residual charges in bilayer devices. This energetic requirement should be a prime consideration in the design of future devices.

V. Trends and Outlook

A. Trends in Materials Research

It is clear from the distribution of the subjects in this report that research efforts on organic photoconductors have been primarily focusing on synthesis and evaluation of new materials. Due to the rapid pace of development, the approach has been semiempirical, but a successful one. Many organic photoconductors have been put to practical use. Now, organic photoconductors are known to be sensitive, highly efficient, stable, and economical. They are not only the materials for today, but also the choice for tomorrow. The photoconductive properties we accomplish now will become the basic requirements of future devices. While a quantum leap in performance improvement is unlikely, there will be a stream of incremental improvements in the next decade. The areas of improvement include (1) mechanical life and abrasion resistivity of the entire device, (2) device performance, stability, and versatility, (3) lower manufacturing cost, and (4) the use of environmentally friendly materials and processes. The first point and part of the second point are related to CTL technology and will partly be discussed in Part B of this section.

1. Basic Studies

The semiempirical approach has led to the development of many practically useful photoconductors. We also understand crudely that the molecular architecture of photoconductive molecules in the microcrystalline state dominates the photoelectrical properties of organic photoconductors. The superior photogeneration efficiency of Y-TiOPc over many other polymorphs of TiOPc illustrates this point very well. The prime focus in the 1990s is not on photosensitivity, but on photoelectrical stability and device reliability. We are at a stage where the semiempirical approach has become inefficient. To realize the stability and reliability goals, a basic understanding of the sciences involved in every step of the photodischarge process becomes a necessity. The steady increase in the number of reports that deal with the science of exciton diffusion, photogeneration, and interfacial electron transfer over the past several years is indicative of the correctness of this assessment. There will be investigations, including molecular modeling and simulation, to search for the "best" possible molecular architecture for an organic photoconductor. The aggressive pursuit of TiOPc or its isoelectronic VOPc will continue. With the recent advent of atomic force microscopy and scanning tunneling microscopy, the architecture of microcrystals of Y-TiOPc may soon be known. As our tool to characterize submicron structure increases, work on structure-photoconductivity relationships will take a sharp upturn. Studies will likely extend to model systems, where the photoconductive assemblies are generated in a "controlled and well-defined" environment and the fundamental processes, such as exciton diffusion, photogeneration, and interfacial electron-transfers can be examined in a very fundamental way. These studies will enable technologists to deconvolute the intricate photoinduced electron-transfer processes in photoreceptors and put the knowledge together for practical use. The understanding will also lead to better

control of electron-transfers at interfaces and ultimately high device stability and reliability.

2. Materials Design Concept

One of the known causes of electrical instability in bilayer xerographic devices is the residual or space charges in the device after photodischarge.³¹³⁻³¹⁵ It is interesting to note that, although phthalocyanines, azo pigments and perylenes are extrinsic photogenerators, the photogeneration processes in bilayer devices of azo pigments and perylenes are at the CGL/CTL interface, whereas that of phthalocyanines is in the bulk of the CGL. The specificity is due to the fact that photogenerations of e-h pairs of perylenes and azo pigments only occur when the excitons react with the hole transporting molecules, whereas in the case of phthalocyanine, photogeneration occurs at the particle surface between the exciton and O₂. The advantage of having an interfacial (interlayer) photogeneration is that, as soon as e-h pairs are formed, opposite charges are separated immediately by the electric field and by hole hopping. Very few free carriers remain in the device. This analysis suggests that photoconductive devices of perylenes and azo pigments should have practically no free carriers after the photodischarge. A high photoelectrical stability is implied and is, indeed, observed.^{180,216} Thus the development of perylenes and azo pigments will continue.

Now, photoreceptor manufacturers make two kinds of photoreceptors, visible photoreceptors for copiers and IR photoreceptors for diode laser (780 nm) printers. One possible improvement would be to have a photoreceptor that can cover the entire spectral range (450–800 nm), so that there is no need to manufacture two kinds of devices. It was proposed that this may be done by incorporating two spectrally complementary CGLs in one photoreceptor³¹⁷ or by mixing two spectrally complimentary photogenerators in a single CGL.³¹⁸ The impracticality of these approaches is quite obvious, considering the difficulty one already experiences in optimizing the performance of a single photogenerator system.

The possibility of using a single photogenerator to cover the entire spectral range, from 400 to 800 nm, has been explored by Law.¹⁷³⁻¹⁷⁵ Unsymmetrical squaraines that are spectrally designed to meet this challenge have been reported. Among the unsymmetrical squaraines synthesized, USq-13 is shown to have the sensitivity and stability that make the approach a reality.¹⁷⁵ In the future, there will be continuous attention to synthesize panchromatic photogenerators to simplify the manufacturing process.

In the past several years, unsymmetrical photoconductors from different chemical classes, squaraines, azo pigments, and perylenes, have been synthesized. While the motivation of introducing asymmetry in the pigment structure may be different among the different laboratories, improvements in photoconductivity have been demonstrated. For example, Law reported that the photoelectrical performance of USq-13 is superior to all known squaraines, most of which are symmetrical.¹⁷⁵ Murakami et al.²⁰² showed that the unsymmetrical azo pigment XIV is more sensitive than an analogous, symmetrical azo pigment. While the origin for the improved photoconductivity has not been clearly elu-

cidated, there is already adequate reason for further efforts in unsymmetrical photoconductors.

3. Visible versus IR

By the end of this century, the time of manufacturing two kinds of (visible and IR) photoreceptors may be over. As indicated in section II, the era for digital xerography has already arrived. The advantage of digitalizing the xerographic process is enormous, it enables editing, color, and image quality improvement. Barring any future breakthrough in visible diode technology, the preferred light source for forming the electrostatic images on the photoconductor will be the near-IR diode laser, which emits at 780 nm.⁴⁷ The copier process will no longer be a light lens process, but just involving laser scanning and digital printing. Thus the pressure of developing a new and improving visible photoreceptor will be gone. Research focus will be on IR photoreceptors.

4. Environmentally Safe Materials

Today, all materials used in photoreceptors are nontoxic and safe for disposal. However, as we become more environmentally conscious, regulation on manufacturing conditions will be more stringent. The rules on industrial waste disposal are tightening and the cost of manufacturing future photoreceptors will be skyrocketing. Now, the urgency is to improve device stability and reliability. The priority, however, can easily be switched when the manufacturing cost becomes unaffordable. Along the line of environmental consciousness, Pacansky and co-workers³¹⁹ reported the use of radiation curing in the coating of the CGL, which minimizes solvent emission into the environment. We expect that the pace of developing solventless coatings or environmentally friendlier materials and processes for photoreceptors will be increased by the end of the century.

B. Trends in Device Development

Photoelectrical stabilities higher than 50–200 kcycles have been reported for several different organic photoreceptors.^{175,180,216} In practice, the machine life varies from a few thousand to 100 thousand cycles. The harsh, operating environment experienced by the photoreceptor, which causes the CTL to wear and mechanically fatigue, limits the practical life of the photoreceptor. Several attempts have been made to improve the robustness of the entire device, so that the full photoelectrical life of the device can be utilized. These attempts include the increase of the thickness of the CTL,²¹⁶ or the use of a mechanically strengthened CTL.³²⁰

Another source of device degradation is induced by reactive species generated during the negative corona charging. These species react with the hole-transporting molecule in the CTL and lead to a deterioration of the transporting properties.³²¹ Efforts to synthesize hole-transporting molecules that are inert to chemical degradation have been reported.^{322,323} The long-term solution, however, is to switch the charging polarity to positive, because positive corona charging is environmentally preferable. To achieve positive charging, one either has to invert the configuration of the bilayer

device (by putting the CGL on the top of the CTL), or alternatively, use an electron-transporting layer. While the former approach is impractical because of the poor wear resistivity of the CGL, the search for electron-transporting materials has been gaining momentum in recent years.³²⁴⁻³²⁷

The manufacturing cost of single-layer photoreceptor devices is extremely, economically attractive. The continuous improvement in the bilayer device technology, in terms of photoelectrical and mechanical properties, has made reintroduction of the single-layer concept difficult. However, there will be frequent revisits of the technology in the future due to the enormous pay-off.

C. Outlook and Other Opportunities

The constant demand for better photoconductors, from the business and competition viewpoint, will continue. As the printer market outgrows the copier market, all engines and processes will become digital. The need for laser addressable photoconductors, particularly the IR photoconductors, is obvious. To meet the stability and reliability goals, basic understanding of the details of the photophysics, photogeneration, electron transfer, and charge recombination of thin-film organic photoconductors will be developed. Undoubtedly, the photoreceptor industry will be the primary beneficiary of the outcome. The similarity in the fundamental steps between xerographic photoreceptors and organic energy conversion devices indicates that better solar cell devices are possibilities with today's improved photoconductors and know-how. In addition, the work on organic photoconductors may find application in molecular electronic devices, where the phenomena of photoconductivity, charge transport and charge recombination are utilized. Indeed, spinoff applications, such as electrophotographic printing master^{328,329} image storage media^{330,331} electroluminescent diodes, etc.,³³²⁻³³⁵ have been reported.

Acknowledgments. The author thanks Mrs. J. Marshall for typing the manuscript, Drs. M. Stolka and I. Morrison for comments and discussion, and Mrs. M. Davidson for proofreading the draft.

References

- Seraphin, B. O., Ed., *Solar Energy Conversion-Solid State Physics Aspects* (Topics in Applied Physics, Vol. 31); Springer-Verlag: New York, 1979.
- Parkinson, B. *Acc. Chem. Res.* 1984, 17, 431.
- Fox, M. A. *Acc. Chem. Res.* 1983, 16, 314.
- Albery, W. J. *Acc. Chem. Res.* 1982, 15, 142.
- Gratzel, M. *Acc. Chem. Res.* 1981, 14, 376.
- Heller, A. *Acc. Chem. Res.* 1981, 14, 154.
- Wrighton, M. S. *Acc. Chem. Res.* 1979, 12, 303.
- Gerischer, H. *Electroanal. Chem. Interfacial Electrochem.* 1975, 58, 263.
- Wohrle, D.; Meissner, D. *Adv. Mater.* 1991, 3, 129.
- Tang, C. W. *Appl. Phys. Lett.* 1986, 48, 183.
- Morel, D. L.; Stogryn, E. L.; Ghosh, A. K.; Feng, T.; Purwin, P. E.; Shaw, R. F.; Fishman, C.; Bird, G. R.; Piechowski, A. P. *J. Phys. Chem.* 1984, 88, 923.
- Piechowski, A. P.; Bird, G. R.; Morel, D. L.; Stogryn, E. L. *J. Phys. Chem.* 1984, 88, 934.
- Hor, A. M.; Loutfy, R. O.; Hsiao, C. K. *Appl. Phys. Lett.* 1983, 42, 165.
- Loutfy, R. O.; Sharp, J. H. *J. Chem. Phys.* 1979, 71, 1211.
- Loutfy, R. O.; Hsiao, C. K.; Kazmaier, P. M. *Photogr. Sci. Eng.* 1983, 27, 5.
- Forster, M.; Hester, R. E. *J. Chem. Soc., Faraday Trans. 1* 1982, 78, 1847.
- Morel, D. L. *Mol. Cryst. Liq. Cryst.* 1979, 50, 127.
- Ghosh, A. K.; Feng, T. *J. Appl. Phys.* 1978, 49, 5982.
- Morel, D. L.; Ghosh, A. K.; Feng, T.; Stogryn, E. L.; Purwin, P. E.; Shaw, R. F.; Fishman, C. *Appl. Phys. Lett.* 1978, 32, 495.
- Merritt, V. Y. *IBM J. Res. Develop.* 1978, 22, 353.
- Merritt, V. Y.; Hovel, H. J. *Appl. Phys. Lett.* 1976, 29, 414.
- Martin, M.; Andre, J. J.; Simon, J. *Nouv. J. Chim.* 1981, 5, 485.
- Borsenberger, P. M.; Weiss, D. S. In *Handbook of Imaging Materials*; Diamond, A. S., Ed.; Marcel Dekker, Inc.: New York, 1991.
- Nakanishi, K. *Nikkei New Mater.* 1987, 41.
- Murayama, T. *Electrophotography* 1986, 25, 290.
- Iskikawa, S.; Kajita, I.; Kondo, E. *Spec. Publ. R. Soc. Chem.* 1986, 60, 82; *Chem. Abstr.* 1987, 106, 93437t.
- Carlson, C. F. U.S. Patent 2,221,776, 1940.
- Mort, J. *The Anatomy of Xerography. Its Invention and Evolution*; McFarland & Company Inc.: London, 1989.
- Kepler, R. G. *Appl. Opt., Suppl.* 1969, 3, 25.
- Schaffert, R. M.; Oughton, C. D. *J. Opt. Soc. Am.* 1948, 38, 991.
- Bixby, W. E.; Ullrich, O. A. U.S. Patent 2,753,278, 1956.
- Dessauer, J. H.; Mott, G. R. *Photogr. Eng.* 1955, 6, 250.
- Weimer, P. K. *Phys. Rev.* 1950, 78, 171.
- Felty, E. J. In *Proceedings of the 2nd International Congress on Reprography*; Helwich, O., Ed.; Cologne, Germany, 1967; p 40.
- Cerlon, P. J.; Myers, M. B.; Felty, E. J. U.S. Patent 3,524,745, 1970.
- Pfister, G.; Melnyk, A. R.; Scharfe, M. *Solid State Commun.* 1977, 21, 907.
- Cheung, L.; Foley, G. M. T.; Fournia, P.; Springett, B. E. *Photogr. Sci. Eng.* 1982, 26, 245.
- Kiyota, K.; Teshima, A.; Tanaka, M. *Photogr. Sci. Eng.* 1980, 24, 289.
- Ishiwata, T.; Fujimaki, Y.; Shimizu, I.; Kokado, H. *J. Appl. Phys.* 1980, 51, 444.
- Shattuck, M. D.; Vahtra, U. U.S. Patent 3,484,327, 1969.
- Light, W. A. U.S. Patent 3,615,414, 1971.
- Regensburger, P. J. *Photochem. Photobiol.* 1968, 8, 429.
- Melz, P. J.; Champ, R. B.; Chang, L. S.; Chiou, C.; Keller, G. S.; Liclican, L. C.; Neiman, R. B.; Shattuck, M. D.; Weiche, W. J. *Photogr. Sci. Eng.* 1977, 21, 73.
- Pai, D. M.; Yanus, J. F. *Photogr. Sci. Eng.* 1983, 27, 14.
- Melnyk, A. R.; Pai, D. M. *Hard Copy and Printing Materials, Media and Process. Proc. SPIE-Int. Soc. Opt. Eng.* 1990, 1253, 142.
- Facci, J. S.; Stolka, M. *Phil. Mag. B* 1986, 54, 1.
- Abkowitz, M.; Bassler, H.; Stolka, M. *Phil. Mag. B* 1991, 63, 201.
- Hug, W. F. *Laser Focus/Electro-Optics* 1986, 92.
- Kakuta, A. In *Infrared Absorbing Dyes*; Matsuoka, M., Ed.; Plenum Press: New York, 1990; Chapter 12.
- Scharfe, M. E.; Pai, D. M.; Gruber, R. J. In *Imaging Processes and Materials*, 8th ed.; Strurge, J., Walworth, V., Shepp, A., Eds.; Van Nostrand Reinhold: New York, 1990.
- Schmidlin, F. W. In *Photoconductivity and Related Phenomena*; Mort, J., Pai, D., Eds.; Elsevier: New York, 1976; Chapter 11.
- Braun, A.; Tcherniac, J. *Ber. Dtsch. Chem. Ges.* 1907, 40, 2709.
- Linstead, R. P.; Lowe, A. R. *J. Chem. Soc.* 1934, 1016.
- Byrne, G. T.; Linstead, R. P.; Lowe, A. R. *J. Chem. Soc.* 1934, 1017.
- Linstead, R. P.; Lowe, A. R. *J. Chem. Soc.* 1934, 1022.
- Dent, C. E.; Linstead, R. P. *J. Chem. Soc.* 1934, 1027.
- Linstead, R. P.; Robertson, J. M. *J. Chem. Soc.* 1936, 1195.
- Robertson, J. M.; Woodward, I. *J. Chem. Soc.* 1937, 219.
- Robertson, J. M. *J. Chem. Soc.* 1935, 615.
- Robertson, J. M.; Woodward, I. *J. Chem. Soc.* 1940, 36.
- Lever, A. B. P. *Adv. Inorg. Chem. Radiochem.* 1965, 7, 27.
- Moser, R. H.; Thomas, A. L. *The Phthalocyanines*; CRC Press: Boca Raton, FL, 1983; Vols. I and II.
- Tucker, R. J. U.S. Patent 3,853,783, 1974.
- Soloveva, L. I.; Mikhailenko, S. A.; Chernykh, E. V.; Lukyanets, E. A. *Zh. Obshch. Khim.* 1982, 52, 90.
- Soloveva, L. I.; Lukyanets, E. A. *Zh. Obshch. Khim.* 1980, 50, 1122.
- Mikhailenko, S. A.; Barkanova, S. V.; Lebedev, O. L.; Lukyanets, E. A. *Zh. Obshch. Khim.* 1971, 41, 2735.
- Mikhailenko, S. A. *Zh. Obshch. Khim.* 1962, 32, 1610.
- Gund, F. *J. Soc. Dyers Colourist* 1960, 76, 151.
- Borodkin, V. F.; Erykalov, Yu. G.; Usacheva, K. V. *Zh. Prikl. Khim.* 1956, 29, 1606.
- Oksengendler, I. G.; Kondratenko, N. V.; Lukyanets, E. A.; Yagupolskii, L. M. *Zh. Org. Khim.* 1977, 13, 2234.
- Borisenkova, S. A.; Erokhin, A. S.; Novikov, V. A.; Rudenko, A. P. *Zh. Org. Khim.* 1975, 11, 1977.
- Barrett, P. A.; Dent, C. E.; Linstead, R. P. *J. Chem. Soc.* 1936, 1719.
- Kiryukhin, I. A.; Lobanova, K. N.; Popov, Yu. A.; Shaulow, Yu. Kh.; Benderskii, V. A. *Russ. J. Phys. Chem.* 1976, 50, 380.
- Loutfy, R. O.; Hsiao, C. K. *Can. J. Chem.* 1979, 57, 2546.
- Kitamura, T.; Imamura, S.; Kawamoto, M. *J. Imaging Technol.* 1988, 14, 136.
- Kitamura, T.; Ueda, N. *Electrophotography* 1989, 28, 269.
- Nukui, Y.; Setoguchi, K.; Oda, M.; Kitamura, T. *Electrophotography* 1991, 30, 30.
- Germano, N. J.; Nealey, R. H. *Xerox Discl. J.* 1978, 3, 377.

- (78) Page, G. A.; Tokoli, E. G.; Cosgrove, R. T.; Spiewak, J. W. U.S. Patent 4,557,868, 1985.
- (79) Liebermann, G.; Hor, A. M.; Toth, A. E. U.S. Patent 4,771,133, 1988.
- (80) Mizuguchi, J. *Cryst. Res. Technol.* 1981, 16, 675.
- (81) Wagner, H. J.; Loutfy, R. O.; Hsiao, C. K. *J. Mater. Sci.* 1982, 17, 2781.
- (82) Edwards, L.; Gouterman, M. *J. Mol. Spectrosc.* 1970, 33, 292.
- (83) Schaffer, A. M.; Gouterman, M.; Davidson, E. R. *Theor. Chim. Acta* 1973, 30, 9.
- (84) Mathur, S. C.; Singh, J. *Int. J. Quant. Chem.* 1972, 6, 57; 1972, 6, 747; 1974, 8, 79.
- (85) Chen, I.; Abkowitz, M.; Sharp, J. H. *J. Chem. Phys.* 1969, 50, 2237.
- (86) Henriksson, A.; Sundborn, M. *Theor. Chim. Acta* 1972, 27, 213.
- (87) Chen, I. *J. Mol. Spectrosc.* 1967, 23, 131.
- (88) Sappok, R. *J. Oil Colour Chem. Assoc.* 1978, 61, 299 and references therein.
- (89) Honigmann, B. *J. Paint Technol.* 1966, 38, 77.
- (90) Suito, E.; Uyeda, N. *Proc. Jpn. Acad.* 1956, 32, 182.
- (91) Miyatake, M.; Tamura, S.; Ishizuka, S. Japanese Kokai 73,76,925, 1973.
- (92) Kumano, I.; Miyatake, M.; Tamura, S.; Ishizuka, S. Japanese Kokai 74,59,136, 1974.
- (93) Arai, Y.; Suzuki, S. Japanese Kokai 72,01,026, 1972.
- (94) Knudsen, B. I.; Rolskov, H. S. U.S. Patent 3,160,635, 1964.
- (95) Yagishita, T.; Ikegami, K.; Narusawa, T.; Okuyama, H. *IEEE Trans. Ind. Appl.* 1984, IA-20, 1642.
- (96) Enokida, T.; Hirohashi, R. *J. Imaging Sci. Technol.* 1992, 36, 135.
- (97) Brown, C. J. *J. Chem. Soc.* 1968, 2488.
- (98) Brown, C. J. *J. Chem. Soc.* 1968, 2494.
- (99) Sharp, J. H.; Lardon, M. *J. Phys. Chem.* 1968, 72, 3230.
- (100) Tarantino, F. R.; Stubbs, D. H.; Cooke, T. F.; Melsheimer, L. A. *Am. Ink Maker* 1950, 35, 425.
- (101) Ebert, A. A.; Gottlieb, H. B. *J. Am. Chem. Soc.* 1952, 74, 2806.
- (102) Karasek, F. W.; Decius, J. C. *J. Am. Chem. Soc.* 1952, 74, 4716.
- (103) Shigemitsu, M. *Bull. Chem. Soc. Jpn.* 1959, 32, 607.
- (104) Byrne, J. F.; Kurz, P. F. U.S. Patent 3,357,989, 1967.
- (105) Kakuta, A.; Mori, Y.; Takano, S.; Sawada, M.; Shibuya, I. *J. Imaging Technol.* 1985, 11, 7.
- (106) Enokida, T.; Hirohashi, R.; Mizukami, S. *J. Imaging Sci.* 1991, 35, 235.
- (107) Enokida, T.; Ehashi, S. *Chem. Lett.* 1988, 179.
- (108) Enokida, T.; Hirohashi, R.; Morohashi, N. *Bull. Chem. Soc. Jpn.* 1991, 64, 279.
- (109) Hackett, C. F. *J. Chem. Phys.* 1971, 55, 3178.
- (110) Enokida, T.; Hirohashi, R.; Nakamura, T. *J. Imaging Sci.* 1990, 34, 234; *Electrophotography* 1990, 29, 373.
- (111) Enokida, T.; Kurata, R.; Seta, T.; Katsura, H. *Electrophotography* 1988, 27, 19.
- (112) Fujimaki, Y.; Tadokoro, H.; Oda, Y.; Yoshioka, H.; Homma, T.; Moriguchi, H.; Watanabe, K.; Kinoshita, A.; Hirose, N.; Itami, A.; Ikeuchi, S. SPSE Proceedings, The Fifth International Congress on Advances in Non-Impact Printing Technologies 1990, 37.
- (113) Oda, Y.; Homma, T.; Fujimaki, Y. *Electrophotography* 1990, 29, 250.
- (114) Takano, S.; Mimura, Y.; Matsui, N.; Utsugi, K.; Gotoh, T.; Tani, C.; Tateishi, K.; Ohde, N. SPSE Proceedings, The Fifth International Congress on Advances in Non-Impact Printing Technologies, 1990, 43; *J. Imaging Technol.* 1990, 17, 46.
- (115) Hor, A. M.; Loutfy, R. O. *Thin Solid Film* 1983, 106, 291.
- (116) Loutfy, R. O.; Hor, A. M.; DiPaola-Baranyi, G.; Hsiao, C. K. *J. Imaging Sci.* 1985, 29, 116.
- (117) Kobayashi, T.; Uyeda, N.; Suito, E. *J. Phys. Chem.* 1968, 72, 2446.
- (118) Enokida, T.; Hirohashi, R. *Chem. Mater.* 1991, 3, 918.
- (119) Arishima, H.; Hiratsuka, H.; Tate, A.; Okada, T. *Appl. Phys. Lett.* 1982, 40, 279.
- (120) Dao, L. H.; Perrier, G.; Cole, K. *Can. J. Chem.* 1988, 66, 1609.
- (121) Loutfy, R. O.; Hsiao, C. K.; Hor, A. M.; DiPaola-Baranyi, G. *J. Imaging Sci.* 1985, 29, 143.
- (122) Loutfy, R. O.; Hor, A. M.; Rucklidge, A. *J. Imaging Sci.* 1987, 31, 31.
- (123) Griffiths, C. H.; Walker, M. S.; Goldstein, P. *Mol. Cryst. Liq. Cryst.* 1976, 33, 149.
- (124) Loutfy, R. O.; Hor, A. M.; Hsiao, C. K.; DiPaola-Baranyi, G.; Kazmaier, P. M. *Pure Appl. Chem.* 1988, 60, 1047.
- (125) Loutfy, R. O.; Hsiao, C. K.; Hor, A. M.; DiPaola-Baranyi, G. *J. Imaging Sci.* 1985, 29, 148.
- (126) Branston, R. E.; Duff, J. M. U.S. Patent 4,557,989, 1985.
- (127) Hung, Y.; Regan, M. T.; Staudenmayer, W. J. U.S. Patent 4,666,802, 1987.
- (128) Yanagi, H.; Douko, S.; Ueda, Y.; Ashida, M.; Wöhrle, D. *J. Phys. Chem.* 1992, 96, 1366.
- (129) Sims, T. D.; Pemberton, J. E.; Lee, P.; Armstrong, N. R. *Chem. Mater.* 1989, 1, 26.
- (130) Klofta, T. J.; Danziger, J.; Lee, P.; Pankow, J.; Nebeany, K. W.; Armstrong, N. R. *J. Phys. Chem.* 1987, 91, 5646.
- (131) Klofta, T.; Linkous, C.; Armstrong, N. R. *J. Electroanal. Chem.* 1985, 185, 73.
- (132) Klofta, T. J.; Rieke, P. C.; Linkous, C. A.; Buttner, W. J.; Nanthakumar, A.; Mewborn, T. D.; Armstrong, N. R. *J. Electrochem. Soc.* 1985, 132, 2134.
- (133) Rieke, P. C.; Armstrong, N. R. *J. Am. Chem. Soc.* 1984, 106, 47.
- (134) Bradbrook, E. F.; Linstead, R. P. *J. Chem. Soc.* 1936, 1744.
- (135) Kovshev, E. I.; Likyanets, E. A. *Zh. Obshchei. Khim.* 1972, 42, 696.
- (136) Hayashida, S.; Tai, S.; Hayashi, N.; Iwakabe, Y.; Kinjo, N.; Numata, S. U.S. Patent 4,886,721, 1989.
- (137) Tai, S.; Hayashida, S.; Hayashi, N. U.S. Patent 4,842,970, 1989.
- (138) Hayashida, S.; Tai, S. U.S. Patent 4,749,637, 1988.
- (139) Sprenger, H. E.; Ziegenbein, W. *Angew. Chem., Int. Ed. Engl.* 1966, 5, 894.
- (140) Treibs, A.; Jacob, K. *Angew. Chem., Int. Ed. Engl.* 1965, 4, 694.
- (141) Sprenger, H. E.; Ziegenbein, W. *Angew. Chem., Int. Ed. Engl.* 1967, 6, 553; 1968, 7, 530.
- (142) Rehak, V.; Israel, G. *Chem. Phys. Lett.* 1986, 132, 236.
- (143) Champ, R. B.; Shattuck, M. D. U.S. Patent 3,824,099, 1974.
- (144) Schmidt, A. H. In *Oxocarbons*; West, R., Ed.; Academic Press: New York, 1980; Chapter 10.
- (145) Kampfer, H. U.S. Patent 3,617,270, 1971.
- (146) Law, K. Y.; Bailey, F. C.; Bluett, L. J. *Can. J. Chem.* 1986, 64, 1607.
- (147) Law, K. Y.; Bailey, F. C. *Dyes Pigm.* 1988, 9, 85.
- (148) Treibs, A.; Jacob, K. *Liebigs Ann. Chem.* 1968, 712, 123; 1966, 699, 153.
- (149) Ziegenbein, W.; Sprenger, H. E. *Angew. Chem., Int. Ed. Engl.* 1966, 5, 893.
- (150) Kuramoto, N.; Natsukawa, K.; Asao, K. *Dyes Pigm.* 1989, 11, 21.
- (151) Keil, D.; Hartmann, H.; Moschny, T. *Dyes Pigm.* 1991, 17, 19.
- (152) Chang, M. S. H.; Edelman, P. G. U.S. Patent 4,353,971, 1982.
- (153) Chang, M. S. H.; Berman, M. F. U.S. Patent 4,391,888, 1983.
- (154) Law, K. Y.; Bailey, F. C. *Can. J. Chem.* 1986, 64, 2267.
- (155) Law, K. Y.; Bailey, F. C. *J. Imaging Sci.* 1987, 31, 172.
- (156) Law, K. Y. *J. Phys. Chem.* 1987, 91, 5184.
- (157) DiPaola-Baranyi, G.; Hsiao, C. K.; Kazmaier, P. M.; Burt, R.; Loutfy, R. O.; Martin, T. I. *J. Imaging Sci.* 1988, 32, 60.
- (158) Kazmaier, P. M.; DiPaola-Baranyi, G.; Loutfy, R. O. U.S. Patent 4,621,038, 1986.
- (159) Champ, R. B.; Vollmer, R. L. U.S. Patent, 4,677,045, 1987.
- (160) Law, K. Y.; Bailey, F. C. U.S. Patent 5,077,160; 1991; *Dyes Pigm.*, in press.
- (161) DiPaola-Baranyi, G.; Burt, R. A.; Hsiao, C. K.; Kazmaier, P. M.; Carmichael, K. M.; Horgan, A. M. U.S. Patent 4,471,041, 1984.
- (162) Bigelow, R. W.; Freund, H. J. *Chem. Phys.* 1986, 107, 159.
- (163) Law, K. Y.; Facci, J. S.; Bailey, F. C.; Yanus, J. F. *J. Imaging Sci.* 1990, 34, 31.
- (164) Wingard, R. E. *IEEE Ind. Appl.* 1982, 37, 1251.
- (165) Tristani-Kendra, M.; Eckhardt, C. J. *J. Chem. Phys.* 1984, 81, 1160.
- (166) Redetermination of the crystal structure of Sq-23 provides accurate structural and packing data of Sq-23 in solid (Law, K. Y.; Ziolo, R. Unpublished results). For original report, see: Farnum, D. G.; Neuman, M. A.; Suggs, W. T. *J. Cryst. Mol. Struct.* 1974, 4, 199.
- (167) Law, K. Y.; Chen, C. C. *J. Phys. Chem.* 1989, 93, 2533.
- (168) Yanus, J. F.; Limburg, W. W. U.S. Patent 4,521,621, 1985.
- (169) Kazmaier, P. M.; Burt, R.; DiPaola-Baranyi, G.; Hsiao, C. K.; Loutfy, R. O.; Martin, T. I.; Hamer, G. K.; Bluhm, T. L.; Taylor, M. G. *J. Imaging Sci.* 1988, 32, 1.
- (170) Law, K. Y.; Kaplan, S.; Crandall, R. K. *Dyes Pigm.* 1988, 9, 187.
- (171) Kazmaier, P. M.; Burt, R.; Baranyi, G. U.S. Patent 4,624,904, 1986.
- (172) Law, K. Y.; Bailey, F. C. *J. Chem. Soc., Chem. Commun.* 1991, 1156; *Can. J. Chem.*, manuscript submitted for publication.
- (173) Law, K. Y.; Bailey, F. C. *J. Chem. Soc., Chem. Commun.* 1990, 864; *J. Org. Chem.* 1992, 57, 3278.
- (174) Law, K. Y. *J. Imaging Sci. Technol.*, in press.
- (175) Law, K. Y. *Chem. Mater.* 1992, 4, 605.
- (176) Rau, H. *Ber. Bunsen-Ges. Phys. Chem.* 1969, 73, 810.
- (177) Champ, R. B.; Shattuck, M. D. U.S. Patent 3,898,084, 1975.
- (178) Law, K. Y.; Tarnawskyj, I. W. *J. Photochem. Photobiol. A: Chem.* 1991, 57, 217.
- (179) Law, K. Y.; Tarnawskyj, I. W. *J. Imaging Sci. Technol.*, in press.
- (180) Murayama, T.; Otsuka, S.; Nagasaka, H. *Res. Dev. Techn.—Mitsubishi Chem.* 1987, 1, 57.
- (181) Hashimoto, M. *Electrophotography* 1986, 3, 230.
- (182) Koyama, T.; Miyazaki, H.; Anayama, H. U.S. Patent 4,895,782, 1990.
- (183) Law, K. Y.; Tarnawskyj, I. W. U.S. Patent 4,797,337, 1989.
- (184) Hashimoto, M.; Sasaki, M. U.S. Patents 4,916,039; 4,925,758, 1990.
- (185) Hashimoto, M. U.S. Patent 4,618,672, 1986.
- (186) Fukagai, T.; Kimura, M.; Ohta, M.; Hashimoto, M. U.S. Patent 4,830,942, 1989.
- (187) Hashimoto, M.; Ohta, M.; Kozima, A.; Sakai, K.; Sasaki, M. U.S. Patent 4,426,327, 1984.
- (188) Tsutsui, K. U.S. Patent 4,540,643, 1985.
- (189) Ohta, M. U.S. Patents 4,663,442, 1987; 4,582,771, 1986.
- (190) Ohta, M.; Sasaki, M.; Shoshi, M. U.S. Patent, 4,567,124, 1986.
- (191) Ohta, M.; Sakai, K.; Hashimoto, M.; Kozima, A.; Sasaki, M. U.S. Patent 4,279,981, 1981.
- (192) Hashimoto, M.; Sakai, K.; Ohta, M.; Kozima, A.; Sasaki, M.; Tsutsui, K. U.S. Patent 4,299,896, 1981.
- (193) Ishikawa, S.; Katagiri, K.; Watanabe, K.; Ohta, S.; Kitahara, M. U.S. Patent 4,356,243, 1982.

- (194) Yamashita, M.; Miyazaki, H.; Takiguchi, T.; Matsumoto, M.; Hiro, M.; Ishikawa, S. U.S. Patent, 4,788,119, 1988.
- (195) Matsumoto, M.; Takiguchi, T.; Yamashita, M.; Umehara, S.; Ishikawa, S.; Miyazaki, H. U.S. Patent 4,760,003, 1988.
- (196) Umehara, S.; Matsumoto, M.; Takiguchi, T.; Ishikawa, S. U.S. Patent 4,830,994, 1989.
- (197) Ishikawa, S.; Katagiri, K.; Watanabe, K.; Sakai, K.; Kitahara, M. U.S. Patent 4,500,619, 1985.
- (198) Takahashi, H.; Ishikawa, S. U.S. Patent, 4,495,264, 1985.
- (199) Hiro, M.; Takasu, Y.; Ishikawa, S.; Katagiri, K.; Takahashi, H. U.S. Patent 4,551,404, 1985.
- (200) Umehara, S.; Matsumoto, M.; Takiguchi, T.; Ishikawa, S. U.S. Patent 4,830,944, 1989.
- (201) Matsumoto, M. U.S. Patent 4,820,602, 1989.
- (202) Murakami, O.; Uenaka, T.; Otsuka, S.; Aramaki, S.; Murayama, T. IS&T Proceedings, The Seventh International Congress on Advances in Non-Impact Printing Technologies 1991, 318.
- (203) Buraway, A.; Salem, A. G.; Thompson, A. R. *J. Chem. Soc.* 1952, 4793.
- (204) Bershtein, I. Ya.; Ginzburg, O. F. *Russ. Chem. Rev.* 1972, 41, 97.
- (205) Ball, P.; Nicholls, C. H. *Dyes Pigm.* 1982, 3, 5.
- (206) Matsunaga, Y.; Miyajima, N. *Bull. Chem. Soc. Jpn.* 1971, 44, 361.
- (207) Kuder, J. E. *Tetrahedron* 1972, 28, 1973.
- (208) Monahan, A. R.; Flannery, J. B. *Chem. Phys. Lett.* 1972, 17, 510.
- (209) Guggenberger, L. J.; Teuffer, G. *Acta Crystallogr.* 1975, B31, 785.
- (210) Whitaker, A. J. *Soc. Dyers Colourists* 1978, 94, 431.
- (211) Kobelt, Von D.; Paulus, E. F.; Kunstmann, W. *Acta Crystallogr.* 1972, B28, 1319.
- (212) Law, K. Y.; Kaplan, S.; Crandall, R.; Tarnawskyj, I. W. Manuscript in preparation.
- (213) Law, K. Y.; Kaplan, S.; Crandall, R.; Tarnawskyj, I. W. Unpublished results.
- (214) DiPaola-Baranyi, G.; Hsiao, C. K.; Hor, A. M. *J. Imaging Sci.* 1990, 34, 224.
- (215) Yoshihara, T.; Kimura, T. U.S. Patent 4,855,202, 1989.
- (216) Seki, K.; Suzuki, Y.; Yamanami, H. SPSE Proceedings, The Fifth International Congress on Advances in Non-Impact Printing Technologies 1990, 60.
- (217) Law, K. Y.; Tarnawskyj, I. W. Unpublished results.
- (218) Khe, C. K.; Takenouchi, O.; Kawara, T.; Tanaka, H.; Yokota, S. *Photogr. Sci. Eng.* 1984, 28, 195.
- (219) Ohta, K. *Electrophotography* 1986, 25, 303.
- (220) Regensburger, R. J.; Jakubowski, J. J. U.S. Patent 3,904,407, 1975.
- (221) Popovic, Z. D.; Hor, A. M.; Loutfy, R. O. *Chem. Phys.* 1988, 127, 451.
- (222) Loutfy, R. O.; Hor, A. M.; Kazmaier, P. M.; Tam, M. *J. Imaging Sci.* 1989, 33, 151.
- (223) Duff, J. M.; Hor, A. M.; Melnyk, A. R.; Teney, D. Hard Copy and Printing Materials, Media, and Process. *Proc. SPIE—Int. Soc. Opt. Eng.* 1990, 183.
- (224) Duff, J. M.; Hor, A. M.; Allen, C. G.; Melnyk, A. R.; Teney, D. IS&T Proceedings, The Seventh International Congress on Advances in Non-Impact Printing Technologies 1991, 284.
- (225) Maki, T.; Hashimoto, H. *Bull. Chem. Soc. Jpn.* 1952, 25, 411.
- (226) Nagao, Y.; Misono, T. *Bull. Chem. Soc. Jpn.* 1981, 54, 1191.
- (227) Takei, Y.; Fujimaki, Y.; Akashi, N.; Nomori, H. U.S. Patent 4,431,722, 1984.
- (228) Duff, J. M.; Hor, A. M.; Hsiao, C. K.; Hamer, G. K. U.S. Patent 4,937,164, 1990.
- (229) Nagao, Y.; Abe, Y.; Misono, T. *Dyes Pigm.* 1985, 6, 303 and references therein.
- (230) Troster, H. *Dyes Pigm.* 1983, 4, 171.
- (231) Iden, R.; Seybold, G.; Stange, A.; Eilingsfeld, H. *Forschungsber.-Bundesminst. Forsch. Technol.* 1984, BMFT-FB-T, 84-164; *Chem. Abstr.* 1985, 102, 150903k.
- (232) Graser, F.; Hadicke, E. *Liebigs Ann. Chem.* 1980, 483, 1994.
- (233) Borsenberger, P. M.; Regan, M. T.; Staudenmayer, W. J. U.S. Patent 4,578,334, 1986.
- (234) Tamizhami, G.; Dodelet, J. P.; Cote, R.; Gravel, D. *Chem. Mater.* 1991, 3, 1046.
- (235) Regensburger, P. J.; Jakubowski, J. J. U.S. Patent 3,879,200, 1975.
- (236) Loutfy, R. O.; Hor, A. M.; Kazmaier, P. M.; Burt, R. B.; Hamer, G. K. *Dyes Pigm.* 1991, 15, 139.
- (237) Hoegl, H.; Sus, O.; Neugebauer, W. German Patent 1,068,115, 1957.
- (238) Hoegl, H. *J. Phys. Chem.* 1965, 69, 755.
- (239) Lardon, M.; Lell-Doller, E.; Weigl, J. W. *Mol. Cryst.* 1967, 2, 241.
- (240) Hayashi, Y.; Kuroda, M.; Inami, A. *Bull. Chem. Soc. Jpn.* 1966, 39, 1660.
- (241) Ikeda, M.; Morimoto, K.; Murakami, Y.; Sato, H. *Jpn. J. Appl. Phys.* 1969, 8, 759.
- (242) Sato, H.; Ikeda, M. *J. Appl. Phys.* 1972, 43, 4108.
- (243) Schaffert, R. M. *IBM J. Res. Dev.* 1971, 15, 75.
- (244) Nakazawa, Y.; Hoshino, K.; Hanna, J.; Kokado, H. *Jpn. J. Appl. Phys.* 1991, 30, 1002.
- (245) Moisan, J. Y.; Andre, B.; Lever, R. *Chem. Phys.* 1991, 153, 305.
- (246) Hirohashi, R.; Kobayashi, N.; Suzuki, T. *Poly. J.* 1990, 22, 191.
- (247) Helmstret, W.; Baumann, H.; Diener, G. *J. Photochem. Photobiol. A: Chem.* 1990, 54, 171; 52, 179.
- (248) Andre, B.; Lever, R.; Moisan, J. Y. *Chem. Phys.* 1989, 137, 281.
- (249) VanAllan, J. A.; Reynolds, G. A. *J. Org. Chem.* 1968, 33, 1102.
- (250) Saeva, F. D.; Olin, G. R.; Turner, S. R.; Yanus, J. F.; Sandman, D. *J. Photogr. Sci. Eng.* 1988, 22, 129.
- (251) Wizinger, R.; Ulrich, P. *Helv. Chim. Acta* 1956, 39, 207.
- (252) Dulmage, W. L.; Light, W. A.; Marino, S. J.; Salzberg, C. D.; Smith, D. L.; Staudenmayer, W. J. *J. Appl. Phys.* 1978, 49, 5543.
- (253) Borsenberger, P. M.; Chowdry, A.; Hoesterey, D. C.; Mey, W. *J. Appl. Phys.* 1978, 49, 5555.
- (254) Perlstein, J. H. In *Electrical Properties of Polymers*; Seanor, D. A., Ed.; Academic Press: New York, 1982; Chapter 2.
- (255) Borsenberger, P. M.; Hoesterey, D. C. *J. Appl. Phys.* 1980, 51, 4248.
- (256) Potts, K. T. U.S. Patent 4,451,659 and 4,476,313, 1984.
- (257) Clark, S. P.; Reynolds, G. A.; Perlstein, J. H. U.S. Patent 4,327,169, 1982.
- (258) Detty, M. R.; Murray, B. J.; Perlstein, J. H. U.S. Patent 4,365,017, 1982.
- (259) Detty, M. R.; Murray, B. J. *J. Org. Chem.* 1982, 47, 5235.
- (260) Mizuguchi, J.; Rochat, A. C. *J. Imaging Sci.* 1988, 32, 135.
- (261) Mizuguchi, J. *J. Appl. Phys.* 1989, 66, 3104.
- (262) Arita, M.; Fukushima, K.; Homma, S.; Kura, H.; Yamamoto, H.; Okamura, M. *J. Appl. Phys.* 1991, 70, 4065.
- (263) Rochat, A. C.; Iqbal, A.; Jeanneret, R.; Mizuguchi, J. U.S. Patents 4,632,893, 1986; 4,760,151, 1988.
- (264) James, T. H. *The Theory of Photographic Processes*, 4th ed.; MacMillan Company: New York, 1977.
- (265) Allen, N. S.; Robinson, E. T.; Stott, C. M.; Thompson, F. *Dyes Pigm.* 1989, 10, 183.
- (266) Takei, Y.; Kijima, E.; Goto, S.; Hiroyuki, N. U.S. Patent 4,835,080, 1989.
- (267) Weiss, D. S.; Burberry, M. *Thin Solid Films* 1988, 158, 175.
- (268) Baranyi, G.; Hor, A. M.; Loutfy, R. O.; Popovic, Z. D. U.S. Patent 4,925,760, 1990.
- (269) Baranyi, G.; Hor, A. M.; Loutfy, R. O. U.S. Patent 4,952,472, 1990.
- (270) Baranyi, G.; Hor, A. M.; Loutfy, R. O. U.S. Patent 4,952,471, 1990.
- (271) Katagiri, K.; Oguchi, Y.; Takasu, Y. *Nippon Kagaku Kaishi* 1986, 387.
- (272) Yokoyama, M.; Endo, Y.; Matsubara, A.; Mikawa, H. *J. Chem. Phys.* 1981, 75, 3006.
- (273) Popovic, Z. D. *Chem. Phys. Lett.* 1983, 100, 227.
- (274) Pai, D. M.; Enke, R. C. *Phys. Rev. B* 1975, 11, 5163.
- (275) Onsager, L. *Phys. Rev.* 1938, 54, 554.
- (276) Onsager, L. *J. Chem. Phys.* 1934, 2, 599.
- (277) Batt, R. H.; Braun, C. L.; Hornig, J. F. *Appl. Opt. Suppl.* 1969, 3, 20.
- (278) Chance, R. R.; Braun, C. L. *J. Chem. Phys.* 1973, 59, 2269.
- (279) Borsenberger, P. M.; Ateya, A. I. *J. Appl. Phys.* 1978, 49, 4035.
- (280) Noolandi, J.; Hong, K. M. *J. Chem. Phys.* 1979, 70, 3230.
- (281) Popovic, Z. D. *Chem. Phys.* 1984, 86, 311.
- (282) Popovic, Z. D.; Hor, A. M. *Proc SPIE—Int. Soc. Opt. Eng.* 1989, 910, 168.
- (283) Loutfy, R. O.; Menzel, E. R. *J. Am. Chem. Soc.* 1980, 102, 4967.
- (284) Popovic, Z. D.; Sharp, J. H. *J. Chem. Phys.* 1977, 66, 5076.
- (285) Popovic, Z. D. *J. Appl. Phys.* 1981, 52, 6197.
- (286) Popovic, Z. D.; Menzel, E. R. *J. Chem. Phys.* 1979, 71, 5090.
- (287) Popovic, Z. D. *J. Chem. Phys.* 1982, 76, 2714; 1983, 78, 1552.
- (288) Tam, A. C. *Appl. Phys. Lett.* 1980, 37, 978.
- (289) Menzel, E. R.; Jordan, K. J. *Chem. Phys.* 1978, 32, 223.
- (290) Menzel, E. R.; Popovic, Z. D. *Chem. Phys. Lett.* 1978, 55, 177.
- (291) Fan, F. R.; Fulkner, L. R. *J. Chem. Phys.* 1978, 69, 3341.
- (292) Ghosh, A. K.; Morel, D. L.; Feng, T.; Shaw, R. F.; Rowe, C. A. *J. Appl. Phys.* 1974, 45, 230.
- (293) Loutfy, R. O.; Sharp, J. H.; Hsiao, C. K.; Ho, R. *J. Appl. Phys.* 1981, 52, 5218.
- (294) Ahuja, R. C.; Hauffe, K. *Ber. Bunsen-Ges. Phys. Chem.* 1980, 84, 68.
- (295) Mizuguchi, J. *Jpn. J. Appl. Phys.* 1982, 21, 822.
- (296) Mizuguchi, J. *Jpn. J. Appl. Phys.* 1981, 20, 1855, 2065; 2073.
- (297) Fujimaki, Y. IS&T Proceedings, The Seventh International Congress on Advances in Non-Impact Printing Technologies 1991, 269.
- (298) Umeda, M.; Nimi, T.; Hashimoto, M. *Jpn. J. Appl. Phys.* 1990, 29, 2746.
- (299) Law, K. Y.; Popovic, Z. D. Unpublished observation.
- (300) Umeda, M.; Hashimoto, M. *J. Appl. Phys.* 1992, 72, 117.
- (301) Grammatica, S.; Mort, J. *Appl. Phys. Lett.* 1981, 38, 445.
- (302) Law, K. Y. *Inorg. Chem.* 1985, 24, 1778.
- (303) Johansson, L. B. A.; Langhals, H. *Spectrochim. Acta* 1991, 47A, 857.
- (304) Bigelow, R. W. *J. Phys. Chem.* 1976, 80, 2694.
- (305) Cressman, P. J.; Hartmann, G. C.; Kuder, J. E.; Saeva, F. D.; Wychick, D. *J. Chem. Phys.* 1974, 61, 2740.
- (306) Law, K. Y. *J. Phys. Chem.* 1985, 89, 2652.
- (307) Ziolo, R.; Griffiths, C. H.; Troup, J. M. *J. Chem. Soc., Dalton Trans.* 1980, 2300.
- (308) Gutman, F.; Lyon, L. E. *Organic Semiconductors*; Krieger: Malabar, FL, 1981; p 168.
- (309) Law, K. Y. *J. Phys. Chem.* 1988, 92, 4226.
- (310) Kakuta, A.; Mori, Y.; Morishita, H. *IEEE Trans. Ind. Appl.* 1981, 1A-17, 382.
- (311) Shi, X. D. *Mater. Sci.* 1990, XVI, 197.
- (312) Kitamura, T.; Yokoyama, M. *J. Imaging Sci.* 1990, 34, 197.

- (313) Kanemitsu, Y.; Funada, H. *J. Phys. D: Appl. Phys.* **1991**, *24*, 1409.
(314) Kanemitsu, Y.; Imamura, S. *J. Appl. Phys.* **1990**, *67*, 3728.
(315) Kanemitsu, Y.; Imamura, S. *J. Appl. Phys.* **1989**, *66*, 997.
(316) Scott, J. C.; Skumanich, A.; Shattuck, M. D.; Nguyen, H. *Hard Copy and Printing Materials, Media and Process. Proc. SPIE—Int. Soc. Opt. Eng.* **1990**, *1253*, 194.
(317) Horgan, A. M. U.S. Patent 4,415,639, 1983.
(318) Loutfy, R. O.; Hor, A. M.; Liebermann, G.; Toth, A. J.; Hsiao, C. K.; Carmichael, K. M.; Tokoli, E. G. U.S. Patent 4,882,254, 1989.
(319) Pacansky, J.; Waltman, R. J.; Coufal, H.; Cox, R. *Radiat. Phys. Chem.* **1988**, *31*, 853.
(320) Limburg, W. W.; Pai, D. M.; Yanus, J. F.; Renfer, D. S.; DeFeo, P. SPSE Proceedings, The Fifth International Congress on Advances in Non-Impact Printing Technologies 1990, 55.
(321) Weiss, D. S. *J. Imaging Sci.* **1990**, *34*, 132.
(322) Akasaki, Y.; Sato, K.; Yabuuchi, N.; Tanaka, K.; Nukada, K. U.S. Patent 4,933,245, 1990.
(323) Pai, D. M.; Yanus, J. F.; DeFeo, P. J. U.S. Patent 4,988,595, 1991.
(324) Ong, B. S.; Keoshkerian, B.; Martin, T. I.; Hamer, G. K. *Can. J. Chem.* **1985**, *63*, 147.
(325) Loutfy, R. O.; Ong, B. S.; Tadros, J. *J. Imaging Sci.* **1985**, *29*, 69.
(326) Murti, D. K.; Kazmaier, P. M.; DiPaola-Baranyi, G.; Hsiao, C. K.; Ong, B. S. *J. Phys. D.* **1987**, *20*, 1806.
(327) Borsenberger, P. M.; Bassler, H. *J. Imaging Sci.* **1991**, *35*, 79.
(328) Bugner, D. E. *J. Imaging Sci.* **1991**, *35*, 377.
(329) Tam, M. C.; Pundsack, A. L.; Gundlach, R. W.; Vincett, P. S.; Kovacs, G. J.; Jennings, C. A.; Loutfy, R. O. *J. Imaging Sci.* **1988**, *32*, 247.
(330) Yokoyama, K.; Yokoyama, M. *Appl. Phys. Lett.* **1989**, *55*, 2141; *J. Imaging Technol.* **1990**, *16*, 219.
(331) Yokoyama, K.; Kishimoto, Y.; Kusabayashi, S. *J. Imaging Technol.* **1989**, *15*, 239.
(332) Tang, C. W.; VanSlyke, S. A. *Appl. Phys. Lett.* **1987**, *51*, 913.
(333) Adachi, C.; Tokito, S.; Tsutsui, T.; Saito, S. *Jpn. J. Appl. Phys.* **1988**, *27*, 269; 713.
(334) Adachi, C.; Tsutsui, T.; Saito, S. *Appl. Phys. Lett.* **1989**, *55*, 1489.
(335) Hiramoto, M.; Miyao, T.; Yokoyama, M. *Appl. Phys. Lett.* **1990**, *57*, 1625.